

A NEW PERMEABILITY PREDICTION FOR
CLEAN SANDS USING 3D RECONSTRUCTION
METHODOLOGY ON THIN SECTIONS

LULUAN ALMANNA LUBIS

MASTER OF SCIENCE
GEOSCIENCES AND PETROLEUM ENGINEERING
DEPARTMENT

UNIVERSITI TEKNOLOGI PETRONAS

MAY 2012

STATUS OF THESIS

Title of thesis

A NEW PERMEABILITY PREDICTION FOR CLEAN SANDS
USING 3D RECONSTRUCTION METHODOLOGY ON THIN
SECTIONS

I, LULUAN ALMANNA LUBIS
hereby allow my thesis to be placed at the Information Resource Centre (IRC) of
Universiti Teknologi PETRONAS (UTP) with the following conditions:

1. The thesis becomes the property of UTP.
2. The IRC of UTP may make copies of the thesis for academic purposes only.
3. The thesis is classified as

☐

Confidential

☒

Non-confidential

If this thesis is confidential, please state the reason:

The contents of the thesis will remain confidential for _____ years.

Remarks on disclosure:

Endorsed by

Signature of Author

Permanent address:

Jl. Tridharma No. 130, Kampus
USU, Medan 20155, North
Sumatera, Indonesia

Date: _____

Signature of Supervisor

Name of Supervisor:

Assoc. Prof. Dr. Zuhar Zahir T.
Harith

Date: _____

UNIVERSITI TEKNOLOGI PETRONAS

A NEW PERMEABILITY PREDICTION FOR CLEAN SANDS USING 3D
RECONSTRUCTION METHODOLOGY ON THIN SECTIONS

by

LULUAN ALMANNA LUBIS

The undersigned certify that they have read, and recommend to the Postgraduate Studies Programme for acceptance this thesis for the fulfillment of the requirements for the degree stated.

Signature : _____

Main Supervisor : ASSOC. PROF. DR. ZUHAR ZAHIR T. HARITH

Signature : _____

Head of Department : ASSOC. PROF. DR. ABDUL HADI A. RAHMAN

Date : _____

A NEW PERMEABILITY PREDICTION FOR CLEAN SANDS USING 3D
RECONSTRUCTION METHODOLOGY ON THIN SECTIONS

by

LULUAN ALMANNA LUBIS

A Thesis

Submitted to the Postgraduate Studies Programme

as a Requirement for the Degree of

MASTER OF SCIENCE

GEOSCIENCES AND PETROLEUM ENGINEERING DEPARTMENT

UNIVERSITI TEKNOLOGI PETRONAS

BANDAR SERI ISKANDAR,

PERAK

MAY 2012

DECLARATION OF THESIS

Title of thesis

A NEW PERMEABILITY PREDICTION FOR CLEAN SANDS
USING 3D RECONSTRUCTION METHODOLOGY ON THIN
SECTIONS

I, LULUAN ALMANNA LUBIS

hereby declare that the thesis is based on my original work except for quotations and citations which have been duly acknowledged. I also declare that it has not been previously or concurrently submitted for any other degree at UTP or other institutions.

Witnessed by

Signature of Author

Permanent address:

Jl. Tridharma No. 130, Kampus
USU, Medan 20155, North
Sumatera, Indonesia

Date: _____

Signature of Supervisor

Name of Supervisor:

Assoc. Prof. Dr. Zuhar Zahir Tuan
Harith

Date: _____

COPYRIGHT PAGE

In compliance with the terms of the Copyright Act 1987 and the IP Policy of the university, the copyright of this thesis has been reassigned by the author to the legal entity of the university,

Institute of Technology PETRONAS Sdn Bhd.

Due acknowledgement shall always be made of the use of any material contained in, or derived from, this thesis.

© Luluan Almann Lubis, 2012
Institute of Technology PETRONAS Sdn Bhd
All rights reserved.

ABSTRACT

There are several methods to predict permeability from thin sections. Conducting numerical simulation of laboratory experiments through 3D pore structure generated from thin section image is one of the methods. To implement this method on a standard personal computer and in real time, the size of the generated 3D should be limited to mm scale. This size is an order of magnitude smaller than the physical core plug. Computed permeability from this size may be over or underestimated when compared with the true laboratory measurement which is conducted at cm scale. The aim of this study is to develop a robust workflow to estimate permeability of reservoir rocks at core plug scale (cm scale) using full thin section images of sandstone which can be implemented in real time on a standard personal computer. The workflow is based on a combination of fluid flow simulation through 3D porous media generated from 2D images at mm scale and grain size vertical profile trends of entire image area of the thin section which covers an area in cm scale. For validation purposes the 2D to 3D porous media methods were tested on 2D images selected from 3D CT-Scan image. The results showed that this methodology had good agreement with the CT-scan data. The workflow was then applied on thin sections of the Berea core plug and three wells in the Malay Basin where their porosity and permeability were tested in the laboratory. The grain size vertical profile trends which cover the entire area of thin sections were used to define the heterogeneity of full thin section images at cm scale. The building blocks for upscaling purposes were created based on these trends. The representative image from each block was selected and the 2D to 3D porous media method was applied. From this information permeability at mm scale from each block was estimated and then upscaled from pore to core plug scale. The upscaling results on each thin section matched well with laboratory data.

ABSTRAK

Terdapat beberapa kaedah untuk meramalkan kebolehtelapan daripada keratan nipis. Menjalankan penyelakuan berangka eksperimen makmal melalui struktur liang 3D yang dijana daripada imej keratan nipis adalah salah satu kaedah. Untuk melaksanakan kaedah ini pada komputer peribadi standard dan dalam masa nyata, saiz 3D yang dijana harus terhad kepada skala mm. Saiz ini adalah suatu perintah magnitud yang lebih kecil daripada palam teras fizikal. Kebolehtelapan dikira dari saiz ini mungkin atau diperkecilkan jika dibandingkan dengan pengukuran makmal sebenar yang dijalankan pada skala cm. Tujuan kajian ini adalah untuk membangunkan satu aliran kerja yang mantap untuk menganggarkan kebolehtelapan batuan takungan pada skala plag utama (skala cm) menggunakan imej seksyen penuh nipis batu pasir yang boleh dilaksanakan secara real time di komputer peribadi piawai. Aliran kerja adalah berdasarkan gabungan simulasi aliran bendalir melalui media berliang 3D yang dijana daripada imej 2D pada skala mm dan saiz bijian trend profil menegak keseluruhan kawasan imej seksyen nipis yang meliputi kawasan dalam skala cm. Untuk tujuan pengesahan 2D kepada media berliang 3D kaedah telah diuji pada imej-imej 2D yang dipilih daripada imej 3D CT-Scan. Hasil kajian menunjukkan bahawa kaedah ini mempunyai perjanjian yang baik dengan data CT-scan. Aliran kerja itu kemudiannya digunakan pada bahagian nipis plag teras Berea dan tiga telaga di Lembangan Melayu di mana keliangan dan kebolehtelapan mereka telah diuji di makmal. Saiz butiran trend profil menegak yang merangkumi seluruh kawasan seksyen nipis digunakan untuk mentakrifkan keheterogenan imej seksyen penuh nipis pada skala cm. Blok-blok bangunan untuk tujuan Penskalaan telah dicipta berdasarkan trend ini. Imej wakil daripada setiap blok telah dipilih dan 2D kepada kaedah media berliang 3D telah digunakan.

ACKNOWLEDGEMENTS

I humbly thank Almighty Allah, the Most Merciful and the Most Beneficent, who gave me health, thoughts and cooperative people to enable me achieve this goal. I would gratefully acknowledge my supervisor Associate Professor Dr. Zuhar Zahir Tuan Harith, for his outstanding guidance, support and valuable discussions throughout the duration of the study. I am fortunate to work and learn from him. I am profoundly indebted to Mr. Khairul Ariffin M. Noh., Project Leader of Short Term Internal Research Fund (STIRF), for providing facilities and funding through STIRF to completing my study of research.

I am grateful to Prof. Deva P. Ghosh (UTP), Dr. Lutz R. (PCSB) and Dr. Budi P. (PMU) for suggestions and discussions which relating my studies more on industrial point of view. Special thanks to Dr. Asiah (EPTC) and Mr. Buang Nasip (PRSB) for helping and providing thin sections from Malay Basin for this study. I am indebted to Dr. Umar Fauzi (Institute of Technology Bandung) for initial discussion through email about Digital Rock Physics. Thank you to Prof. Blunt (Imperial College London), Dr. J. Dvorkin (Stanford University) and Dr. Zhang (University of Science and Technology of China) for discussions and quick reply by email and permission to use their CT-Scan images for this study.

I would also like to thank: my parents Prof. Dr. Ir. Zulkifli Lubis, and Lily Adriany for their thoughts, constant love and support during my whole live; my brothers, Qisthi Aufa Lubis and Aqwam Sakinata Lubis, my beloved one Diesta R. Purba for all their support and prayers. Without them, this thesis would have not been completed.

Special thanks are extended to the following people and institutions for their help in conducting this research: Mr. Ridwan and laboratory technologists at the UTP Core Analysis, for their technical advice and materials procurement; Aryo, Septian, Fikri, Chandra, Kiki, Hermawan, Firman, Surya, Ariyanti, Belinda, fellow postgraduate students of Universiti Teknologi PETRONAS and housemates for their advice and insightful discussion with them while doing this research; Dr. Hilfan, Maman, Eko, Sajid, Najmi, Hazim, Ifti, Cuya, Habib, Sara and Siti as colleagues at the Geoscience and Petroleum Engineering Department of the university.

Finally, I acknowledge the graduate assistantship scheme financial support from Universiti Teknologi PETRONAS for giving the opportunity in pursuing Master's degree.

TABLE OF CONTENTS

| | |
|--|------|
| STATUS OF THESIS | ii |
| APPROVAL PAGE | iii |
| TITLE PAGE | iii |
| DECLARATION | iv |
| COPYRIGHT OF THESIS | v |
| ABSTRACT..... | vi |
| ACKNOWLEDGEMENTS | viii |
| TABLE OF CONTENTS..... | x |
| LIST OF TABLES | xiii |
| LIST OF FIGURES | xv |
| | |
| CHAPTER 1 : INTRODUCTION | 1 |
| 1.1 Introduction..... | 1 |
| 1.2 Problem Statement..... | 3 |
| 1.3 Objectives..... | 3 |
| 1.4 Scope of study..... | 4 |
| 1.5 Thesis Outline..... | 5 |
| | |
| CHAPTER 2 : LITERATURE REVIEW | 7 |
| 2.1 Introduction..... | 7 |
| 2.2 Porosity..... | 8 |
| 2.3 Permeability..... | 9 |
| 2.4 Kozeny-Carman Relation and Permeability Prediction..... | 10 |
| 2.5 Fluid Flow Simulator..... | 13 |
| 2.5.1 Fluid Flow Simulator using Pore Network Modeling (PNM)..... | 13 |
| 2.5.2 Fluid Flow Simulator using The Lattice Boltzmann Method (LBM)... | 15 |
| 2.6 Method of Generating 3D Porous Media of Rock..... | 17 |
| 2.6.1 X-Ray Computed Tomography (CT-Scan) | 17 |

| | | |
|--|---|----|
| 2.6.2 | 3D Porous Media Reconstruction using 2D Image..... | 19 |
| 2.7 | Summary..... | 22 |
| CHAPTER 3 : METHODOLOGY | | 27 |
| 3.1 | Introduction..... | 27 |
| 3.2 | Simulation Study..... | 30 |
| 3.2.1 | Samples: 3D CT-Scan Image for Simulation Study..... | 32 |
| 3.2.2 | Preliminary Study on Image Size and Resolution for Fluid Flow Simulation..... | 32 |
| 3.2.3 | Study on Sample Points as New Input Parameter for 2D to 3D Porous Media Reconstruction Method..... | 34 |
| 3.2.4 | Representative Elementary Volume (REV) | 35 |
| 3.2.5 | Selection of Training Image (TI) | 36 |
| 3.2.6 | Two Point Correlation Functions (TPCF) | 37 |
| 3.2.7 | Parameters for Simulation: Porosity, Variogram and Sample Points.... | 39 |
| 3.2.8 | Stochastic Simulation: 2D to 3D Porous Media..... | 42 |
| 3.2.9 | Permeability Estimation Using Fluid Flow Simulation..... | 43 |
| 3.3 | Measurement..... | 45 |
| 3.3.1 | Sample: Berea Sandstone Core Plug..... | 45 |
| 3.3.2 | Measurement Procedure..... | 46 |
| 3.4 | Thin Sections..... | 48 |
| 3.4.1 | Thin Section Preparation..... | 49 |
| 3.4.2 | Image Collection..... | 51 |
| 3.4.3 | Image Processing and Segmentation: 2D Binary Image..... | 55 |
| 3.4.4 | Image Stitching: Full Thin Section Image..... | 57 |
| 3.5 | Upscaling Permeability: Pore to Core-Plug Scale..... | 58 |
| 3.5.1 | Grain Size Vertical Profile from Thin Section Image..... | 60 |
| 3.5.2 | Building Blocks..... | 62 |
| CHAPTER 4: RESULTS AND DISCUSSIONS | | 65 |
| 4.1 | Introduction..... | 65 |
| 4.2 | Preliminary Study on Image Size and Resolution for Fluid Flow Simulation.... | 66 |
| 4.3 | Study on Sample Points as New Parameter Input for 2D to 3D Porous Media Reconstruction Method..... | 74 |
| 4.4 | Reconstruction from 2D to 3D Porous Media of Sandstone..... | 80 |

| | | |
|--|--|-----|
| 4.4.1 | Berea Sandstone Reconstruction..... | 80 |
| 4.4.2 | Sandstone S (8) Reconstruction..... | 88 |
| 4.4.3 | Fontainebleau Sandstone Reconstruction..... | 96 |
| 4.5 | Validation of 2D to 3D Porous Media Reconstruction..... | 105 |
| 4.6 | Effectiveness of Grain Size Vertical Profile..... | 106 |
| 4.7 | Upscaling Permeability: Pore to Core Plug Scale..... | 108 |
| 4.7.1 | Application of Upscaling Permeability Workflow to Berea Sandstone Thin Section..... | 109 |
| 4.8 | Case Studies: Application of Upscaling Permeability Workflow to Thin Sections from the Malay Basin..... | 119 |
| 4.8.1 | Application of Upscaling Permeability Workflow to Thin Section from Well A..... | 119 |
| 4.8.2 | Application of Upscaling Permeability Workflow to Thin Section from Well B..... | 127 |
| 4.8.3 | Application of Upscaling Permeability Workflow to Well C Thin Section..... | 135 |
| 4.9 | Discussion..... | 145 |
| CHAPTER 5 : CONCLUSIONS AND RECOMMENDATIONS..... | | 147 |
| 5.1 | Conclusions..... | 147 |
| 5.2 | Recommendation..... | 149 |
| REFERENCES | | 150 |
| PUBLICATIONS..... | | 161 |
| IN PREPARATION PUBLICATIONS | | 162 |
| APPENDIX A..... | | 163 |
| APPENDIX B | | 175 |

LIST OF TABLES

| | |
|---|-----|
| Table 2.1 Summary of Literature Review..... | 23 |
| Table 3.1 Comparison between the proposed method and Keehm (2003). | 34 |
| Table 4.1 Comparison of running time between different types of conditional data. . | 74 |
| Table 4.2 Comparison of physical properties obtained from reconstruction and CT- Scan image..... | 105 |
| Table 4.3 Estimation of porosity and permeability from each representative building block of the Berea sandstone thin section. | 116 |
| Table 4.4 Comparison between the porosity and permeability from upscaling workflow on thin section and core plug measurement on the Berea sandstone. | 117 |
| Table 4.5 Estimated porosity and permeability from each representative building block of thin section from Well A. | 125 |
| Table 4.6 Comparison between the porosity and permeability from upscaling workflow on thin section and core plug measurement on sandstone from Well A. | 125 |
| Table 4.7 Estimated porosity and permeability from each representative building block of thin section from Well B. | 133 |
| Table 4.8 Comparison of porosity and permeability obtained by upscaling permeability workflow and core plug measurement from Well B. | 133 |
| Table 4.9 Porosity and permeability estimated from each representative building block of the thin section from Well C. | 142 |

| | |
|---|-----|
| Table 4.10 Comparison of porosity and permeability obtained by upscaling permeability workflow on thin section and core plug measurement from Well C..... | 142 |
| Table 4.11 Comparison of running time between upscaling permeability workflow with core plug measurement..... | 146 |

LIST OF FIGURES

| | | |
|------------|--|----|
| Figure 2.1 | a) Volume of simple cubic centred packing. b) Area or 2D image selected from simple cubic centred packing [26]. | 9 |
| Figure 2.2 | Illustration of Darcy's Law..... | 10 |
| Figure 2.3 | Three cylindrical tube models with different diameters used by Keehm et.al to compare permeability simulation on LBM with theoretical prediction [17]. The lower images show the local flux from each cylindrical tube model. | 16 |
| Figure 2.4 | Red dots show results of permeability simulation using LBM. Permeability from theoretical theory is shown on blue solid line [17]. . | 16 |
| Figure 2.5 | The 3D rendering of raw CT-Scan cubic image of rock (Courtesy of Ingrain). The image shows that CT-Scan captured the details of the rock. | 19 |
| Figure 2.6 | (a) Process Based Reconstruction image of the Fontainebleau sandstone as compared with (b) CT-Scan image of the same sandstone [18]. | 22 |
| Figure 3.1 | Research Flowchart | 29 |
| Figure 3.2 | Detailed flow chart of simulation work..... | 31 |
| Figure 3.3 | The 3D CT-Scan images for simulation study a) Berea sandstone, b) Sandstone (S8), c) Fontainebleau sandstone. | 32 |
| Figure 3.4 | Workflow for fluid flow simulation test on different sizes and resolutions on the same sample. | 33 |
| Figure 3.5 | Schematic graph of how a measured property (porosity) varies with sample volume and the domain of the REV [73]. | 36 |
| Figure 3.6 | Porosity Fluctuations within 3D CT-Scan Image Samples. | 37 |

| | | |
|-------------|--|----|
| Figure 3.7 | Two Point Correlation Functions Plot. $S_2(r)$ is unitless as it the probability of certain simple geometrical arrangements [28]..... | 39 |
| Figure 3.8 | Input Parameters for Simulation: Porosity, Variogram and Sample Points Extracted from Training Image. | 40 |
| Figure 3.9 | Three dimensional isosurface plot of a 3D reconstructed pore structure from SISIM [17]. | 42 |
| Figure 3.10 | Illustration of a fluid forced through 3D digital image (Courtesy Ingrain). | 43 |
| Figure 3.11 | Photograph of a Berea sandstone core plug. | 45 |
| Figure 3.12 | Poroperm equipment to measure porosity and permeability at ambient confining pressure. | 46 |
| Figure 3.13 | Details of the flow chart outlining the experiment procedure to measure porosity and permeability. | 47 |
| Figure 3.14 | Thin section preparation flow chart..... | 48 |
| Figure 3.15 | Impregnation equipment is used to vacuum and impregnate the samples with blue-dyed epoxy. | 49 |
| Figure 3.16 | Computerized grinding machines is used to produce a deformation free and smooth sample surface..... | 50 |
| Figure 3.17 | Flow chart of image collection. | 51 |
| Figure 3.18 | Microscope for image acquisition. The two magnifications used in this study are 12.5 and 40 times magnification. | 52 |
| Figure 3.19 | Image collected using a 12.5 times magnification. The coverage area is 9 x 11 mm ² . The yellow bar shows scale of the image. Polarization type is cross-polarized..... | 53 |
| Figure 3.20 | Thin section images of cross-polarized (a) and plane-polarized (b). The cross-polarized images are used as an input for full thin section image and the plane-polarized images are used as an input for 3D reconstruction method. | 54 |

| | | |
|-------------|---|----|
| Figure 3.21 | Flow chart of image processing and segmentation of thin section image. | 55 |
| Figure 3.22 | Steps for image processing and segmentation..... | 56 |
| Figure 3.23 | Steps for image collections of the full thin section image. Nine images (middle) are collected as an input for full thin section image. A full thin section image is produced by stitching the nine images..... | 57 |
| Figure 3.24 | Flow chart of Upscaling permeability pore to core plug scale..... | 59 |
| Figure 3.25 | Grain Size Vertical profile calculated in a digital image of bed sediment. [79]. | 61 |
| Figure 3.26 | Building blocks created based on the grain size vertical profile calculated from digital image. Building blocks were created based on the coarsening and fining trends calculated from digital image..... | 63 |
| Figure 4.1 | Relation between image size and computational time of fluid flow simulation. The bigger the size of the cube (75 to 200 voxels) the computational time will be longer. | 66 |
| Figure 4.2 | 3D porous media with the reduced scale to 200, 100, 75 voxels cubes of 19.6% porosity of 3D CT-Scan Berea sandstone from the original 400 voxels cube. The loss of image complexities are shown as the resolution decreased. | 68 |
| Figure 4.3 | The fractional changes value (unitless) of porosity and simulated permeability with respect to the original 400 voxels cube of Berea sandstone. L is unitless as it is a fraction of the size (e.g. 400 voxels/200 voxels = 2). | 68 |
| Figure 4.4 | 3D porous media with the reduced scale to 150, 75 and 50 voxels cubes of 34% porosity of 3D CT-Scan Sandstone (S8) from the original 300 voxels cube. The loss of image complexities are shown as the resolution decreased. | 69 |

| | | |
|-------------|---|----|
| Figure 4.5 | The fractional changes value (unitless) of porosity and permeability with respect to the original 300 voxels cube of Sandstone S (8). L is unitless as it the fraction of size (e.g. 300 voxels/150 voxels = 2). | 70 |
| Figure 4.6 | 3D porous media with the reduced scale to 120 to 100 voxels cubes of 14.6% porosity of 3D CT-Scan Fontainebleau sandstone from original 144 voxels cube. The loss of images complexities are shown as the resolution decreased. | 71 |
| Figure 4.7 | The fractional changes value (unitless) of porosity and permeability with respect to the original 144 voxels cube of Fontainebleau sandstone. L is unitless as it is the fraction of size (e.g. 144 voxels/108 voxels = 1.2). . | 72 |
| Figure 4.8 | Computational time and time efficiency chart on different types of conditional data. (a) Proposed workflow to reconstruct 3D porous media, (b) using training image as conditional data and (c) the non-modified method (Keehm, 2003). | 75 |
| Figure 4.9 | Structural and variogram (x=50, y=50 and z=50) using sample points as conditional data. The structure showed that the complexities of porous media are well preserved. The variograms are align showed that the image is isotropic..... | 77 |
| Figure 4.10 | Structural and variogram (x=50, y=50 and z=50) using training image as conditional data. The structure showed that the complexities of porous media are well preserved. The variograms are align showed that the image is isotropic..... | 78 |
| Figure 4.11 | Structural and variogram (x=50, y=50 and z=50) without conditional data. The structure showed that the complexities of porous media are well preserved. The variograms are align showed that the image is isotropic. | 79 |
| Figure 4.12 | The REV graph for porosity on 3D CT-Scan of Berea Sandstone. The cube on the right shows the original size of 3D image and the cube on the left shows the selected REV cube..... | 81 |

| | | |
|-------------|--|----|
| Figure 4.13 | Porosity fluctuations within the 3D CT-Scan of Berea Sandstone sample. Arrow indicates the slice which was taken as training image. | 82 |
| Figure 4.14 | Horizontal and vertical TPCF graph from Berea sandstone training image. The graphs of TPCF are align showed that the training image is isotropic. | 83 |
| Figure 4.15 | Berea sandstone Training image on SGEMS user interface. The image was reformatted from JPEG format to SGEMS format..... | 85 |
| Figure 4.16 | Variogram calculated from training image from x and y direction. The variograms are aligned showing that the image is isotropic..... | 85 |
| Figure 4.17 | Sample points extracted from Berea sandstone training image..... | 86 |
| Figure 4.18 | Cross sectional areas ($x = 50$, $y = 50$ and $z = 50$) of a reconstructed 3D porous media from 2D image of Berea sandstone. The structure showed that the complexities of Berea sandstone porous media are well preserved..... | 87 |
| Figure 4.19 | Variogram comparison between training image (2D image) and reconstructed 3D porous media. The variograms are aligned for 2D and 3D showing that the images are isotropic..... | 87 |
| Figure 4.20 | Exterior 3D realization of Berea sandstone by geostatistics. The pores are shown in white and grains in black color. | 88 |
| Figure 4.21 | The REV graphs for porosity on 3D CT-Scan of Sandstone S (8). The cube on the right shows the original size of 3D image and the cube on the left shows the selected REV cube..... | 89 |
| Figure 4.22 | Porosity fluctuations within the 3D CT-Scan Sandstone S (8) sample. Arrow indicates the slice which was taken as training image. | 90 |
| Figure 4.23 | Horizontal and vertical TPCF graph from Sandstone S (8) training image. The graphs of TPCF are aligned showing that the training image is isotropic. | 91 |
| Figure 4.24 | Sandstone S (8) training image on SGEMS user interface. The image was reformatted from JPEG format to SGEMS format..... | 92 |

| | | |
|-------------|---|-----|
| Figure 4.25 | Variogram calculated from x and y direction of training image. The variograms are aligned showing that the image is isotropic..... | 93 |
| Figure 4.26 | Sample points extracted from Sandstone S (8) training image. | 93 |
| Figure 4.27 | Cross sectional areas of a reconstructed 3D porous media from 2D image of Sandstone S (8). The structure showed that the complexities of Sandstone S(8) porous media are well preserved. | 94 |
| Figure 4.28 | Variogram comparison between training image (2D image) and reconstructed 3D porous media. The variograms are aligned for 2D and 3D showing that the images are isotropic..... | 95 |
| Figure 4.29 | Exterior 3D realization of Sandstone S (8) by geostatistics. The pores are shown in white and grains in black color. | 96 |
| Figure 4.30 | The REV graph for porosity on 3D CT-Scan of Fontainebleau sandstone. The cube on the right shows the original size of 3D image and the cube on the left shows the selected REV cube..... | 97 |
| Figure 4.31 | Porosity fluctuations within the 3D CT-Scan Fontainebleau sample. Arrow indicates the slice which was taken as training image. | 98 |
| Figure 4.32 | Horizontal and vertical TPCF graph from Fontainebleau sandstone training image. The graphs of TPCF are aligned showing that the training image is isotropic. | 99 |
| Figure 4.33 | Fontainebleau sanstone training image on SGEMS user interface. The image was reformatted from JPEG format to SGEMS format. | 100 |
| Figure 4.34 | Variogram calculated from x and y direction of training image. The variograms are aligned showing that the image is isotropic..... | 101 |
| Figure 4.35 | Sample points extracted from Fontainebleau sandstone training image..... | 101 |
| Figure 4.36 | Cross sectional areas of a reconstructed 3D porous media from 2D image of Fontainebleau. The structure showed that the complexities of Fontainebleau sandstone porous media are well preserved..... | 102 |

| | | |
|-------------|---|-----|
| Figure 4.37 | Variogram comparison between training image (2D image) and reconstructed 3D porous media. The variograms are aligned for 2D and 3D showing that the images are isotropic..... | 103 |
| Figure 4.38 | Exterior 3D realization of Fontainebleau sandstone by geostatistics. The pores are shown in white and grains in black color..... | 104 |
| Figure 4.39 | Grain size vertical profile in a thin section. The arrow <i>a</i> with the yellow line is the coarse area (porous) and the arrow <i>b</i> with the yellow line is the fine area (tight). | 107 |
| Figure 4.40 | Scale comparison between a core plug and the full length of a thin section of the Berea sandstone. The length of a full thin section image is 4.5 cm. | 109 |
| Figure 4.41 | Image acquisition and stitching processes on full thin section image of Berea sandstone. Nine images were acquired (middle) by using the 12.5 times magnification. The length of the image (right) after the stitching process is 4.5 cm..... | 110 |
| Figure 4.42 | Grain size vertical profile trends on full thin section image of Berea sandstone. The pink trends show the profile before smoothing and the blue trends show the profile after smoothing. | 112 |
| Figure 4.43 | Building blocks for upscaling permeability workflow on a full thin section image of the Berea sandstone. The building blocks and fractions of heterogeneity are shown in the middle and the pore scale permeability estimations on each block of the Berea sandstone thin section are shown on the right..... | 115 |
| Figure 4.44 | Berea sandstone permeability comparison: Estimated permeability of building blocks representative image (blue dots), upscaling permeability workflow (green line and green ellipse) and laboratory data (red line and red ellipse). The y axis is has no unit. | 118 |
| Figure 4.45 | Thin section of sandstone from Well A..... | 120 |
| Figure 4.46 | Image acquisition and stitching processes on a full image of a thin section of sandstone from Well A. Nine images were acquired (middle) | |

| | | |
|-------------|--|-----|
| | by using the 12.5 times magnification. The length of the image (right) after stitching is 2.8 cm. | 121 |
| Figure 4.47 | Grain size vertical profile trends on a full thin section image of sandstone from Well A. The pink trends show the profile before smoothing and the blue trends show the profile after smoothing..... | 122 |
| Figure 4.48 | Building blocks for upscaling permeability workflow on a full thin section image of sandstone from Well A. The building blocks and fractions of heterogeneity are shown on the middle and the pore scale permeability estimations on each block of sandstone from Well A thin section are shown on the right. | 124 |
| Figure 4.49 | Sandstone from Well A permeability comparison: Estimated permeability of building blocks representative image (blue dots), upscaling permeability workflow (green line and green ellipse) and laboratory data (red line and red ellipse). The y axis has no unit..... | 126 |
| Figure 4.50 | Thin section of sandstone from Well B..... | 128 |
| Figure 4.51 | Image acquisition and stitching processes on a full image of thin section of sandstone from Well B. Nine images were acquired (middle) by using the 12.5 times magnification. The length of the image (right) after stitching is 2.8 cm. | 129 |
| Figure 4.52 | Grain size vertical profile trends on a full thin section image of sandstone from Well B. The pink trends show the profile before smoothing and the blue trends show the profile after smoothing..... | 130 |
| Figure 4.53 | Building blocks for upscaling permeability workflow on a full thin section image of sandstone from Well B. The building blocks and fractions of heterogeneity are shown on the middle and the pore scale permeability estimations on each block of sandstone from Well B thin section are shown on the right. | 132 |
| Figure 4.54 | Sandstone from Well B permeability comparison: Estimated permeability of building blocks representative image (blue dots), | |

| | | |
|-------------|--|-----|
| | upscaling permeability workflow (green line and green ellipse) and laboratory data (red line and red ellipse). The y axis has no unit..... | 134 |
| Figure 4.55 | Thin section of sandstone from Well C..... | 136 |
| Figure 4.56 | Image acquisition and stitching processes on a full image of thin section of sandstone from Well C. Nine images were acquired (middle) by using the 12.5 times magnification. The length of the image (right) after stitching processes is 2.8 cm..... | 137 |
| Figure 4.57 | Grain size vertical profile trends on a full thin section image of sandstone from Well C. The pink trends show the profile before smoothing and the blue trends show the profile after smoothing..... | 139 |
| Figure 4.58 | Building blocks for upscaling permeability workflow on a full thin section image of sandstone from Well C. The building blocks and fractions of heterogeneity are shown on the middle and the pore scale permeability estimations on each block of sandstone from Well C thin section are shown on the right. | 141 |
| Figure 4.59 | Sandstone from Well C permeability comparison: Estimated permeability of building blocks representative image (blue dots), upscaling permeability workflow (green line and green ellipse) and laboratory data (red line and red ellipse). The y axis has no unit..... | 143 |

CHAPTER 1

INTRODUCTION

1.1 Introduction

Porosity and permeability are the most important physical properties for reservoir characterization. As opposed to porosity which can be obtained insitu from seismic studies, well testing and logging, spatial distribution of permeability cannot be directly obtained insitu. Currently, up to now, collecting physical core plugs along selected depths of petroleum wells and measuring the permeability of the core plugs in the laboratory is the most reliable way to obtain spatial distribution of permeability [1] [2].

Conducting measurements in a laboratory requires time and resources. Another limitation is that, due to the economics of business, most of the wells (almost 90%) are not cored. Even if the wells are cored, core plug measurements are not carried out along the entire depth of the wells and sometimes leave behind gaps between the measurements. Upscaling is usually carried out to obtain the effective physical properties of the rock formations.

As opposed to core plugs, samples like chips, cuttings and rotary sidewall cores could be sampled along the entire depth of each well [3]. The spacing of sampling for rotary sidewall core covers almost the entire depth of the wells. However, these samples are not easy to be measured as the equipment for measuring need a regularly shaped sample as an input for measurement. Most of these samples were used to make

thin sections for geological evaluation and mineralogy studies [4] [5] and to be stored as sample database.

To be able to extract physical properties such as permeability from chips and cuttings has been a dream of geoscientist. Several studies have revealed that conducting rigorous numerical simulation of physical experiments in a realistic porous media can be used to overcome these problems. This technology can be used as a compliment for laboratory data [6] [7] [8]. Such porous media can be obtained from high-resolution X-ray tomography, also known as Computed Tomography (CT)-scanning. CT-scan produces multiple closely spaced 2D slice images of a rock that, when stacked together, represent the 3D volume [9] [10]. The absolute permeability can be accurately calculated by applying Darcy's law numerical simulation through 3D volume such as Pore Network Modeling (PNM) and Lattice-Boltzmann method (LBM) [11] [12]. However, high-resolution scanning devices are still prohibitively expensive and the scanning time is too long to be practically useful in massive numerical experimentation [9]. Another problem is that the numerical simulation on a large digital sample (i.e. core plug scale) needs a supercomputer or parallel computing of a good workstation to run the simulation [9].

An alternative to reconstruct 3D volume from thin section (2D image) has been discussed by several researchers [13] [14] [15] [16] [17] [18]. The information from a thin section image where the pore space appears in a blue color because it is impregnated with blue dyed epoxy and easily distinguishable from the grains can be used for this purpose. Another reason is that thin sections are relatively easy and cheap to prepare either from core plugs, side wall core plugs or cuttings are often made at the drill site. Thin sections are also stored in a database storage for geological evaluation. Employing geostatistical simulation to reconstruct 3D porous media from 2D image can still be used to correctly simulate connectivity in clastic sediments and the computed permeability through this methodology matched laboratory data [9] [17].

1.2 Problem Statement

Even though many researchers have conducted researches on the reconstruction of 2D to 3D porous media using geostatistical simulation, the accuracy and time of computation still need to be improved especially when running the simulation on a standard personal computer which is portable enough to be used in the field.

Studies showed that the representativeness of the 3D porous media also needs to be improved since the size of the reconstructed porous media through geostatistical simulation is only at millimeter scale. The input samples used to measure permeability in the laboratory are usually conducted at core plug scale (centimeter scale).

The aim of this study is to develop a new workflow to predict permeability at laboratory or core plug scale which can be implemented in real time on a standard personal computer using information from thin section images.

1.3 Objectives

This study focuses on the improvement of computational time to reconstruct 3D porous media from thin section images of clastic sediments on a personal computer. The effect of scale is highlighted in this study. Modification of workflow to solve permeability anisotropy at core plug scale and relate them to laboratory data also highlighted in this study. Thus the objectives of this study are:

1. To develop workflow to reconstruct pore scale 3D porous media from thin section images by using sample points as conditional data. For this study, the geostatistical algorithm used is Sequential Indicator Simulation (SISIM). Workflow to reconstruct 3D porous media is developed by using sample points as new parameter. The purpose of workflow modification is to improve computational time to generate 3D porous media from 2D image on standard personal computer. This method is applied to 2D image from available 3D CT-Scan image. The accuracy of this method is validated by comparing the reconstructed porous media with CT-Scan image.

2. To calculate permeability at pore scale level using fluid flow simulation. Once the 3D porous media is generated, fluid flow simulation is applied. Lattice Boltzmann Method is used to calculate permeability on digital sample by applying physical measurement concept on the simulation. The scale of digital sample in this part is at pore scale level.

3. To improve laboratory scale permeability prediction using upscaling method with combination of fluid flow simulation on 3D porous media generated from 2D image and grain size vertical trends of full thin section image. The prediction of permeability is conducted at laboratory scale using information from full thin section image. Full thin section image has the same scale with laboratory scale (cm scale). The reconstruction of 3D porous media and simulation of fluid flow on large digital sample (i.e. core plug scale) cannot be implemented in real time on standard personal computer. The Upscaling method combine with 2D to 3D porous media reconstruction and fluid flow simulation is chosen as part of workflow. The result is compared with laboratory data to show the accuracy of the workflow.

1.4 Scope of study

The scope of this study comprises the following:

1. Conducting 2D to 3D porous media reconstruction on selected 2D images from 3D CT-Scan samples
2. Validating the 2D to 3D porous media reconstruction method with 3D porous media from experimental CT-Scan
3. Identifying the minimum representative scale range volume of CT-Scan samples using the representative elementary volume (REV) concept
4. Selecting training images for 2D to 3D porous media reconstruction based on the average porosity of each slice within the 3D CT-Scan image
5. Determine the heterogeneity and isotropy of the training image by calculating Two Point Correlations Function (TPCF)

6. Calculate the porosity and variogram from the training images as an input for 2D to 3D porous media reconstruction.
7. Increase computational time by using sample points extracted from training images as conditional data.
8. Measure the physical properties of Berea core plug using poroPerm.
9. Calculate grain size vertical profile from full thin section images
10. Create building blocks for upscaling purposes based on trends from grain size vertical profile
11. Improve permeability predictions at core plug scale using the combination of 2D to 3D porous media reconstruction methods, fluid flow simulation, grain size vertical profile from thin sections and upscaling methods

1.5 Thesis Outline

This thesis consists of five (5) chapters namely Introduction, Literature Review, Methodology, Results and Discussions and Conclusions and Recommendations. A whole range of simulation studies and experimental works have been performed to meet the objectives of this study.

Chapter 1 consists of the background and problem statement of this study. The aim of conducting this research is described in this section. The objectives and scope of study are also stated in this chapter.

Chapter 2 presents a review of literature related to this study. Reference is also drawn from many studies on permeability prediction method. Previous studies on 2D to 3D porous media reconstruction distress together with the benefits and non benefits of each method are also described in this chapter.

Chapter 3 describes the workflow of research methodology in this study. The list of 3D image CT-Scan samples and thin sections used in this study are also presented with detailed steps of simulation studies conducted in this research. This section also highlighted the thin sections, measurement and upscaling procedure.

Chapter 4 is divided into three main parts which are results of preliminary study on size and resolution, simulation study and application of upscaling permeability workflow to sandstone thin section (Berea core plug and Malay basin). The first part shows the impact of image size and resolution for fluid flow simulation. The second part presents results and validation of the 2D to 3D porous media reconstruction method. The last part describes in detail the workflow and results of application of upscaling permeability pore to core plug scale. Detailed discussions on the results are also given.

Chapter 5 presents the conclusions of this study based on the results, discussions made and recommendations for future study.

CHAPTER 2

LITERATURE REVIEW

2.1 Introduction

The determination of porosity and permeability in a reservoir is most important in oil and gas exploration. Porosity determines the amount of fluid that can be stored in rock, and permeability determines the potential in which fluid will flow through the rock. Permeability is one parameter that is difficult to describe. Unlike porosity, detailed distribution of permeability cannot be remotely mapped since it correlates poorly with the elastic properties of rocks, a parameter that is usually obtained from remote acquisition such as seismic and well log.

There are several empirical methods to predict permeability. One of the more common methods is the Kozeny-Carman relation. This empirical method is based on simple cylindrical pore geometry. These models have been widely applied because they are easy to use and simple to understand [19] [20].

Currently, with the development of technology, numerical fluid flow simulation through porous media has been used to predict permeability. The numerical simulation is derived by applying Darcy's Law Equation. The input for numerical simulation is a digital representation of porous media in three dimensions. These 3D porous media can be obtained using CT-Scan [21] [22] [23].

Viable approaches have been proposed by several researchers to reconstruct the 3D porous media from the readily available 2D images of the rock. Adler [13] used porosity and two-point correlation function (TPCF) which obtain from binary phase from 2D thin section images to reconstruct the structure of the 3D porous media using a truncated Gaussian random function. Oren and Bakke [18] developed a process which reconstructs the porous media by modeling the geological process based on the information extracted from 2D images. Okabe and Blunt [24] used high order statistics to reconstruct a structure of porous media from 2D images. A sequential indicator simulation (Geostatistics) was used by Keehm et.al [9] [17] to reconstruct the structure of the 3D porous media.

2.2 Porosity

Porosity can be determined as the storage capacity or the total rock volume that can be filled with oil, gas, water or a mixture of these fluids. The total porosity (ϕ) is defined as the fraction of bulk volume of the reservoir rock that is occupied by pore space. This can be expressed in mathematical form as [25]:

$$\phi = \frac{V_b - V_{gr}}{V_b} = \frac{V_p}{V_b} \quad (2.1)$$

where ϕ is porosity (fraction), V_b is bulk volume of the reservoir rock, V_{gr} is grain volume and V_p is pore volume.

For example in the case of a simple cubic centred packing below (Figure 2.1 a), V_b can be calculated from L^3 (L is the length of the cube) and V_{gr} , can be calculated from the number of packing inside the cube times volume of the packing which is shown in the equation below:

$$V_{gr} = (L/d_{sphere})^3 \left(\frac{4}{3} \pi r^3 \right) \quad (2.2)$$

if r is equal to $\frac{1}{2} d_{sphere}$,

$$V_{gr} = (L/d_{sphere})^3 (\pi d_{sphere}^3 / 6) \quad (2.3)$$

where $(L/d_{\text{sphere}})^3$ is the number of packing inside the cube and $(\pi d_{\text{sphere}}^3/6)$ is volume of the packing. From this information, Equation 2.1 becomes:

$$\phi = \frac{L^3 - (L/d_{\text{sphere}})^3 (\pi d_{\text{sphere}}^3/6)}{L^3} \quad (2.4)$$

The final result from this equation is equal to $1 - (\pi/6) = 0.4764$ or 47.6 %. In the context of 2D image, the calculation of porosity can be defined by using stereological concept which was introduced by Underwood (1970). Stereological concepts show that in a homogenous and isotropy medium the 2D area fraction is identical to the 3D volume fraction of that constituent [25]. The homogeneity is related to the sizes which are representative of that part of the pore system (Figure 2.1 b). The rock can be considered to be isotropic when image features are independent of orientation. This consideration can be identified from 2D image using the Two Point Correlation Functions (TPCF) method by applying Fourier Transform [28] [29].

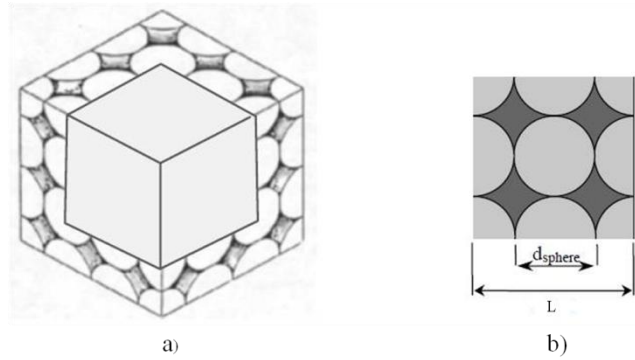


Figure 2.1 a) Volume of simple cubic centred packing. b) Area or 2D image selected from simple cubic centred packing [26].

2.3 Permeability

Permeability is defined as the ability of rock to allow fluids to flow through interconnected pores. Henry Darcy developed a fluid flow equation that is used as standard mathematical tools to determine permeability. This equation which is expressed in differential form is as follows [25]:

$$Q = \frac{KA_{tube}(p_i - p_o)}{\mu L} \quad (2.5)$$

where Q is the flow rate, K is the permeability of the porous rock, A_{tube} is the cross sectional area of the tube, μ is the viscosity of the fluid, L is the length or the rock sample and $p_i - p_o$ is pressure gradient in the direction of the flow. Figure 2.2 shows the illustration of Darcy's Law.

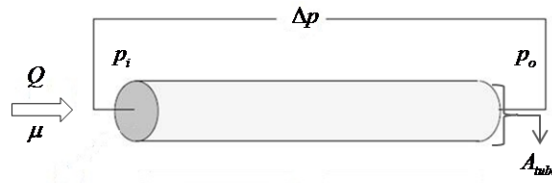


Figure 2.2 Illustration of Darcy's Law.

Figure 2.2 illustrates Darcy's Law on a tube. It shows the proportionality that exists between the fluid flow rate and the applied pressure drop in a unidirectional flow. The derivation of Darcy's Law is derived based on this linear relationship.

2.4 Kozeny-Carman Relation and Permeability Prediction

Permeability is perhaps one of the most important yet elusive reservoir properties, since it correlates poorly with the elastic properties of rock. As a result, permeability cannot be mapped remotely. Since the permeability of rocks is difficult to measure or simulate, empirical relations are often used to estimate permeability through other pore structure parameters that can be measured more easily. The Kozeny and Carman Relation provides a good empirical relation between fluid permeability and other measurable properties of porous media. The Kozeny-Carman Relation is based on simple cylindrical pore geometry [27].

Mavko and Nur [19] [27] stated these models have been widely used because they are easy to use and simple to understand. However, these models are only valid for certain conditions, in this case, fluid-flow in rocks. Furthermore, parameters from these models are difficult to relate in detail to rocks in the field.

The Kozeny-Carman Relation was applied for low porosity and low permeability granites by Walsh and Brace [20]. The permeability was related to several parameters such as porosity, geometrical factor, formation factor and specific surface area. These kinds of relationships provide a way of relating the permeability of a porous media to other rock parameters, such as porosity, specific surface area, tortuosity and grain size. There is however, it is not easy to measure the parameters from samples or thin sections. Porosity is the only parameter that is easy to measure, whilst specific surface area is very difficult to measure accurately from thin sections.

Another study by Berryman [28] suggested a relationship for estimating the specific surface area from spatial correlation functions of thin section images. Blair et al. [29] combined the formulae by Walsh and Brace and Berryman. The porosity and the specific surface area were calculated from thin section using Berryman's formula, and then permeability was estimated using the relationship by Walsh and Brace [20]. Estimation of the permeability using this method matched well with data from the laboratory. There are however, some difficulties when this method is applied on thin section images. The calculation of the specific surface area from images is sensitive to the resolution of thin section images.

The estimation of permeability has a relatively large error when the resolution of thin section image changes. Though the porosity and the specific surface area may be estimated from thin sections, the formation factor and the geometrical factor in the formula are not directly measurable from thin sections. Empirical estimates or laboratory measurements are required for these parameters.

Schaap [30] used the Kozeny-Carman Relation to estimate the permeability of soil. A Scanning Electron Microscopy (SEM) image with 50 times magnifications was used. The specific surface area and porosities of the SEM image was derived using the Berryman Formula. The results indicated that after developing the model

using microscopic information, only macroscopic data are necessary to predict the permeability of soils in a semi-physical manner with the Kozeny-Carman Relation.

Torabi [31] modified the Kozeny-Carman Relation to estimate the permeability of deformation bands. Permeability was calculated based on information obtained from image processing. Torabi devised a means to estimate the porosity and permeability on a micro scale and mapped out the variations along and across deformation bands and similar structures. In so doing, the anisotropy of physical properties in deformed band was shown.

Fauzi [32] applied combination of the Kozeny-Carman Relation and renormalization group to estimate the permeability anisotropy of a rock. The Specific surface area and local porosity was estimated from two point correlation functions calculated from thin section images and the permeability was estimated using the Kozeny-Carman Relation. The permeability estimation tended to conform to the laboratory measurement as the renormalization step increased.

Dvorkin [33] revised an alternative form for the Kozeny-Carman equation from several rocks. These forms have an advantage over the traditional one in which the grain size and tortuosity parameters remain constant. Dvorkin stated that empirical solution cannot replace measurement but can be used to mimic some experimental trends which can be used as a quality control tool for physical and digital experimentation.

Previous studies have indicated that applying the Kozeny-Carman Relation to predict permeability from thin section images might be easy to be applied. This empirical approach can be used as a quality control tool once all parameters are obtained. However, there may be some problems if the image resolution is changing. The changes of resolution give large errors on the determination of permeability. Some of parameters also need to be obtained from measurement, which means this method cannot be used directly from thin section image [17].

2.5 Fluid Flow Simulator

There are several permeability simulation derived from Darcy's equation. In this study the discussion on permeability simulation only focused on two main numerical simulations, namely, Pore Network Modeling (PNM) and Lattice Boltzmann Method (LBM).

2.5.1 Fluid Flow Simulator using Pore Network Modeling (PNM)

Network Modeling is a method to simulate fluid flow which simplifies the pore spaces into pores and connecting bonds. The simplification gives a possibility to simulate fluid flow in simple form for large networks. The use of network models to study fluid flow was first introduced by Fatt [34]. The models were based on interconnected network within a porous media. The initial work was conducted on two-dimensional and did not represent the real porous media. However, it is still the basis of the current use of networks for the prediction of transport properties.

Chatzis and Dullien [35] modified Fatt's models. They used a 3D model that consisted of sites which are connected to each other by bonds. Fatt's initial network assumed that the bond intersections do not possess any volume of their own. The basis of these network models is that the void space of a porous medium can be represented by a graph of connected sites. The sites correspond to pore bodies while the interconnecting bonds are analogous to pore throats connecting the pore bodies. They compared models to laboratory data from sandstones and noted that regular networks combined with circular capillaries did not yield a realistic description of real sandstones.

Bryant et al. [36] [37] used network models which were derived from a real porous media. The spatial coordinates of every sphere were measured thereby, enabling the microstructure of the medium to be completely determined; a network model which replicates the pore space was then extracted. Transport properties were then predicted from network models which were successfully compared with experimental values measured on real porous media. However, the permeability was

over predicted by a factor of two [38]. It is unlikely that most porous media will comprise equal-sized grains resulting in a constant coordination number, as such the application of the method used for network extraction by Bryant et.al [36] [37] [38] to more complex porous media is limited.

A common method of extracting networks from microstructures involves defining the skeleton of the pore space as a set of points (voxels) at equal distances from two or more points of the solid grain [13]. This skeleton may be regarded as the centre line of the pore network; this line contains points where two or more lines meet. These points are the network nodes which are connected to other nodes through the pore throats.

Lindquist et.al [39] [40] [41] extended a thinning algorithm in which the pore space is eroded until only the centrelines remain in order to analyze geometric properties such as connectivity and tortuosity of skeletons generated from various micro-CT imaged rock samples.

Silin et.al [42] [43] [44] [45] introduced the maximal ball method to extract pore network from 3D images. The maximal ball method is a network model from 3D images without the need to first extract a skeleton. This method involves finding the largest inscribed spheres (maximal ball) that touch grain surfaces. Maximal balls (MB) are the basic elements used to define the pore space and detect the geometrical changes and connectivity. A maximal ball is defined as a set of voxels assembling the largest sphere, as such, a maximal ball must touch the grain surface and it cannot be a subset of any other maximal ball. Every maximal ball possesses at least one voxels that is not contained in any other maximal ball; the aggregate of all maximal balls defines the void space in a rock image.

From previous studies it can be concluded that network modelling is one widely used technique to predict physical properties. The benefit of this method is a reasonable amount of pore geometry information that can be incorporated since it simplifies the pore space into pores and connecting bonds. With this assumption the flow simulation is simple enough for very large networks. However, this method has its limitation since the approach of this method is dividing the pore structure into

discrete pores and throats. Sometimes this approach arbitrarily alters the real pore structure. This method can be precise if the resolution of the 3D image is in very good resolution. However, for 3D images that are stochastically simulated from thin sections which have quite complex geometry and may contain statistical noise, this approach cannot handle this complexity [54] [58] [51] [17].

2.5.2 Fluid Flow Simulator using The Lattice Boltzmann Method (LBM)

The Lattice Boltzmann Method (LBM) is a class of computational fluid dynamics methods for fluid flow. This method describes fluid motion as collisions of particle model which illustrates the physics at microscopic scale and averaged properties of the particle model to satisfy the Navier-Stokes equations.

LBM first originated from Lattice Gas Automata (LGA) and was proposed by Hardy et.al. Hardy et.al [46] used this to study transport properties of fluids through discrete particles in a square lattice. The particles capture the essential physics and are distributed on discrete points and averaged properties on a square lattice and reproduced macroscopic properties.

Frisch et.al [47] used the LGA method on a hexagonal lattice. The results showed the model was very close to solutions of the incompressible Navier-Stokes equation. McNamara and Zanetti [48] proposed the use of the Boltzmann equation to simulate LGA. The results showed LBM simulated the macroscopic equations more efficiently than LGA. Rothman [49] used the LGA to simulate fluid flow through simple and complicated geometries and compared the result with Darcy's Law. Succi et.al [50] used the LBM to calculate permeability in a 3D random medium and showed good agreement with the laboratory data. Many studies have successfully applied the LBM to a wide range of fluid phenomena such as single-phase flow [51] [17] and two-phase flow [49] [52].

Keehm et.al [17] verified the implementation of LBM on a simple cylindrical tube model. The permeability was simulated on three different cylindrical tube models

with different diameters. Figure 2.3 shows the three cylindrical tube models used by Keehm et.al.

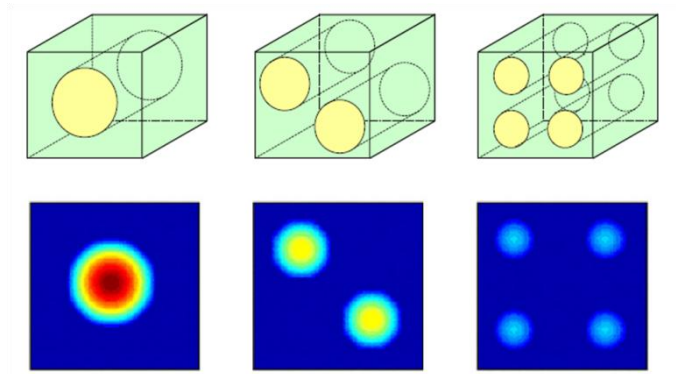


Figure 2.3 Three cylindrical tube models with different diameters used by Keehm et.al to compare permeability simulation on LBM with theoretical prediction [17]. The lower images show the local flux from each cylindrical tube model.

The simulated permeability showed excellent agreement with the theoretical prediction. Figure 2.4 shows the simulated permeability using LBM simulation (dots) and predicted permeability from theoretical theory.

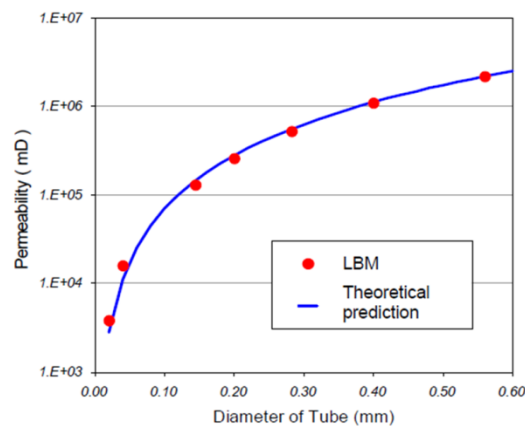


Figure 2.4 Red dots show results of permeability simulation using LBM. Permeability from theoretical theory is shown on blue solid line [17].

Several researches mentioned that the biggest advantage of the LBM is that it is readily applied to any arbitrary discrete geometry [53] [54] [55] [56]. LBM describes fluid motion as collisions of imaginary particles that are larger than the real fluid molecules but show almost the same flow behaviour at the macroscopic scale. While other methods for example, pore network modelling discretize either the geometry or the governing equations. LBM solves and recovers the governing Navier-Stokes equations from the collision rules between the particles that move on a lattice. The algorithm is easy and simple to implement. LBM can handle complicated pore geometry without simplifications or modifications [57] [58]. The LBM is a strong contender for the best fluids simulation approach currently available [59] [60].

2.6 Method of Generating 3D Porous Media of Rock

Numerical fluid flow simulation through porous media can be used to predict permeability [6] [7] [8]. The input for this numerical simulation is an accurate 3D representation of the rock microstructure. Without this permeability cannot be accurately predicted. The most common method to achieve this 3D porous media is by using one of the following two methods: (1) X-Ray Computed Tomography (CT-Scan), (2) 3D porous media reconstructed from 2D image.

2.6.1 X-Ray Computed Tomography (CT-Scan)

X-ray Computed Tomography (CT-Scan) can be used to generate the 3D porous media of reservoir rock. X-ray computed tomography can visualize the internal structure of rocks in three-dimensional visualization by determining the density variations of the rocks. Density variations usually correspond to pores or grains of the rocks. This technology is established and rapidly evolves in the image analysis of a porous media. It was initially developed for use in the field of medicine, but nowadays its use has been extended to a wide variety of fields.

Dunsmuir et.al [21] have developed and extended the usage of CT-Scan to provide 3D images of reservoir rocks with a resolution down to pore scale.

Preliminary studies of fluid flow were performed through 3D images of reservoir rock. Another study demonstrated the usefulness of CT-Scan for two-phase flow in porous media [22]. Other researchers also stated about the derivation of physical properties from the topology of rocks such as conductivity [8]. It is believed many other physical properties can be derived from topology of rocks such as permeability, conductivity and elastic properties [23] [61].

The interest in carbonate reservoirs has made several researchers apply this method to carbonate samples. High resolution X-ray tomography was used by Arns et.al [62] to image a carbonate core plug from a vuggy reservoir in high resolution. Pore scale morphology and petrophysical properties were derived directly on the highest resolution digitized tomographic images and the computed permeability was in agreement with the experimental values.

Dong et.al [45] imaged rock cuttings of poorly consolidated sandstone and vuggy carbonate using high resolution X-ray tomography and validated the extracted topologically equivalent networks through comparisons with networks derived by a different method.

Riepe et.al [63] [64] applied a combination of high resolution X-ray tomography and Pore Network Modeling technology to unconventional reservoirs, namely, a tight gas reservoir in Oman and a fracture based reservoir in Vietnam. The computed static and dynamic petrophysical properties were simulated from 3D images and showed good agreement with the laboratory data. It is believed that this technology can be used as an alternative approach as a development concept for these types of reservoirs.

There are several companies working on imaging through CT-Scan and developing simulation for petrophysical properties through 3D images of rocks. Digital Core (Australia), Ingrain (U.S.) and Numerical Rock AS (Norway) are some of the companies working on this area. Figure 2.5 showed 3D image from Ingrain.

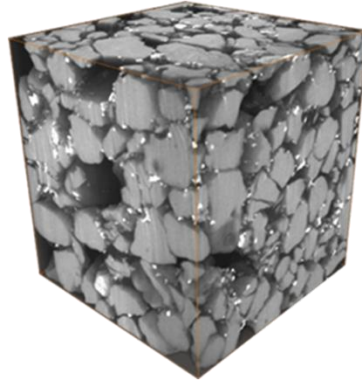


Figure 2.5 The 3D rendering of raw CT-Scan cubic image of rock (Courtesy of Ingrain). The image shows that CT-Scan captured the details of the rock.

Though the imaging technique of using X-ray tomography (high resolution) is a direct methodology to obtain 3D porous media structures at high resolution, it is still a very expensive and time-consuming task. Conducting such a test on a fragment of rock will take around 4-5 hours depending on the size of rock and resolution. Segmentation and the simulation processes of petrophysical properties is another problem which can only be run using a supercomputer or parallel computing of a very powerful workstation.

2.6.2 3D Porous Media Reconstruction using 2D Image

The 2D image of a thin section, in contrast to the 3D image, is often readily available. Thin sections are often taken from formations and imaged for geological evaluation such as for mineralogy study and sorting purposes. In the past, such 2D images have formed the basis for the reconstruction technique to generate 3D pore structure.

Adler et.al [13] used the unconditional truncated Gaussian method to generate a 3D image of pore structure. Porosity and two point correlation functions were used as an input. However, the use of the truncated Gaussian method for the correlation of the 2D image is not always appropriate. Hilfer and Manwart [65] investigated the results from Adler et.al and calculated the local percolation probabilities. Results showed that

the reconstructed 3D pore structure has lower connectivity than the original 3D image from X-ray tomography. It means that connectivity cannot be properly reproduced.

Several researchers proposed a hybrid method that combines the truncated Gaussian method and simulated annealing to reduce the computation time [4] [14] [15]. As studied by Manwart et.al [66], this method still does not improve the connectivity of the reconstructed 3D porous media.

Okabe and Blunt [24] used a more sophisticated statistical technique. Multiple point statistics (MPS) was used to reconstruct the 3D porous media of a rock. This methodology was applied to sandstone and carbonate samples. The application of multiple point statistics to reconstruct 3D images using 2D image data has successfully been used to reconstruct the connectivity of sandstone and carbonate samples. The results showed through comparison between the original and the 3D X-ray tomography image. However, applying such statistical properties to capture important features of a porous media and then generate 3D pore structure still needs an excessive amount of computational time. A reconstruction of a 128 voxel cube using a 512 square pixels size training image took around 10 hours CPU time using an Intel Xeon 1.7GHz computer with 1GB memory.

Zhang et.al [67] modified the work of Okabe and Blunt by using sample points extracted from a training image as conditional data. Using MPS and sample points, each 2D newly reconstructed image is taken as a new training image to generate the next layer and at the end all the 2D images are successively stacked to reconstruct a 3D structure. However, this method is still not practical and easily repeatable. Implementing this method on a 2G Athlon CPU processor with 2GB memory needed 4779 seconds computational time for one realization of a 3D porous media.

Keehm et.al [17] showed that porosity and two point correlation functions can still be used to correctly simulate connectivity and permeability in clastic sediments if a sequential indicator simulator (SISIM) is used [68]. This reconstruction method is commonly used in geostatistics to fill 3D volume with properties known at wells. This method used information of pores and grains extracted from a 2D image and used the same concept to reconstruct the 3D porous media. This method appears to produce the

correct connectivity when compared with 3D X-ray tomography. However, since the 3D porous media reconstructed from this method is only in millimetre scale, this method sometimes failed to predict the anisotropy of permeability at core plug scale [68].

Kameda used the same method and modified the workflow. A combination of 2D to 3D porous media and the Upscaling method was applied. Kameda classified the input for the reconstruction method into three types: porous, patchy and tight, based on the observation on thin section images [9]. Keehm et.al [69] used the same approach. This modified method was applied to compacted bands of sandstone. Permeability measurements on the compacted bands are difficult to obtain since test samples of the compaction bands are not easily available and the material is poorly consolidated. By applying the appropriate volume fraction and building blocks this modification can compute correctly the permeability and is able to estimate the permeability anisotropy at core plug scale. However, to classify into the three types of input, detailed observation of thin section images is needed.

Oren and Bakke [18] chose a different approach. Instead of applying the statistical reconstruction technique, a process based model was used. This method which accounts for the physical processes such as sedimentation, compaction and diagenesis can be extracted from a 2D image. Although this method reproduces local percolation probabilities and predicts permeability accurately, simulating the physical processes requires very intensive calculations and laboratory information such as grain size distribution. Figure 2.6 shows the comparison of pore space using the process based reconstruction method with a CT-Scan of the Fontainebleau sandstone. A comparison of the two images shows that the pore space is correctly simulated.

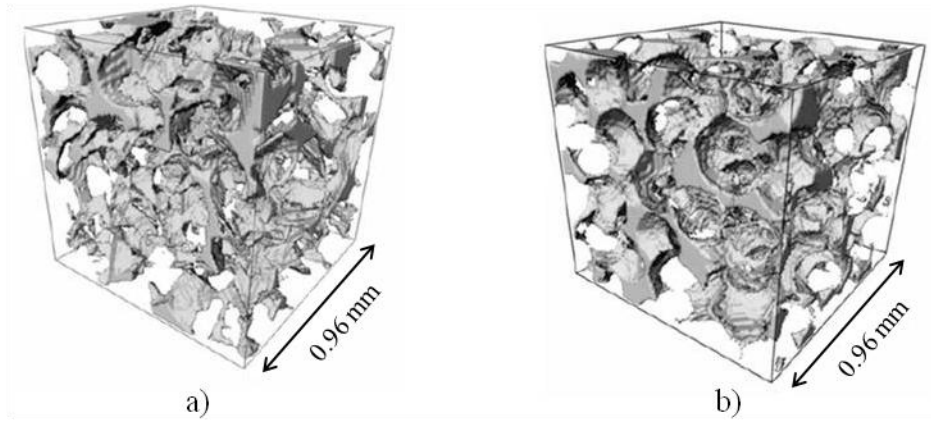


Figure 2.6 (a) Process Based Reconstruction image of the Fontainebleau sandstone as compared with (b) CT-Scan image of the same sandstone [18].

Jin et.al [70] used a similar approach to the process-based reconstruction method. A Physics-based depositional model was used to reconstruct natural sedimentary rock, and generated 3D images of the pore space at an arbitrary resolution.

Amongst the methods discussed for the generation of a 3D porous media of rock microstructure, X-ray tomography (CT-Scan) despite its limitations, is the most promising since it is a direct measurement of the actual microstructure. Process-based reconstructions may be problematic for rocks if their depositional and diagenetic history is complex or unknown. Statistical methods, despite having limitation, still can be used to reconstruct connectivity correctly, at least for a clastic system.

2.7 Summary

There are many literatures on permeability prediction through the depiction of 2D and 3D images of rocks. The Kozeny-Carman relation can be applied to thin section images to predict permeability. Although this method is easy to use the parameter is difficult to obtain and changing the resolution can be a problem and results in errors on the prediction. This method cannot be used directly from thin section images. PNM is a robust fluid flow simulator and can predict the permeability precisely depending on the resolution of the 3D porous media. A combination of the high

resolution 3D porous media and PNM can be very useful and precise even for unconventional reservoirs, such as tight gas and fracture based reservoirs. Although this combination is very useful, it is still a very expensive and time-consuming to obtain high resolution 3D porous media. This approach cannot be applied to 3D images that are stochastically simulated from thin sections which have quite complex geometry and may contain statistical noise. On the other hand, LBM can handle complicated pore geometry without simplifications or modifications. The combination of 2D to 3D porous media reconstruction using SISIM, fluid flow simulation (LBM) and upscaling method can be used to predict permeability at core plug scale in a clastic system.

Table 2.1 Summary of Literature Review.

| Methodology | Advantage | Disadvantage |
|-----------------------------|--|--|
| Kozeny-Carman | <ul style="list-style-type: none">• Easy to implement and gives good correlation between permeability and other parameters | <ul style="list-style-type: none">• Specific surface area sensitive to resolution• Formation factor and geometrical factor from measurement |
| | Input scale for permeability prediction: mm scale | |
| Fluid Flow Simulator | | |
| Pore Network Modeling (PNM) | <ul style="list-style-type: none">• Pore geometry information that can be incorporated for very large networks• Precise estimation if the resolution of 3D image is in very good resolution | <ul style="list-style-type: none">• Arbitrarily alters the real pore structure• Cannot handle complexity of stochastically generated porous media |

| | | |
|--|--|--|
| Lattice Boltzmann Method (LBM) | <ul style="list-style-type: none"> • Shows almost the same flow behaviour at macroscopic scale • No simplification • LBM can handle complex geometry without simplification | <ul style="list-style-type: none"> • Time consuming if implemented on large size digital sample |
| Method of Generating 3D Porous Media of Rock | | |
| CT-Scan | <ul style="list-style-type: none"> • Direct methodology to obtain 3D porous media structures | <ul style="list-style-type: none"> • Take around 4-5 hours depending on the size of rock and resolution • Needs a supercomputer for segmentation and numerical simulation processes |
| | Input scale for reconstruction: mm and cm scale | |
| 2D to 3D: Process Based Reconstruction | <ul style="list-style-type: none"> • Accounts for the physical processes such as sedimentation, compaction and diagenesis which are extracted from 2D images | <ul style="list-style-type: none"> • Requires intensive calculations • Some input from experiment such as grain size study • Problematic for rocks if their depositional and diagenetic history is complex or unknown |
| | Input scale for reconstruction: mm scale | |
| 2D to 3D: Multiple Point Statistics | <ul style="list-style-type: none"> • Applying high order statistics to reconstruct porous media | <ul style="list-style-type: none"> • Need an excessive amount of computational time |
| | Input scale for reconstruction: mm scale | |

| | | |
|--|--|--|
| 2D to 3D: Sequential Indicator Simulation | <ul style="list-style-type: none"> • SIS simulates connectivity and permeability in sandstone | <ul style="list-style-type: none"> • Reconstruction in real time on standard personal computer can only be implemented at mm scale • 3D must statistically represent the measurement scale |
| | Input scale for reconstruction: mm scale | |

CHAPTER 3

METHODOLOGY

3.1 Introduction

The main purpose of this study is to develop a new workflow to predict permeability at laboratory or core plug scale using information from full thin section images which can be implemented in real time on a standard personal computer. Several methods are combined as part of the workflow. The porous media reconstruction method from thin section image, fluid flow simulation and Upscaling method is part of the workflow. The first step in this study is to improve the computational time of 2D to 3D porous media reconstruction. This method is based on work by Keehm [17] [68] [69]. The sample points as conditional data are added as part of the modification to improve the computational time. This method was tested and compared with known samples from 3D CT-Scan image. Details of this method will be discussed in Section 3.2.

The algorithm of 2D to 3D porous media method is tested on thin section images with known values of measured porosity and permeability. The porosity and permeability of the Berea sandstone core plug were measured using Poroperm. The results of the measurement will be used as a benchmark for permeability prediction from full thin section images. Details of the test will be provided in Section 3.3.

Full thin section images are needed as an input for the new workflow to determine permeability at laboratory scale. Full thin section images have a similar scale with core plugs. To obtain this objective, a thin section was made from a vertical cut

through the core plug. The core plug was first saturated with blue dyed epoxy. The core plug was then cut into thin slice to be bonded on to glass slide. The thin slice was then grounded with carborundum on a rotating steel mortar into thin section. This part will be discussed in Section 3.4. Image collection from thin section images will be discussed in detail in Sections 3.4.2 to 3.4.3.

Once a full thin section image is obtained, the grain size vertical profile trends were calculated from image. The trends showed the coarsening and fining parts of a thin section image and solve the heterogeneity at core plug scale. The building blocks were determined based on the trends shown from the grain size vertical profiles. The building blocks were used as a benchmark to upscale permeability from pore to core plug scale. The results from this workflow were compared with data from measurements. A general flow chart of this research is shown in Figure 3.1.

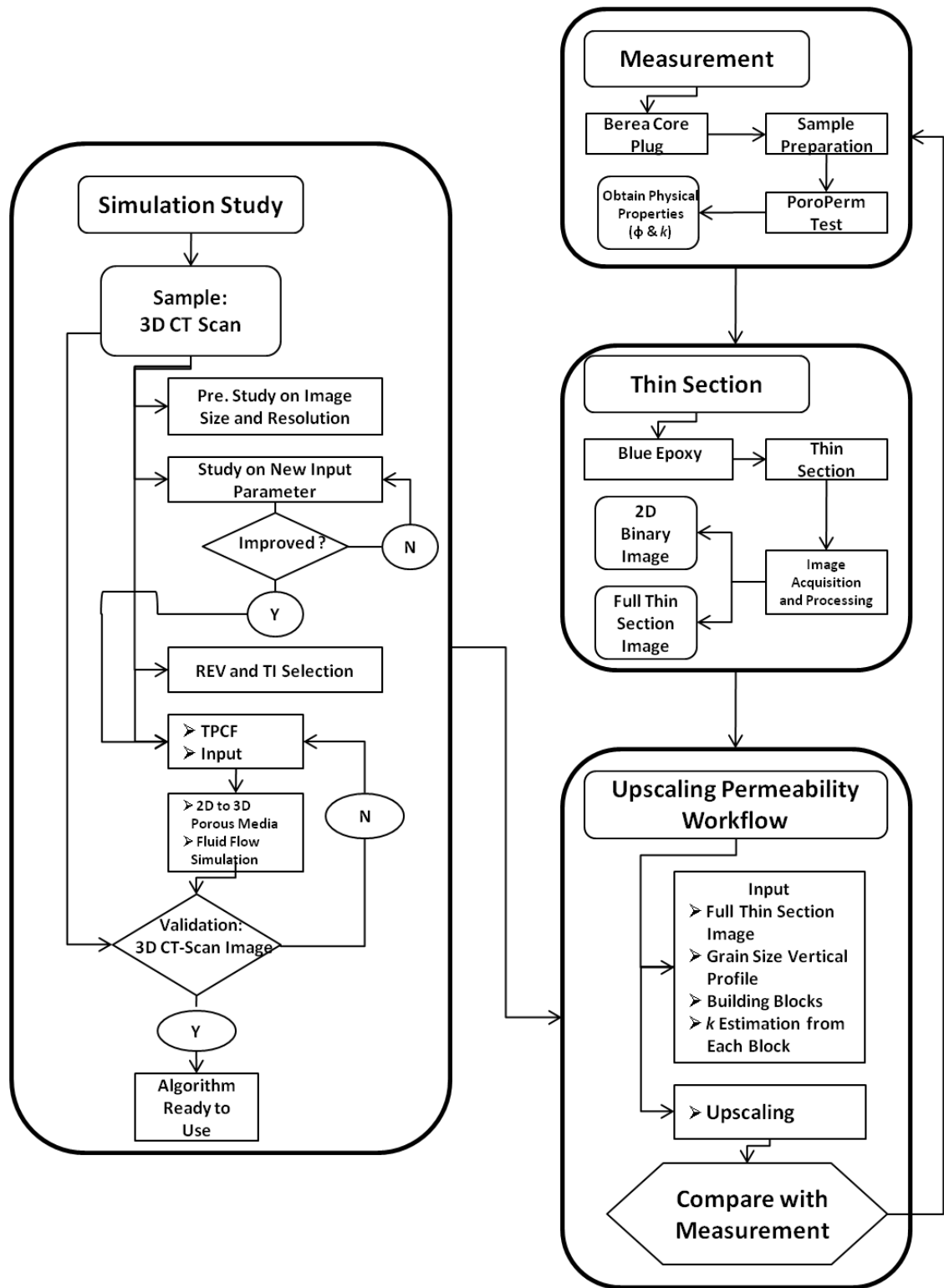


Figure 3.1 Research Flowchart

3.2 Simulation Study

Simulation work in this thesis is part of a number of studies that analyze the steps to reconstruct 3D porous media from a thin section image (2D) and determine the accuracy of this method through comparison with a CT-Scan image. The first study was a preliminary study on image size and resolution to identify the minimum effective size and resolution to conduct fluid flow simulation. The Representative Elementary Volume (REV) concept was used in this study. A training image as an input to reconstruct 3D porous media was selected from a range of REV size of CT-Scan image. The second study was a study on new input parameter to improve 2D to 3D porous reconstruction running time on a standard personal computer. To determine the accuracy of this method, simulation work was conducted on a 2D image cut from a 3D CT-Scan image.

The microstructure geometry of the rock was determined using Two Point Correlation Functions (TPCF). The porosity and variogram were calculated from a training image and used for input parameters. Sample points were added as new input parameter. This modification reduces the computational time to reconstruct the porous media. Sequential Indicator Simulation (SISIM) from Geostatistical Algorithm was used to reconstruct 3D porous media based on input parameters. Once the porous media is generated, fluid flow is simulated using the Lattice Boltzmann Method (LBM). The accuracy of this method is shown by comparing fluid flow simulation from reconstructed porous media with CT-Scan. All simulation studies were run on a personal computer Intel (R) Xeon CPU 2.67 GHz with 8 GB of RAM. Figure 3.2 shows the detailed flow chart of the simulation work.

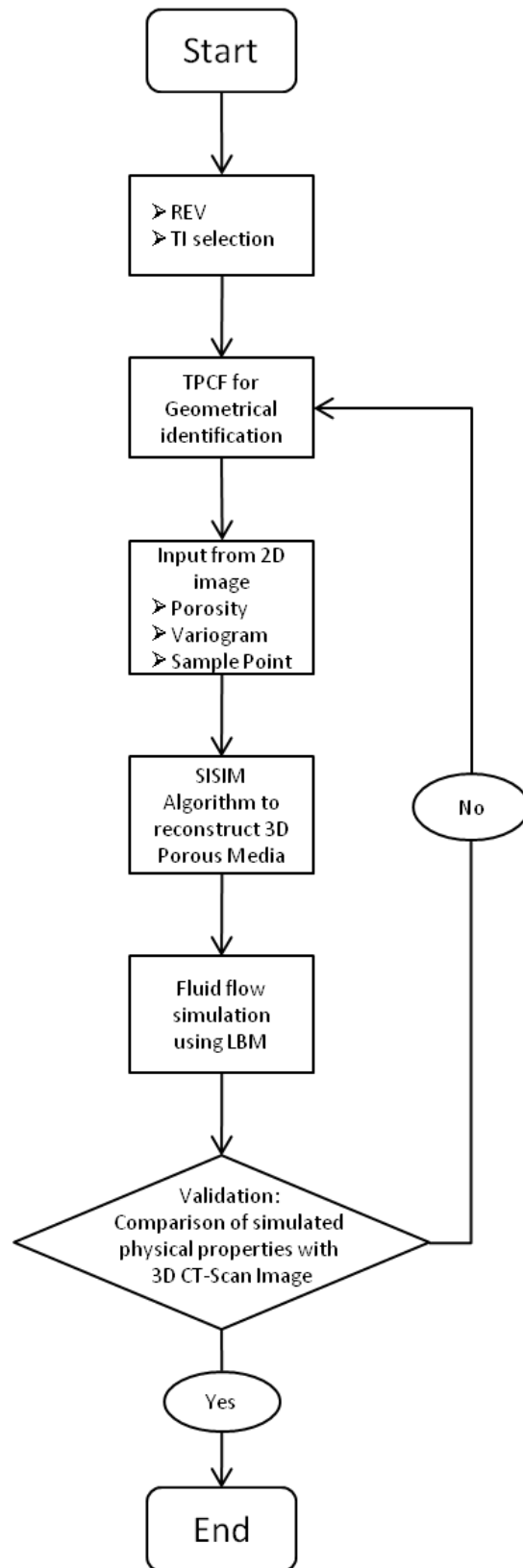


Figure 3.2 Detailed flow chart of simulation work

3.2.1 Samples: 3D CT-Scan Image for Simulation Study

3D porous media reconstructed from a 2D image was tested on sandstone samples. 3D CT-Scan images of sandstone were used as the experimental data, which can provide reference data to evaluate the simulated results through comparison. Parts of the CT-Scan images were used as an input for training image to reconstruct 3D from 2D images. The size ranges of the CT-Scan images are 400, 300 and 144 voxels (400 voxels equal to $400 \times 400 \times 400$ pixels) with a resolution of 4 to $15 \mu\text{m}$ per pixel. All CT-Scan image data used in this study were taken from the Imperial College London CT-Scan image library website. The image for the Fontainebleau Sandstone was from the Stanford University CT-Scan image library. Three of the six 3D CT-Scan image samples used in this study are shown below:

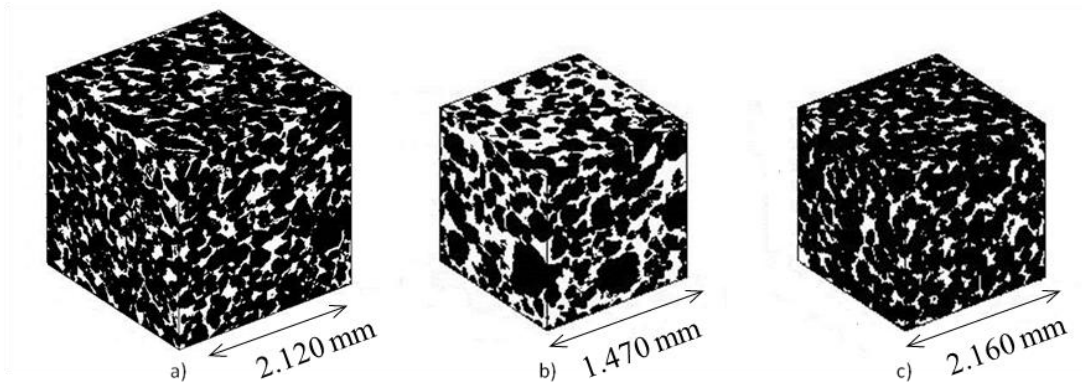


Figure 3.3 The 3D CT-Scan images for simulation study a) Berea sandstone, b) Sandstone (S8), c) Fontainebleau sandstone.

3.2.2 Preliminary Study on Image Size and Resolution for Fluid Flow Simulation

The 3D cube image of the porous media is an input for fluid flow simulation. This image can be generated using CT-scanning experiment or 2D to 3D porous media reconstruction method. For CT-scanning, the size and resolution of the image acquired depend on the topology of the rock.

The end product of the simulation study is to produce a robust workflow to reconstruct 3D porous media from 2D images. To validate the result, a 2D image is cut from part of the 3D CT-Scan image. Permeability estimation will be compared on both images to show the accuracy of the reconstruction method.

Based on previous study [9], 100 square pixels is the maximum input size to reconstruct 3D porous media in real time on a standard personal computer. Since the six 3D CT-Scan image samples used in this study have various sizes (400 to 144 voxels) and resolutions (4 to 15 μm per pixel), image size and resolution tests need to be conducted. Figure 3.4 shows the work flow to conduct the image size and resolution test. For example a 3D CT-Scan image of the Berea sandstone has a size of 400 voxels. This size will be reduced to 200 and 100 voxels, and the porosity and permeability of each image will be calculated and the fraction will be compared to the original size of 400 voxels. The results will show if there is any effect of resolution for fluid flow simulation.

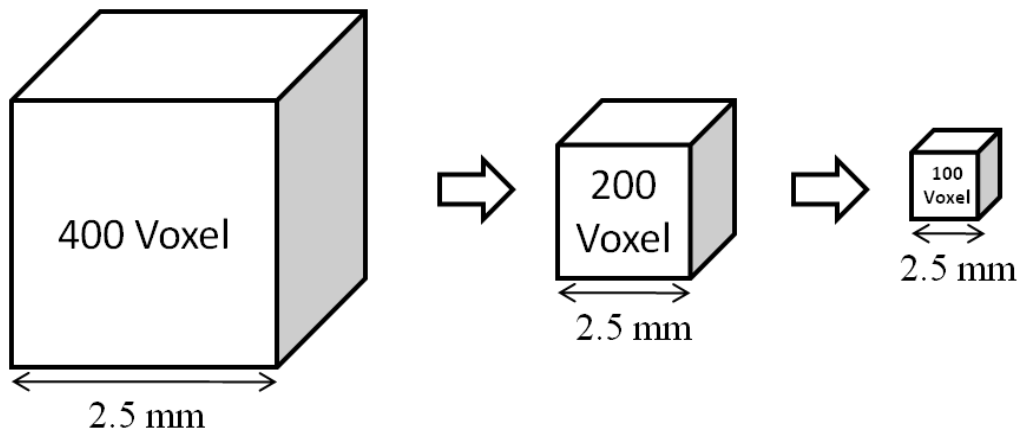


Figure 3.4 Workflow for fluid flow simulation test on different sizes and resolutions on the same sample.

3.2.3 Study on Sample Points as New Input Parameter for 2D to 3D Porous Media Reconstruction Method

The method of generating 3D porous medias from 2D image using SISIM algorithm (geostatistics) was initially introduced by Keehm [17]. Several researchers stated that this method shows high accuracy in the reconstruction of connectivity of porous media in a clastic system. The input is porosity and variogram calculated from a 2D image. PC clones and parallel computing is mentioned in Keehm's previous work.

In order to improve the running time, new input parameter is needed. Sample points as conditional data are added as new input parameter. Sample point terms were introduced by Zhang [67] and used to reconstruct porous media using Multiple Point Statistics (MPS) method. Using this parameter improved the running time to reconstruct porous media as compared to the Okabe and Blunt method [24]. However, the reconstruction method using this algorithm is still tedious and not in real time on a standard personal computer.

SISIM algorithm can still be used, since we are dealing with sandstone samples. Sample points extracted from a training image (2D image) are adopted and used as conditional data for the reconstruction. Table 3.1 shows the comparison between the method proposed by the author with Keehm's method.

Table 3.1 Comparison between the proposed method and Keehm (2003).

| | Comparison | |
|---------------------|--|---|
| | Proposed Method | Keehm (2003) |
| Input Parameter | <ul style="list-style-type: none"> ➤ Porosity ➤ Variogram ➤ Sample Points | <ul style="list-style-type: none"> ➤ Porosity ➤ Variogram |
| Algorithm | SISIM from SGEMS | SISIM from GSLIB |
| Reconstructed Scale | mm scale | mm scale |

| | | |
|----------------------|---------------------|--------|
| Visualization | ➤ Matlab ➤ SGEMS | Matlab |
| Fluid Flow Simulator | LBM | LBM |

3.2.4 Representative Elementary Volume (REV)

Measurement scales in the petroleum industry have a large span from seismic, to log, to laboratory core sample and finally to CT-Scanned micro scale [71] [72]. In order to deal with such a large range of scale, geoscientists usually refer to a representative elementary volume (REV). The REV is defined as the smallest volume over which a measurement can be made that will yield a value representative of the whole. In other words, the properties obtained at a scale smaller than the REV fluctuate considerably, while at a scale larger than the REV these fluctuations are significantly less [4] [45] [71] [73].

In this study, the REV concept was used to define the smallest size ranges that represent the whole size of 3D CT-Scan image. The limited size to reconstruct 3D porous media through a standard personal computer (PC) is around 10^6 nodes (100 voxels) [9]. The input ranges from samples are 400, 300 and 144 square pixels. Directly squeezing the size of images to 100 square pixels will affect information loss of the images as the resolution of the images are decreasing [17] [71] [74]. In this research, the REV for porosity is calculated based on the definition by Bear as [73]:

$$n_i = \frac{(\Delta U_v)_i}{\Delta U_i} \quad (3.1)$$

where n_i is the porosity of sub-volume i and $(\Delta U_v)_i$ is the volume of the void space in the volume ΔU_i .

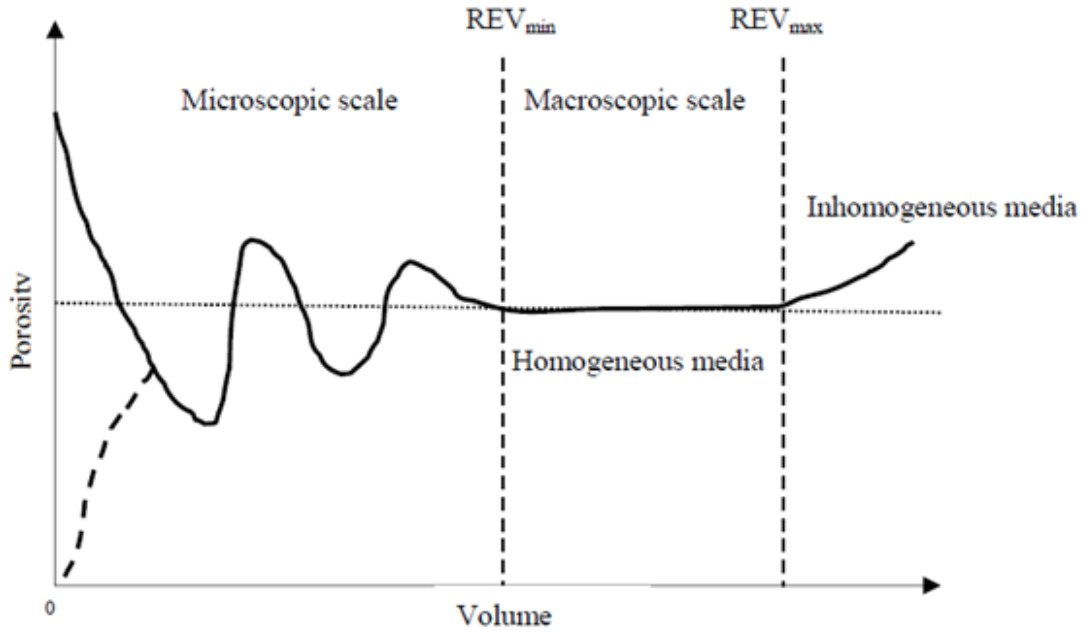


Figure 3.5 Schematic graph of how a measured property (porosity) varies with sample volume and the domain of the REV [73].

Figure 3.5 illustrates the concept of REV for porosity. The REV ranges from a minimum limit, which is the transition from the microscopic to the macroscopic level, to a maximum limit, which is the transition from homogenous to heterogeneous state. REV analysis is performed to ensure that the sample of concern is homogenous and therefore representative.

3.2.5 Selection of Training Image (TI)

Once the REV is confirmed, a training image to reconstruct 3D from 2D image was taken from REV scale ranges of 3D CT-Scan image, which also used as reference data to validate the reconstructed results. The 3D CT-scan image is a set of closely spaced consecutive 2D slices. These slices can be analogous as thin sections from core-plug or drill cuttings [9] [24] [67].

In order to reconstruct a 3D structure effectively from a 2D cut, a representative 2D image should be selected especially in terms of porosity [24] [67].

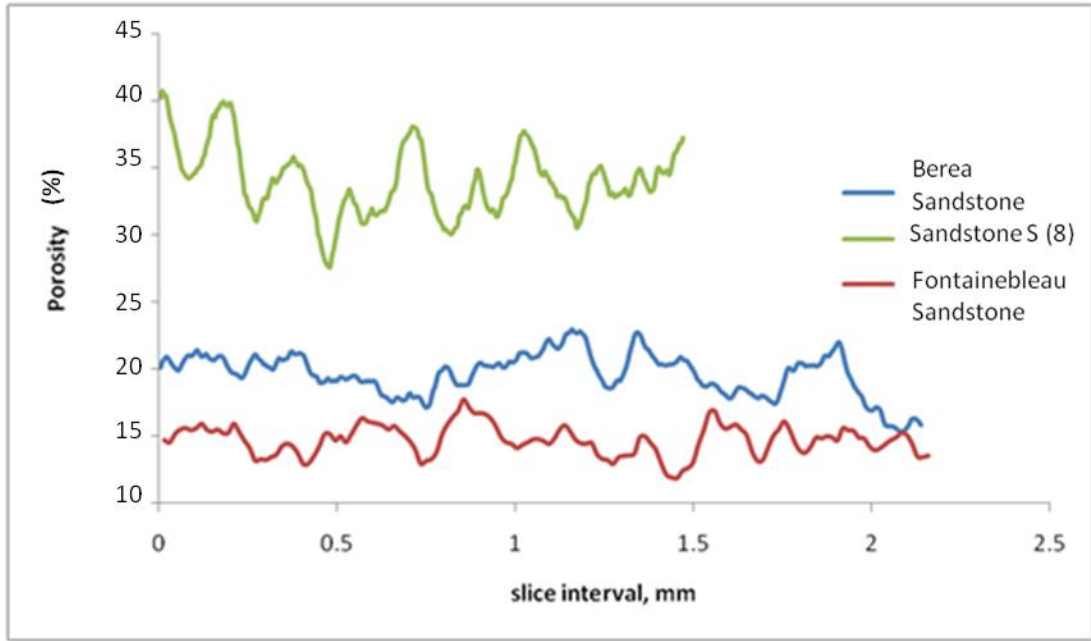


Figure 3.6 Porosity Fluctuations within 3D CT-Scan Image Samples.

Figure 3.6 shows porosities calculated from 2D slices of three 3D CT-Scan samples. For example, for Berea sandstone, the 3D has a size of 400 voxels with a resolution 5.3 μm . It means that the 3D images contain 400 stacking images with a real length 2.120 mm. For Berea sandstone, the fluctuations show different porosity values from 400 slices of the 2D image.

3.2.6 Two Point Correlation Functions (TPCF)

There are two assumptions to reconstruct 3D porous media from 2D image [17] [24] [67]. The training image (2D image) should be homogenous and isotropic. Two point correlation functions (TPCF) can be used to characterize the spatial arrangement and heterogeneity of micro structural rock geometry [28]. Conducted TPCF calculation on

images of rock can be used to determine whether the images are homogenous, isotropic or not.

Rocks are usually composed of at least two phases; pores and grains. The physical properties of rocks (i.e. porosity and permeability) depend on the properties, amount and spatial distribution of each phase. Two point correlation functions is the possibility of finding the two end points of a segment with a certain length in the same phase, pore or grain. These functions can be defined by the statistical average of the spatial arrangement, denoted by $\langle \cdot \rangle$,

$$A(\mathbf{h}) = \langle f(r)f(r + \mathbf{h}) \rangle \quad (3.2)$$

A 2D image contains of row and column of matrices pixels. Each pixel has its own value. From equation 3.2, \mathbf{h} can be identified as lag vector between two data points (pixels). Two point correlation functions contain statistical information about the arrangement of the constituents in a composite material by measuring the probability of certain simple geometrical arrangements of the constituents. The two point correlation functions can be easily obtained using Fourier transforms [28] [29],

$$A(\mathbf{h}) = F^{-1}\{F\{f(r)\} \times F^*\{f(r)\}\} \quad (3.3)$$

where $F\{.\}$, $F^{-1}\{.\}$ denotes Fourier and inverse Fourier transforms and $*$ denotes the complex conjugate.

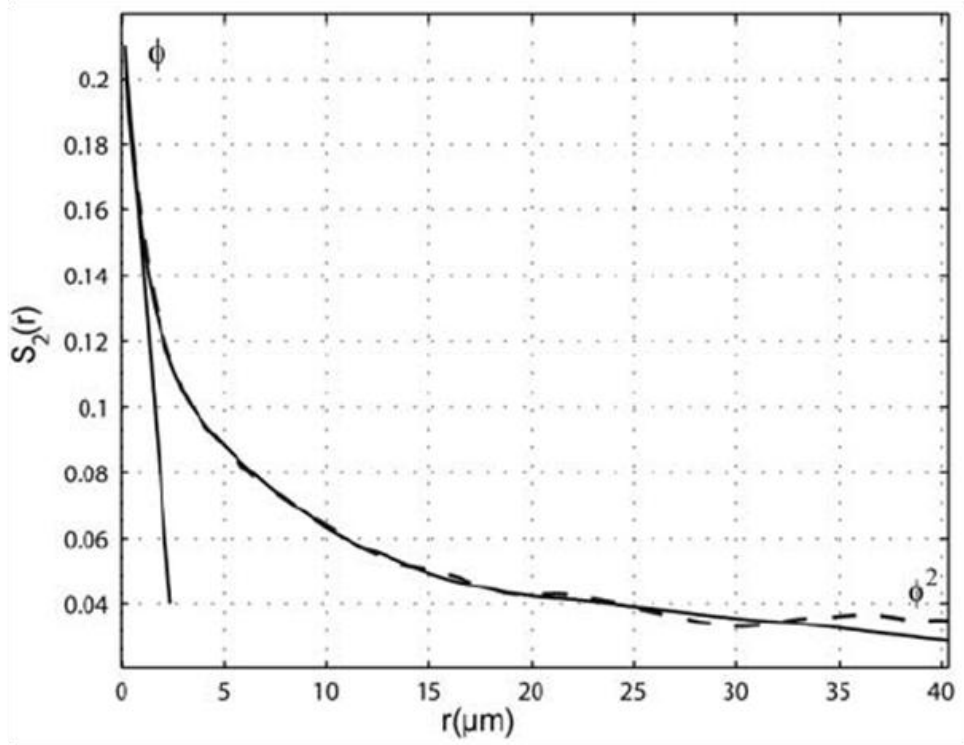


Figure 3.7 Two Point Correlation Functions Plot. $S_2(r)$ is unitless as it is the probability of certain simple geometrical arrangements [28].

Figure 3.7 illustrates a TPCF plot calculated from a thin section image using Equation 3.3. Since the plot is based on the identification of lag vector between two data points in the 2D image, porosity can be obtained by averaging these values (using Equations 3.4 and 3.5). The isotropy parameter can be obtained by applying TPCF on different directions of the 2D image, for example from the x and y direction. If the plots from different directions are negligible, the image can be assumed as isotropic.

3.2.7 Parameters for Simulation: Porosity, Variogram and Sample Points

Based on the previous study [9] [17], there are two input parameters to reconstruct 3D porous media from 2D image (training image), first, porosity and second, variogram calculated from the training image. For computational purposes, sample points

extracted from the training image is added as the new parameter. Sample points are used as conditional data. The use of conditional data is to reduce the computational time to reconstruct 3D porous. Details of the results are discussed in Section 4.3.

A 2D digitized image can be numerically converted into a binary 2D image (Figure 3.8 a). Pore space can be assigned as 1 (white color) and grain phase as 0 (black color). Porosity on 2D binary image is determined by counting the number of pore pixels and dividing by the total number of pixels in the image.

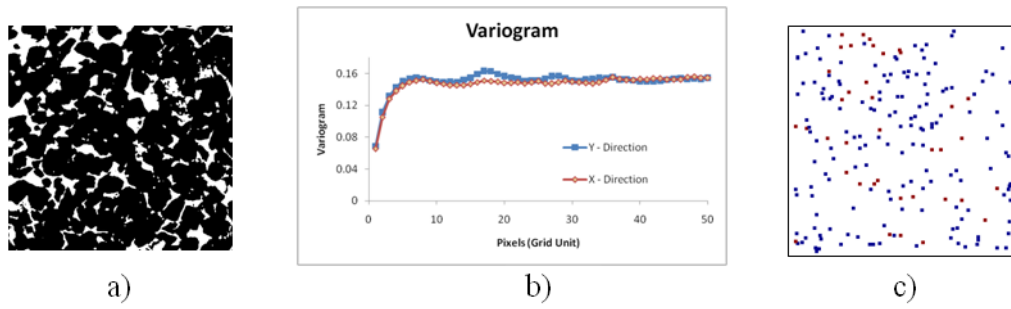


Figure 3.8 Input Parameters for Simulation: Porosity, Variogram and Sample Points Extracted from Training Image.

The porosity can also be derived from two point correlation functions (Equations 3.2 and 3.3) and can be defined by the statistical averages, denoted by $\langle \cdot \rangle$,

$$\phi = \langle f(r) \rangle \quad (3.4)$$

Replacing r from Equation 3.2 by 0, porosity can be calculated using following formula,

$$A(0) = \phi \quad (3.5)$$

The second parameter is variogram. The variogram has nearly the same meaning as two point correlation functions. Variogram reflects the dissimilarity of an image in spatial distributions; TPCF reflects similarity in spatial distributions. The equation to compute variogram [75] is as follows:

$$\gamma(\mathbf{h}) = \frac{1}{2N(\mathbf{h})} \sum_{i=1}^{N(\mathbf{h})} [f(r_i) - f(r_i + \mathbf{h})] \quad (3.6)$$

From Equation 3.6, $N(\mathbf{h})$ is the number of pairs of data locations spaced a distance of \mathbf{h} apart. The variogram of the thin section image is related to the TPCF as follows:

$$\gamma(\mathbf{h}) = A(0) - A(\mathbf{h}) \quad (3.7)$$

The exponential variogram of the image is reproduced by an exponential function to ensure positive-definiteness of the variogram model. The equation of the exponential function is as follows:

$$\gamma(\mathbf{h}) = c \left[1 - \exp\left(-\frac{3\mathbf{h}}{a}\right) \right] \quad (3.8)$$

where a is the practical range in geostatistics and c is the sill of the variogram. The range and sill are obtained by least-squares fit to the experimental variogram. Figure 3.8 b shows the variogram calculated from the x and y directions of the 2D image on Figure 3.8 a.

An additional parameter is sample points. There are only two phases on a 2D image, pore and grain. A 2D image comprises a number of continuous regions of pore spaces and grain spaces. MATLAB was used to extract the sample points. The porosity of the image is used as an input. 0.5% pixel is extracted using *Tem* with a size of 3x3 pixels. An example of sample points is shown in Figure 3.8 c. The red color represents the pore spaces region and blue color represents the grain spaces. For example, if a 2D image has a size of 200^2 pixels which comprises 400000 matrices row and column then the sample points extracted are 200 points.

3.2.8 Stochastic Simulation: 2D to 3D Porous Media

The use of 2D image to reconstruct 3D porous media can be justified under two conditions: the 2D image or training image should be homogenous and isotropic. The statistical averages can be replaced by volume averages when a rock is homogenous. The volume (3D) averages can be replaced by surface (2D) averages if it is also isotropic [17].

Realizations of 3D porous media were simulated using sequential indicator simulation (SISIM) conditioned to porosity and variogram of training image. The algorithm was taken from Stanford Geostatistical Modeling Software (SGEMS) by Remy et.al [75]. SGEMS is the next generation of Geostatistical Software Library (GSLIB) [76]. The training image was first reformatted from jpeg to sgems format using MATLAB and used as an input on SGEMS.

In this algorithm, all the nodes in the 3D grid are visited along a random path. At each node, a local conditional cumulative distribution function (*ccdf*) for $f(r)$ is computed. The *ccdf* is obtained by indicator kriging. First, a value for $f(r)$ is drawn from the local *ccdf*. Next, this value is preserved as conditioning data and the algorithm proceeds to the next node along the random path. Finally when all the nodes are visited, one realization of the 3D binary field with the correct spatial statistics is generated. Figure 3.9 shows an example of a simulated 3D porous media [17].

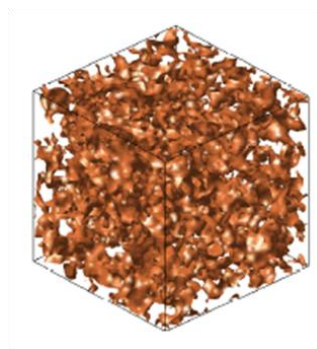


Figure 3.9 Three dimensional isosurface plot of a 3D reconstructed pore structure from SISIM [17].

3.2.9 Permeability Estimation Using Fluid Flow Simulation

Once the 3D porous media is generated, permeability is estimated by conducting numerical flow simulations on the 3D porous media. The reconstructed 3D porous media are geometrically very complex and may contain statistical noise due to the stochastic nature of their construction [17]. The Lattice Boltzmann Method (LBM) for fluid simulation is an appropriate choice for these cases. This method is a robust technique that simulates flow according to simple rules governing local interactions between individual particles and recovers the Navier-Stokes equations at the macroscopic scale [54].

Its accuracy in describing flow through a porous media and the way it treated the complex pore geometry without any modifications or simplifications are the prime advantages of this method [17] [54] [51]. The LBM is a discrete computational method based upon the Boltzmann equation that considers a typical volume element of fluid to be composed of a large number of particles, represented by a particle velocity distribution function for each fluid component at each grid point following simple local rules.

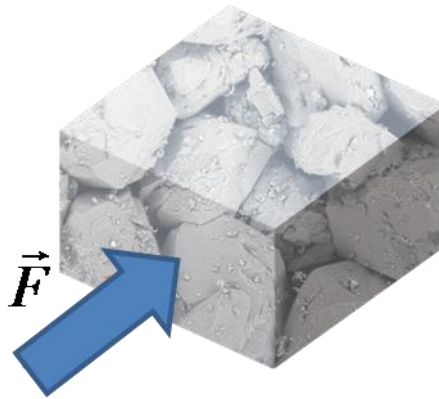


Figure 3.10 Illustration of a fluid forced through 3D digital image (Courtesy Ingrain).

Figure 3.10 shows a simple illustration on how LBM works and solves the Navier-Stokes equations:

$$\rho \vec{u} \nabla \vec{u} = -\nabla p + \mu \Delta \vec{u} + \vec{F} \quad (3.9)$$

where ρ is the density, \vec{u} the velocity of flow, p pressure, μ viscosity and \vec{F} body force. The Navier-Stokes equation can be solved as mentioned before by solving the discrete Boltzmann equation. The operation count is linear to the number of pore nodes where the fluid resides. Regardless of the complexity of the pore structure, the operation count per iteration is the same for the same number of pore nodes. The Boltzmann equation is solved by counting the particle density distribution at time t and location of r . From the local flux, a volume averaged flux can be calculated. Then, the absolute permeability is computed in a manner analogous to a laboratory measurement: a pressure head or body force is directly applied to a digital sample. The resulting fluid flux is computed and permeability is calculated according to the Darcy's law.

$$k = \frac{\langle Q \rangle}{\nabla P} \mu \quad (3.10)$$

The flow simulation is performed with pressure gradient (∇P) assigned across the opposite faces of the 3D cube. Next, a volume averaged flux $\langle Q \rangle$ is computed from the local flux. μ is the dynamic viscosity of the fluid.

3.3 Measurement

3.3.1 Sample: Berea Sandstone Core Plug

Berea sandstone is one of the rocks which have been widely used for laboratory experiments in the petroleum industry. This sandstone has been used for many years as a standard material in core analysis research and laboratory core flooding experiments. The rock is relatively well characterized and homogenous. It is well sorted with closely spaced planar bedding and well rounded predominately quartz grains, but it also contains minor amount of feldspar, dolomite and clays. This sandstone also occurs in the oil and gas producing formation in the Michigan basin. [18] [24]. The particular Berea sample that is used in this study has a size of 2 inch length and 1 inch diameter. The average of three measurements taken in the laboratory showed that the porosity is 17.5 % and the Klinkenberg-corrected air permeability 196.3 mD. Figure 3.11 shows the core plug of the Berea sandstone that was used for the measurement.



Figure 3.11 Photograph of a Berea sandstone core plug.

3.3.2 Measurement Procedure

The equipment used to measure the porosity and permeability of a core plug sample is the Poroperm. The Poroperm instrument is a porosimeter and permeameter used to determine properties of plug sized core samples at ambient confining pressure. In addition to the direct properties measurement, the instrument offers reporting and calculation facilities. Two types of gases are required to operate this equipment. Firstly, Nitrogen is used as the confining pressure conditioning and valve operation, and secondly, Helium is used for porosity measurement purpose. The Poroperm equipment is shown in Figure 3.12. This equipment is available at the Universiti Teknologi PETRONAS core laboratory.



Figure 3.12 Poroperm equipment to measure porosity and permeability at ambient confining pressure.

Details of the flow chart to measure porosity and permeability is shown in Figure 3.13 below:

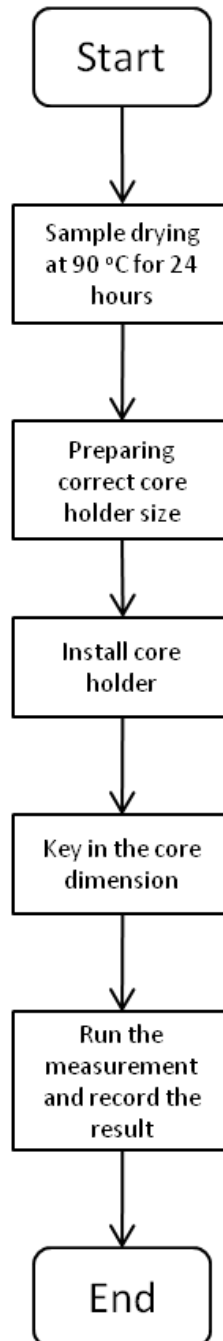


Figure 3.13 Details of the flow chart outlining the experiment procedure to measure porosity and permeability.

3.4 Thin Sections

A thin section is a very thin slice of rock which is mounted on a glass plate (usually 2" x 1") called microscope glass. Usually the thickness of geological thin section is between 30 to 40 micrometers. At this thickness, light easily gets transmitted through the slides and most minerals can be observed through an optical microscope. The objective to carry out thin section analysis is usually for geological studies such as mineralogy and sorting of the rock formation. Blue dyed epoxy is used for grains fixation. The epoxy fills the pore space in the rock and blue is a color that does not normally occur in reservoir rock; therefore the blue areas can be recognized as pore space. On this section, measured Berea core plug was used to create thin section. To fulfil the objective of this study, the thin section was cut in vertical direction due to the length of the plug. The size of the thin section is assumed as the scale of the core plug. Preparations of the thin sections were conducted at PETRONAS Research Sdn. Bhd. (PRSB). Figure 3.14 shows the flow chart of thin section preparation.

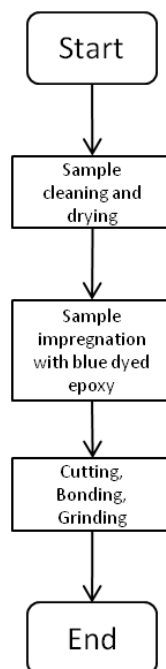


Figure 3.14 Thin section preparation flow chart.

3.4.1 Thin Section Preparation

To produce a good thin section from a reservoir rock, the rock sample has to be cleaned and remnants of the reservoir fluids and drilling mud removed. This step is very important since good bonding and complete impregnation of the sample depends on this step. After cleaning and drying, the samples are vacuum-impregnated with blue-dyed epoxy resin to assist the recognition of porosity. Blue dyed epoxy is also used as a protection from damage, such as fracturing or plucking. The impregnation equipment at PRSB is shown in Figure 3.15 below,



Figure 3.15 Impregnation equipment is used to vacuum and impregnate the samples with blue-dyed epoxy.

The next step is face lapping of the cut material that is used to produce a deformation free, smooth sample surface. This surface will be bonded to the glass slide. The last part is fine grinding to reduce the section thickness to 30 to 40 micrometers. The section must be monitored carefully to detect any plucking that can damage the glass during the grinding process. The computerised grinding machine at PRSB is shown in Figure 3.15.



Figure 3.16 Computerized grinding machines is used to produce a deformation free and smooth sample surface.

3.4.2 Image Collection

A microscope equipped with a high-resolution digital camera and a personal computer (PC) was used for image collection. The equipment is located at the South East Asia Carbonate Research Laboratory (SEACARL), Universiti Teknologi PETRONAS. Figure 3.17 shows the flow chart of image collection using microscope.

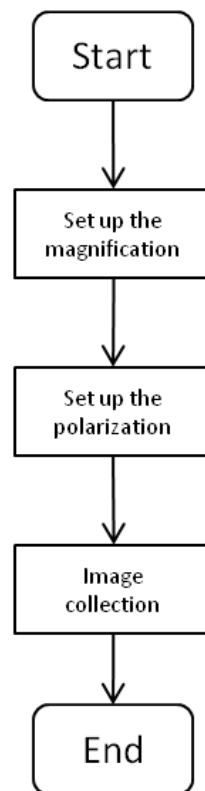


Figure 3.17 Flow chart of image collection.

The microscope is an Olympus petrographic microscope BX-51 that is specifically designed for thin section observation. The high resolution digital camera is a mounted camera Olympus DP-72 that enables the collection of a full color image of 4140 x 3096 pixels and gives a file size of 1.51 Mb for one image. Because of high storage requirements and processing time involved, the image size was limited to 600

x 400 pixels and gave an image size of 500 kb. Figure 3.18 shows the microscope used for image acquisition.

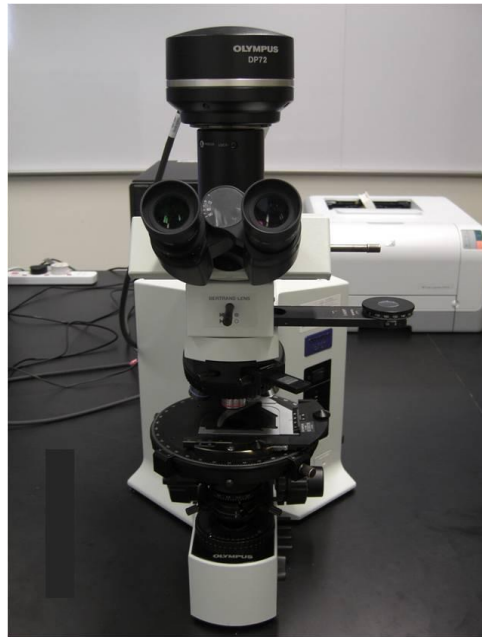


Figure 3.18 Microscope for image acquisition. The two magnifications used in this study are 12.5 and 40 times magnification.

Magnification

There are two types of magnification that were used for image collection in this study. The first was a 12.5 times magnification and second, 40 times magnification. These magnifications are provided from the objective lens and ocular lens. For example, a 12.5 times magnification is from a 1.25 times objective lens and a 10 times ocular lens. The output of this magnification was an image with a coverage area of about $0.9 \times 11 \text{ mm}^2$. Figure 3.19 shows an image collected using a 12.5 times magnification. Images collected from this magnification will be the inputs to obtain full thin section images. Details of the processes to stitch these images into full thin section image will be discussed in Section 3.4.4.

The second magnification was 40 times. The 40 times magnification was used as an input for 2D to 3D porous media reconstruction. The output of this magnification was an image which covered an area of about $2 \times 3 \text{ mm}^2$ of thin section. Figures 3.20 (a) and (b) show images acquired by a magnification of 40 times.

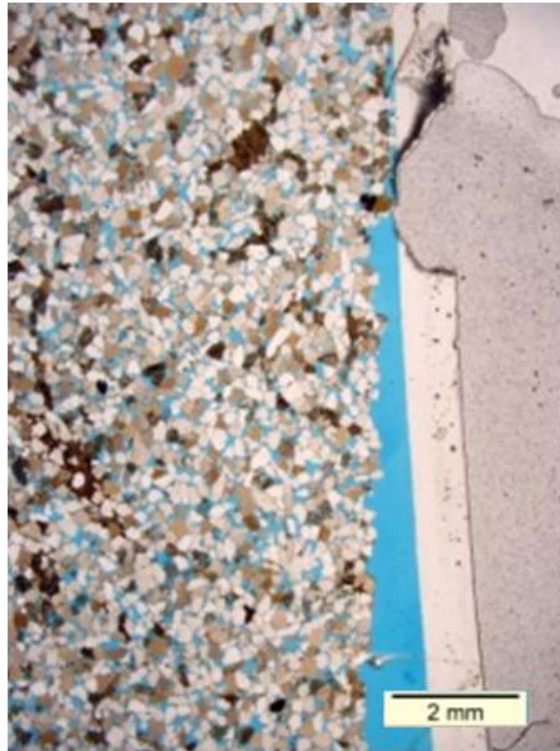


Figure 3.19 Image collected using a 12.5 times magnification. The coverage area is $9 \times 11 \text{ mm}^2$. The yellow bar shows scale of the image. Polarization type is cross-polarized

Cross-polarized and plane-polarized

Different types of polarization were used in this study. The polarizations are cross-polarized and plane-polarized. Full thin section images were produced by stitching nine images subsection into an image mosaic. The mosaic construction is based on finding the locations of co-located objects and minimizing the transition zone between the individual subsections. The optical reaction of minerals to cross-polarized light is

a good indicator of the material properties independent of their color [77]. The independence of material properties through color with this polarized eased the merging and stitching of subsections. With cross-polarization, a 12.5 times magnification and about 30% overlay from individual subsection, the result of mosaic construction is excellent for the input of grain size vertical profile method. The full image of thin sections using mosaic construction is shown in Sections 4.7 and 4.8.

The input for the 2D to 3D porous media reconstruction method is a binary image. Images produce by cross-polarized light give many colors. In this condition the pore and grain segmentation is difficult to be implemented. Plane-polarization differentiates only pores with color of blue and others (usually almost all color in white). With these conditions the binary image through image processing and segmentation is easy to obtain [26] [71] [78]. Figure 3.20 shows photomicrographs from cross-polarized and plane-polarized image acquisitions.

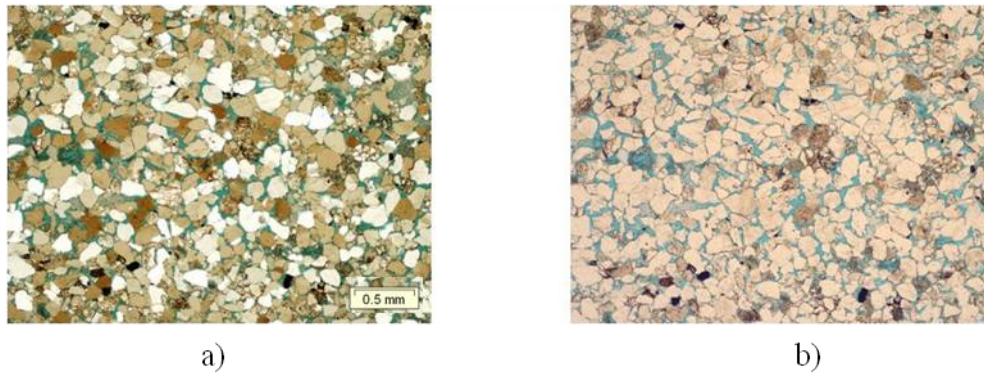


Figure 3.20 Thin section images of cross-polarized (a) and plane-polarized (b). The cross-polarized images are used as an input for full thin section image and the plane-polarized images are used as an input for 3D reconstruction method.

3.4.3 Image Processing and Segmentation: 2D Binary Image

One of the parameters for simulation is the porosity of thin sections. The general methodology for calculating porosity from thin sections involves conversion of a colored image to a binary image. The average of the binary image gives the value of porosity. As most thin sections use blue epoxy impregnation, the conversion to binary image requires computationally identifying pixels that are blue. Figure 3.19 shows the flow chart of image processing and segmentation of thin section image

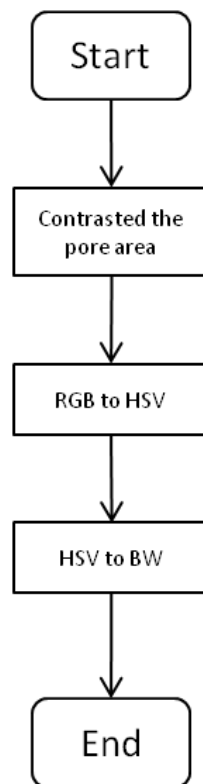


Figure 3.21 Flow chart of image processing and segmentation of thin section image.

Jmicrovision image analysis program was used for image processing and segmentation. Jmicrovision is an open source software for image processing and analysis. Several features of the program were therefore used to automate the method. The software allows one to “threshold” the images using HSV (Hue Saturation Value) histogram, a process also known as segmentation. Figure 3.22 shows the steps for image processing and image segmentation.

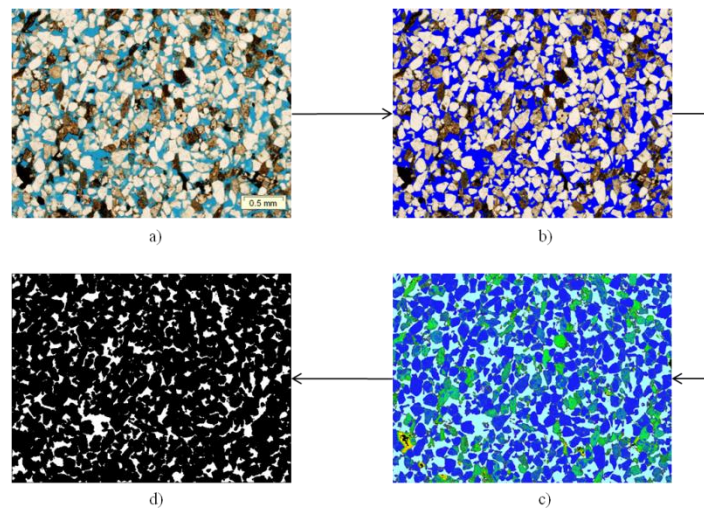


Figure 3.22 Steps for image processing and segmentation.

Plane-polarized image as an input is shown in Figure 3.22 a. To enhance the color of pores, threshold using HSV histogram was used. The results of threshold and segmentation shown in figure 3.22 b. The next step is converting RGB (Red Green Blue) to HSV format. Several studies have confirmed that converting the image from RGB to HSV will enhance the contrast of the pores [26] [68] [71] [78]. The HSV image is shown in Figure 3.22 c. The last step is converting HSV image into a black and white (BW) image (Figure 3.22 d). The last two steps were implemented using MATLAB.

3.4.4 Image Stitching: Full Thin Section Image

The 12.5 times magnification with cross-polarized was used to cover the whole image area of thin section. The full image of the thin section can be obtained by nine image collections from different parts of the thin section with each image having about 30% overlay. Full thin section images were produced by merging and stitching individually acquired subsections into an image mosaic. An Autostitch program and MATLAB were used as a tool for this purpose.

The objective of having a full thin section image is to give a representative image of thin section in centimetre scale [76]. This full image of thin section will be an input for grain size vertical profile (Section 3.5.1). Figure 3.23 shows the steps to acquire a full thin section image.

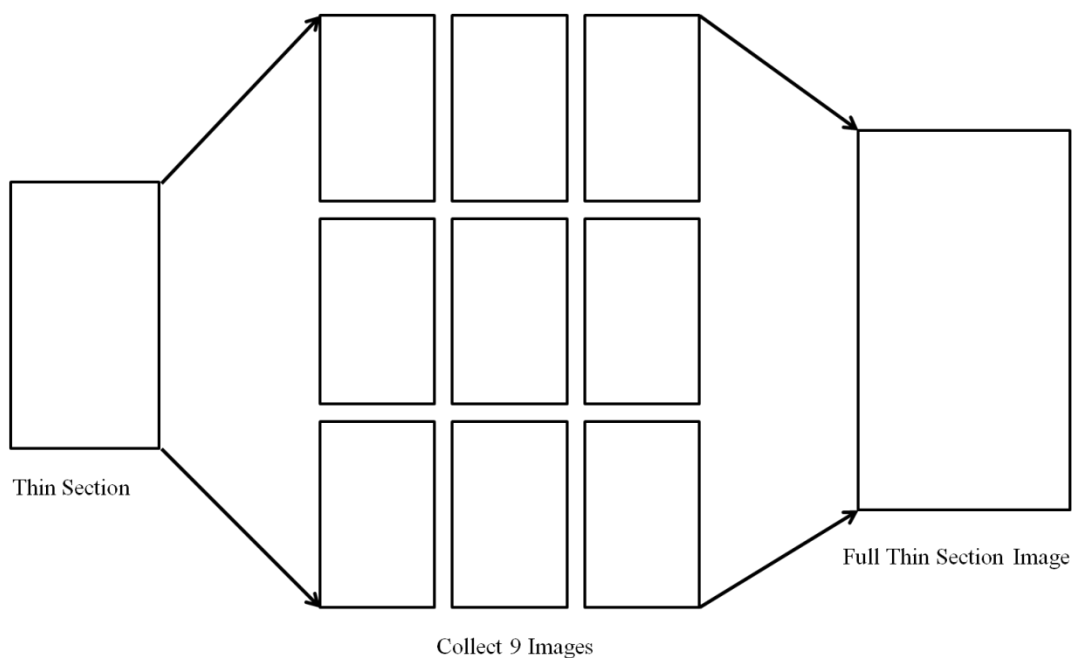


Figure 3.23 Steps for image collections of the full thin section image. Nine images (middle) are collected as an input for full thin section image. A full thin section image is produced by stitching the nine images.

3.5 Upscaling Permeability: Pore to Core-Plug Scale

Permeability prediction using 2D image from thin sections is sometimes overestimated and higher than the laboratory measurement permeability values of core plugs. The heterogeneity of the core plugs rendered an impossible permeability prediction from a single 2D image which is not representative of the sample. These images are very small (mm scale) and permeability prediction from these images needs to be upscaled to match the core plug measurements. In this study, a different approach was used to cover the heterogeneity of the sample. The grain size vertical profile from an image of the whole area thin section was used to determine the heterogeneity of the image at core plug scale. This profile gives the trends of coarsening and fining area of the whole thin section image. Figure 3.24 shows the flow chart of upscaling permeability.

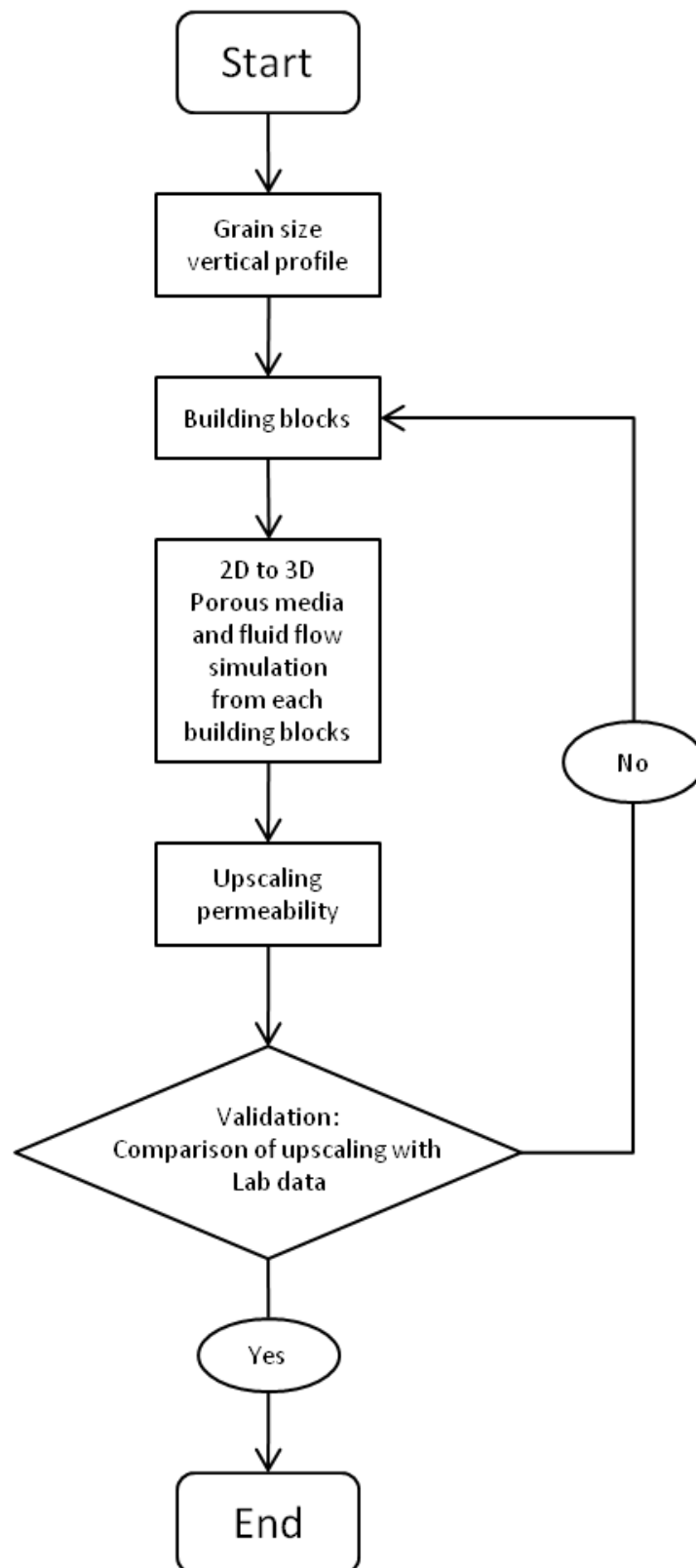


Figure 3.24 Flow chart of Upscaling permeability pore to core plug scale.

3.5.1 Grain Size Vertical Profile from Thin Section Image

Determining changes in bed sediment grain size from digital images was first employed by Rubin [79] [80]. Rubin used autocorrelation between two rectangular regions in digital images of sediment to determine the coarsening and fining trends. The actual grain size cannot be estimated with this method but sufficient for tracking changes in sediment grain size, which in some settings are related to flow changes. The spatial autocorrelation r between two rectangular regions (plaquettes) in an image is:

$$r = \frac{\sum_i (x_i - \bar{x})(y_i - \bar{y})}{\sqrt{\sum_i (x_i - \bar{x})^2} \sqrt{\sum_i (y_i - \bar{y})^2}} \quad (3.11)$$

where x_i and y_i are the intensities of corresponding pixels in two plaquettes, and \bar{x} and \bar{y} are the mean intensities of pixels in the two plaquettes. An autocorrelation curve is determined by calculating r as a function of distance between the two plaquettes. Grain size vertical profile can be implemented using autocorrelation curve which is computed for each row of pixels in the image.

Figure 3.25 shows a Grain Size Vertical profile calculated in a digital image of bed sediment. The digital image of sediments in four beds with a total thickness is 6 cm is presented in Figure 3.22 a. Figure 3.22 b shows the documentation of autocorrelation statistics of the bedding. Each of the four beds is inversely graded (gradually coarsening upward to the top contact and then abruptly fining at the base of the overlying bed). The overall sequence also coarsens upward [79].

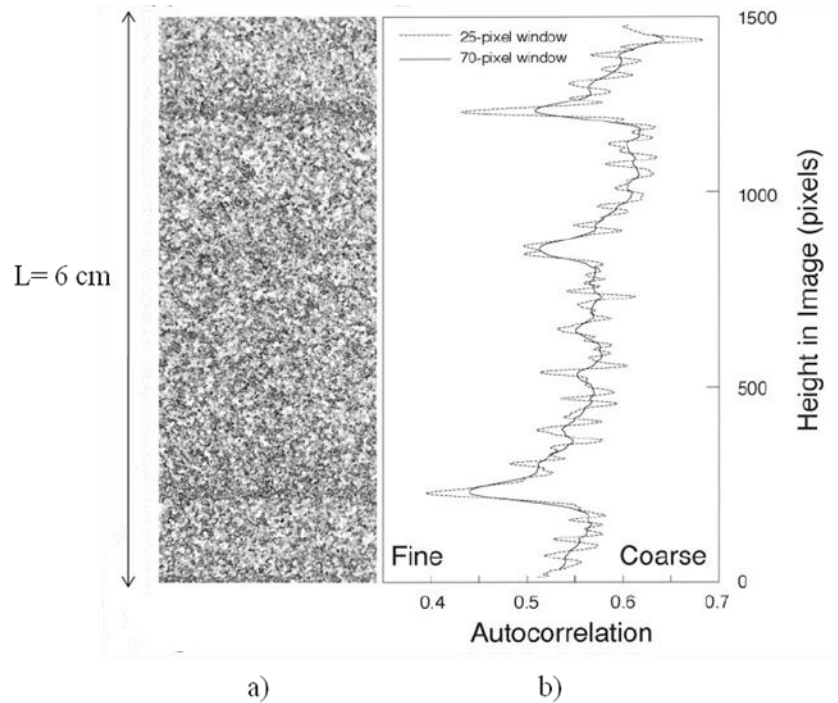


Figure 3.25 Grain Size Vertical profile calculated in a digital image of bed sediment. [79].

In this study, this methodology was used to classify the building blocks. This method can be used for all sediments with good resolution. For image acquisition, a magnification of 12.5 times was used to cover the whole area in the thin section (usually 2.54 sq. cm). The usefulness of this magnification is that it can cover the entire image fast, with only 9 image collections are required to cover the whole area of thin section. The vertical grain size profile can be calculated easily from the whole area of the thin section. The calculations for this grain size vertical profile (autocorrelation curves for about 3000 rows of pixels, smoothed at two scales) took 1 second on a 2.67 GHz computer.

3.5.2 Building Blocks

The computed permeability values of small sub-volumes sometimes overestimated the laboratory-measured permeability values since the input to compute permeability is in millimetre scale and the measured scale in centimetre scale [9] [68]. The overestimation is caused by permeability heterogeneity in the relatively large physically measured sample. To overcome these problems, upscaling on the basis of small building blocks can be combined with computed permeability.

The effective permeability of a 3D network of building blocks (each with a known permeability) may take values between the harmonic and arithmetic average of the block permeability values, depending on their spatial arrangement. The bulk permeability parallel and normal to beddings are calculated as weighted arithmetic and harmonic averages, respectively, using the corresponding values [81] [82]. Figure 3.23

In this study, the grain size vertical profile was used as the basis for creating the building blocks. Previous studies showed that rocks which are coarse grained are more porous than the fine grained. We can assume that the coarser part is more porous and the finer part less porous.

Figure 3.26 a. shows building blocks created based on the grain size vertical profile calculated from digital image. Building blocks were created based on the coarsening and fining trends calculated from digital image. Based on the gradation of the trends, there are three main trends which can be used as the base to create building blocks. Part *c* is the finest area with length l_c . There are two similar trends on part *b*. Based on the trends, we can assume that these areas have the same characteristics as the medium grain size. The coarser part is shown on *a*.

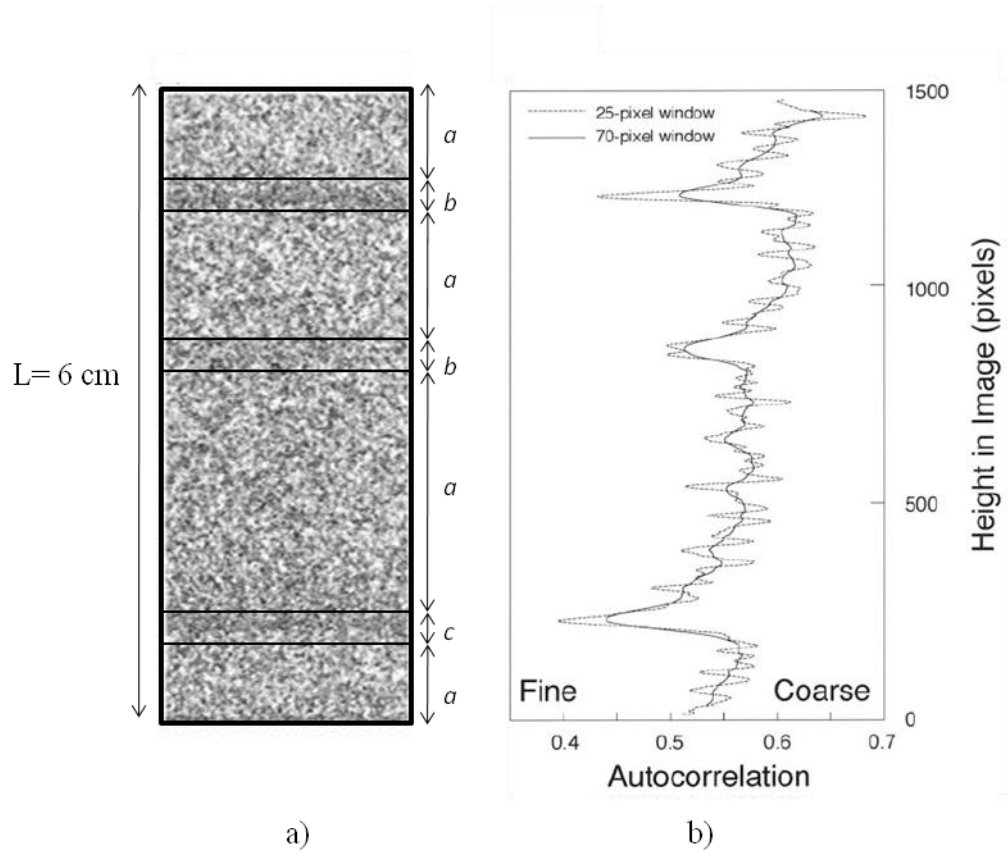


Figure 3.26 Building blocks created based on the grain size vertical profile calculated from digital image. Building blocks were created based on the coarsening and fining trends calculated from digital image.

The volume fraction that is used for upscaling can be determined based on this information. The formula to calculate effective permeability is expressed as follows:

$$K_p = \frac{k_a l_a + k_b l_b + k_c l_c}{L} \quad (3.12)$$

$$K_n = \frac{k_a k_b k_c L}{k_a k_b l_c + k_c k_b l_a + k_c k_a l_b} \quad (3.13)$$

CHAPTER 4

RESULTS AND DISCUSSIONS

4.1 Introduction

This chapter presents the results and subsequent discussions of the results that are obtained in this work. The results would first describe the impact of image resolution and image size for fluid flow computation. The effectiveness of porous media reconstruction method from 2D to 3D image with comparison on 3D CT-Scan image is also presented.

The computational generation of 3D porous media and fluid flow simulation which can be handled by a standard personal computer and in real time only can only be implemented at mm scale. Comparison through this method can only be précised if it is compared on the same scale. This size sometimes cannot cover the heterogeneity of a sample at laboratory scale (cm scale). The full image of a thin section (usually 2.54 cm^2), in principle has the similar size scale with the laboratory scale.

To overcome these problems the upscaling method is applied. Grain size vertical profile which shows the trends of coarser and finer parts of a full thin section image is used as a benchmark to create building blocks for upscaling purposes. Each image which represents the coarse and fine parts of a thin section is used as an input for 2D to 3D porous media reconstruction method. The porosity and permeability are calculated from each reconstructed porous media (mm scale) and used as an input for upscaling (mm to cm scale). These workflows were applied to the Berea thin section and thin sections from the Malay Basin.

4.2 Preliminary Study on Image Size and Resolution for Fluid Flow Simulation

Input for the fluid flow simulator (PNM or LBM) is a 3D image cube of a rock sample. Each cube has resolution and size which are used as input parameters for fluid flow simulation. In this subsection, three samples are discussed in detail on the impact of image resolution and size. The samples are the Berea sandstone, Sandstone S (8) and the Fontainebleau sandstone. These tests were conducted to decide the effective minimum size to run the fluid flow simulation.

Image Size

The impact of image resolution will be discussed in the next section on image resolution. Changes on the resolution will reduce the size of the 3D porous media. The bigger the size of the cube, the computational time will be longer. Figure 4.1 shows the impact of image size with computational time on Berea Sandstone:

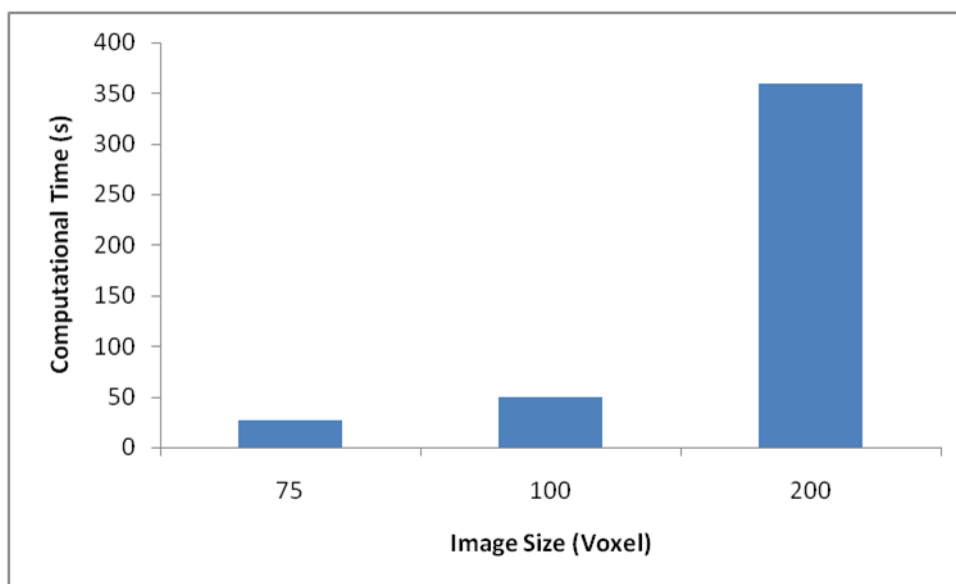


Figure 4.1 Relation between image size and computational time of fluid flow simulation. The bigger the size of the cube (75 to 200 voxels) the computational time will be longer.

Based on previous studies, the effective size to run fluid flow simulation on a standard personal computer (PC) is 100 voxels [9] [17] [68]. A size more than 100 voxels will make the computational time not effective and not in real time. However, results on the impact of resolution shows that a direct reduction of the resolution without good arrangement will result in a loss of geometry information and will affect the connectivity of porous media (will be discussed on the image resolution section). Therefore to obtain the effective size, the Representative Elementary Volume (REV) needs to be identified before conducting the simulation. By applying REV, the minimum size that represents the whole sample can be determined. Reducing the resolution with proper steps will give effective size for simulation.

Image Resolution

The impact of image resolution was first tested on 3D CT-Scan image of sandstone. The test was first conducted on 3D CT-Scan of Berea Sandstone with an original size of 400 voxels (volume pixel) and resolution $5.3 \mu\text{m}$ ($400^3 \times 5.3 \mu\text{m} = 2.120 \text{ mm}^3$ in physical volume). The resolution was reduced to 75 voxels with $28.2 \mu\text{m}$ per pixel, the same physical volume of 2.120 mm^3 .

Figure 4.2 shows the impact of resolution on Berea sandstone sample. The images showed that the connectivity of porous media is largely reduced with decreasing resolution. The biggest impact of pore structure and connectivity was severely compromised in the model with cell size resolution $28.2 \mu\text{m}$. The porosity and permeability were calculated and simulation started from the original size of 400 voxels, reduced to 200 voxels and decreasing to 75 voxels. The results were plotted based on the fractional change relative to the original 400 voxels with a resolution of $5.3 \mu\text{m}$ per pixel.

Figure 4.3 is the plot which showed that porosities were relatively unaffected with a reduction of resolution. The impacts on the simulated permeabilities were quite poor and affected the simulation results. A marked decrease in permeability was observed when the cell size changed from a resolution of 10.6 (200 voxels) to $28.26 \mu\text{m}$ (100 voxels) per pixel. In contrast when the resolution reduced from 5.3 (400 voxels) to

10.6 μm (200 voxels) per pixel there was relatively little change in the permeability because the pore throats were fairly well resolved.

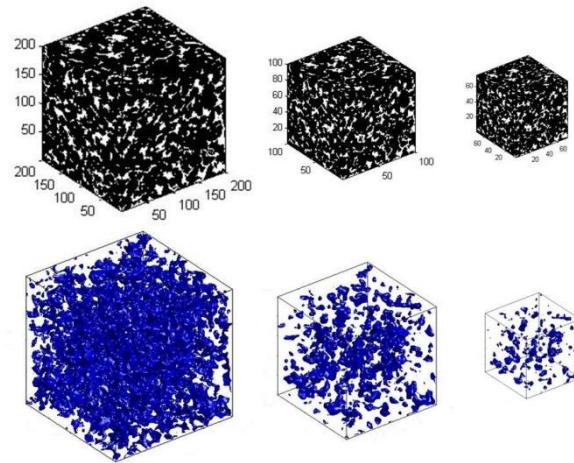


Figure 4.2 3D porous media with the reduced scale to 200, 100, 75 voxels cubes of 19.6% porosity of 3D CT-Scan Berea sandstone from the original 400 voxels cube. The loss of image complexities are shown as the resolution decreased.

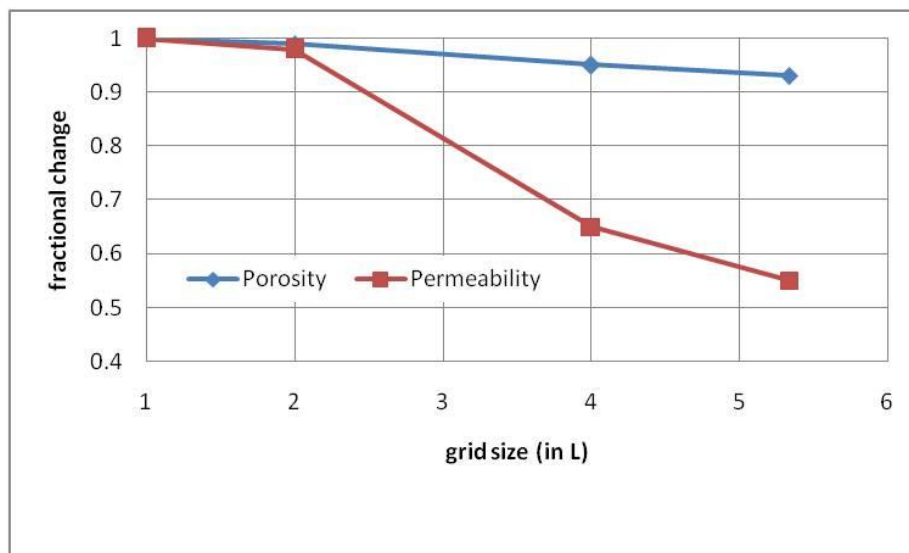


Figure 4.3 The fractional changes value (unitless) of porosity and simulated permeability with respect to the original 400 voxels cube of Berea sandstone. L is unitless as it is a fraction of the size (e.g. 400 voxels/200 voxels = 2).

The second test was conducted on 3D CT-Scan of Sandstone S (8) with an original size of 300 voxels and resolution 4.9 μm per pixel ($300^3 \times 4.9 \mu\text{m} = 1.470 \text{ mm}^3$ physical volume). The image size was reduced to 50 voxels with a resolution of 29.4 μm per pixel, which has the same physical volume as the original 1.470 mm^3 . Figure 4.4 shows the impact of resolution on Sandstone S (8) sample.

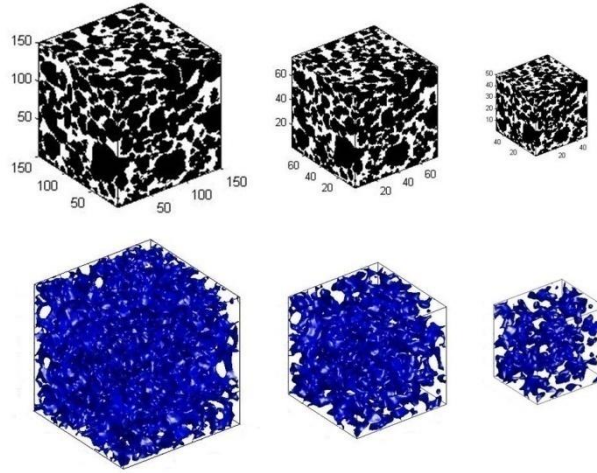


Figure 4.4 3D porous media with the reduced scale to 150, 75 and 50 voxels cubes of 34% porosity of 3D CT-Scan Sandstone (S8) from the original 300 voxels cube. The loss of image complexities are shown as the resolution decreased.

Figure 4.4 shows that the connectivity of porous media is largely reduced with decreasing resolution. The biggest impact of pore structure and connectivity was severely compromised in the model with cell size 29.4 μm (50 voxels). The porosity and permeability were calculated and simulated starting from the original size of 300 then 150, 75, and 50 voxels. The results were plotted based on the fractional change relative to the original 300 voxels with a resolution of 4.9 μm per pixel.

Figure 4.5 shows that porosities were relatively unaffected with a reduction of the resolution. The impacts on the simulated permeabilities were quite poor and affected the simulation results. A marked decrease in permeability was observed when the cell size changed from a resolution of 9.8 (150 voxels) to 29.4 (50 voxels) μm per pixel. In

contrast when the resolution reduced from 4.9 (300 voxels) to 9.8 (50 voxels) μm per pixel there was relatively little change in permeability because the pore throats are fairly well resolved. As noted in this second test, the fractional changes of the simulated permeability on cell size with a resolution of 19.6 μm (75 voxels) per pixel is still in good agreement with respect to the original cube. This is shown in Figure 4.4 that the pore throats are still well preserved. In contrast with the Berea sandstone sample where the pore throats were not fairly resolved on 4 times reduction from the original cube, the results showed that the pore throats are fairly well resolved on Sandstone S (8) sample. The analysis from this is because Sandstone S (8) which has a porosity of 34 % is more porous than the Berea sandstone, which has a porosity of only 19.6 %. Since Sandstone S (8) is more porous, a reduction of 4 times from original cube could still fairly resolve the pore throats.

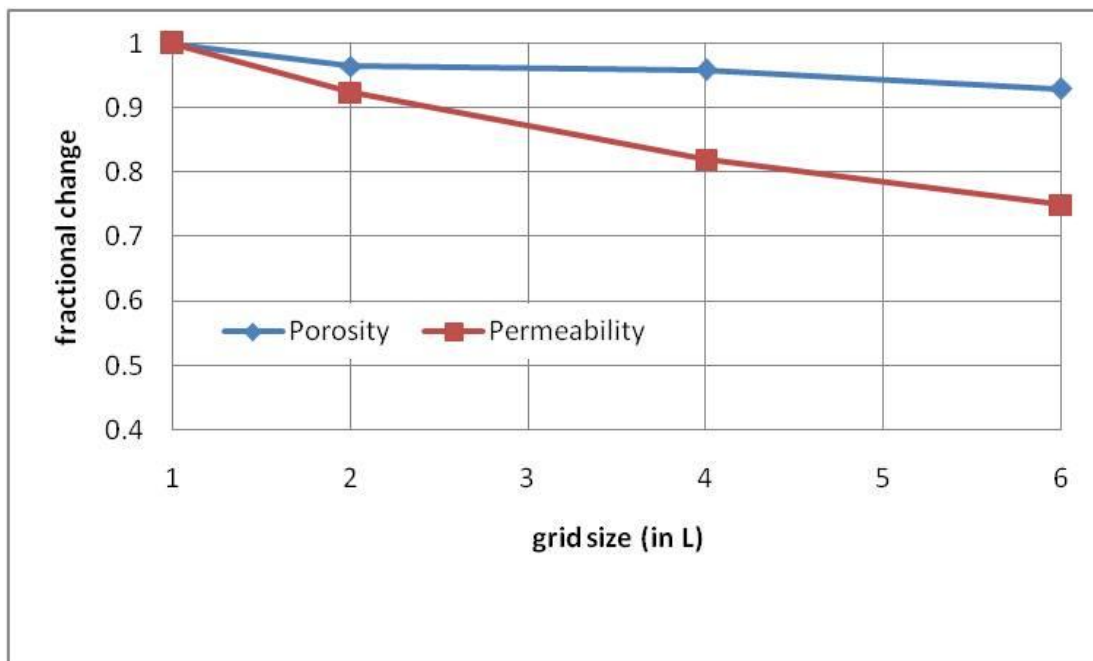


Figure 4.5 The fractional changes value (unitless) of porosity and permeability with respect to the original 300 voxels cube of Sandstone S (8). L is unitless as it the fraction of size (e.g. 300 voxels/150 voxels = 2).

The third test was conducted on a 3D CT-Scan of the Fontainebleau sandstone with an original cube of 144 voxels and a resolution of 15 μm ($144^3 \times 15 \mu\text{m} = 2.160 \text{ mm}^3$ physical volume). In contrast with the Berea Sandstone and Sandstone S (8) tests which were tested on 1, 2 and 4 times reduction of resolution from the original cube, the test on the Fontainebleau sandstone was conducted by reducing the resolution to 1, 1.2, 1.33 and 1.4 times from original cube. The reason for choosing these reductions is because the size of the Fontainebleau sandstone sample is not as big as other two samples. The resolution is also not as good as other two samples. Figure 4.6 shows the impact of resolution on Fontainebleau sandstone:

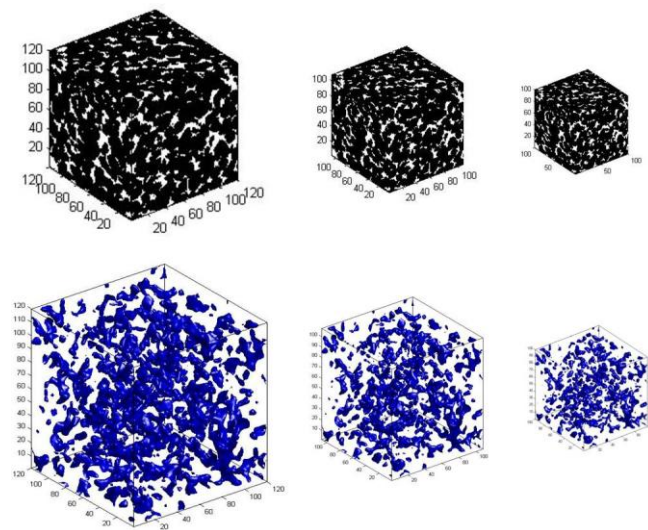


Figure 4.6 3D porous media with the reduced scale to 120 to 100 voxels cubes of 14.6% porosity of 3D CT-Scan Fontainebleau sandstone from original 144 voxels cube. The loss of images complexities are shown as the resolution decreased.

The images showed that the connectivity of porous media is largely reduced with decreasing resolution. The biggest impact of pore structure and connectivity was severely compromised in the model with cell size 21.6 μm (100 voxels). The porosity and permeability were calculated and simulated starting from the original size of 144, 120 to 100 voxels. The results were plotted based on the fractional change relative to original 144 voxels with 15 μm resolution per pixel.

Figure 4.7 showed that porosities were relatively unaffected with a reduction of the resolution. The impacts on the simulated permeabilities were quite poor and affected the simulation results. A marked decrease in permeability was observed when the cell size changed from a resolution per pixel of 20 (108 voxels) to 21.6 μm (100 voxels) per pixel. In contrast when we changed from 15 (144 voxels) to 18 μm (120 voxels) there was relatively little change in the permeability because the pore throats were fairly well resolved. The image resolution on the Fontainebleau sandstone (15 μm per pixel) was not as good as the Berea sandstone (5.3 μm per pixel) and Sandstone S (8) (4.9 μm per pixel). The resolutions decreased less than twice from the original size of 144 voxels, since the original resolution is 15 μm per pixel. As shown in Figure 4.6 and Figure 4.7 the loss of complexity information of the porous media gave a great impact to the pore throats and the simulated permeability.

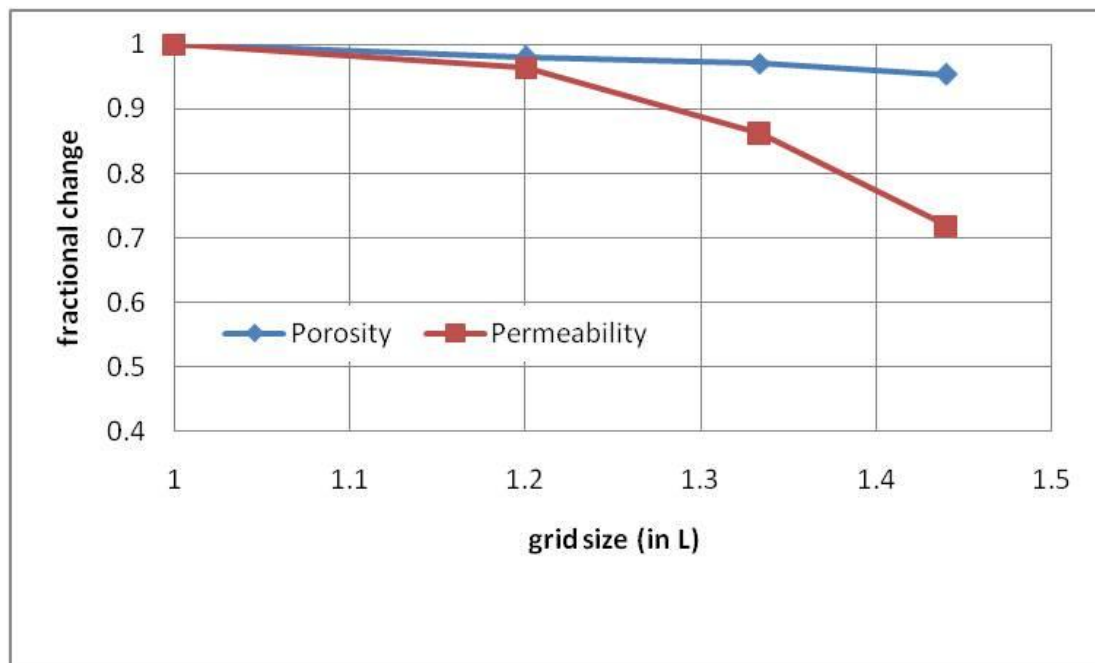


Figure 4.7 The fractional changes value (unitless) of porosity and permeability with respect to the original 144 voxels cube of Fontainebleau sandstone. L is unitless as it is the fraction of size (e.g. 144 voxels/108 voxels = 1.2).

The conclusion can be taken from these three tests is that the image resolutions affect fluid flow simulation. Porosities values shown on each plot indicate that porosities are relatively unaffected by reduction of resolution. The reason for these phenomena is because porosity is just a fraction of the pore nodes over the total volume which will not affect much on the changes of resolution. For permeability, at lower resolutions the 3D images lose details in structural complexity which leads to a sharp overestimate of the computed permeability.

The resolution requirements of rock samples through CT-Scan are also highlighted. The first two samples, Berea sandstone and S (8) sandstone were acquired using CT-Scan with a good resolution (5.3 μm and 4.9 μm per pixel) respectively. The resolution reductions of 50 % on Berea sandstone CT-Scan image (5.3 to 10.6 μm per pixel) and Sandstone S (8) (4.9 to 9.8 μm per pixel) are still in good agreement on the simulated permeability. However, for Fontainebleau sandstone, where its resolution (15 μm) is not as good as Berea and S (8), the reduction of resolution still in good agreement at 80% of the resolution reduction (15 μm to 18 μm per pixel). The results showed that the complexity information of the porous media is well preserved at a resolution more than 18 μm per pixel for the size of a cube more than 100 voxels cube.

4.3 Study on Sample Points as New Parameter Input for 2D to 3D Porous Media Reconstruction Method

The reconstruction of porous media from a 2D image using geostatistical (SISIM) method was initially introduced by Keehm [17] [68]. This methodology is good enough to reconstruct 3D porous media from 2D image especially on a clastic system [9]. In this study, the modification was made to improve the computational time of porous media reconstruction method. Sample points extracted from a training image were used as a conditional data which will improve the computational time without changing the output of this methodology. Table 4.1 shows the computational time between the modification and non-modified method (Keehm, 2003).

Table 4.1 Comparison of running time between different types of conditional data.

| Type of Conditional Data | Computational Time (Sec) |
|--------------------------|--------------------------|
| Cond. SP | 30 |
| Cond. TI | 92 |
| No Cond. | 998 |

Cond. SP (the modification and proposed method) is the reconstruction of a porous media using sample points as conditional data, Cond. TI is the reconstruction of a porous media using training image as conditional data and No Cond. (the non-modified method / Keehm, 2003) is the reconstruction of a porous media without conditional data. The modification method using sample points as conditional data shows an improvement on computational time. The results were plotted as a function of efficiency.

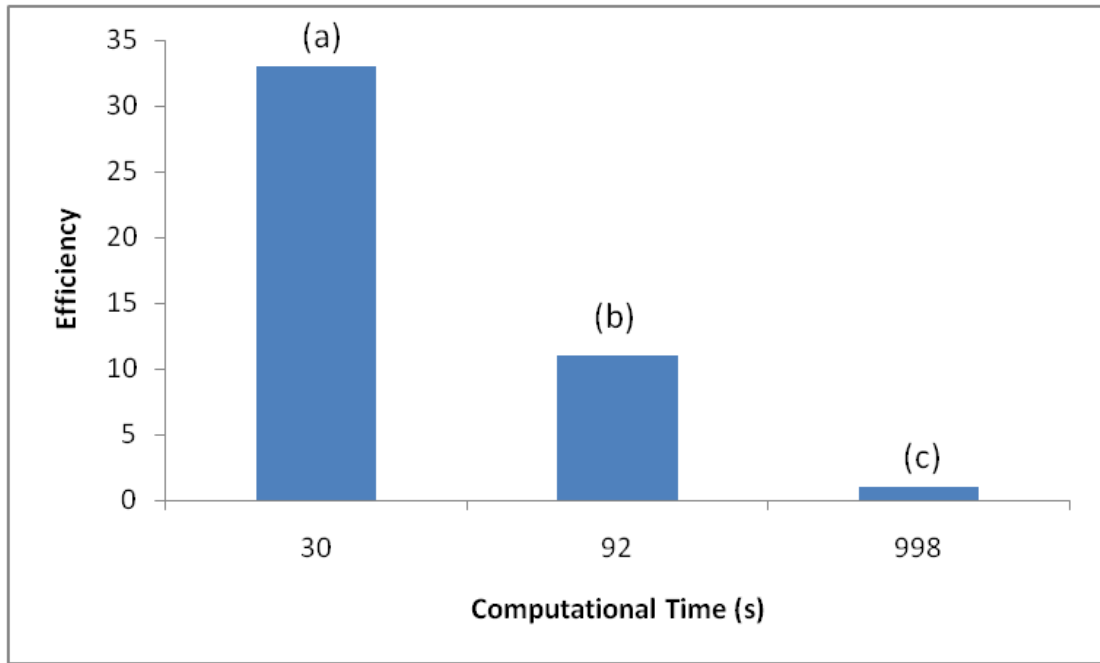


Figure 4.8 Computational time and time efficiency chart on different types of conditional data. (a) Proposed workflow to reconstruct 3D porous media, (b) using training image as conditional data and (c) the non-modified method (Keehm, 2003).

Figure 4.8 shows the graph between the non-modified and the modification method. The methodology without conditional data needs 998 seconds to reconstruct one realization of porous media. The methodology using training image as conditional data only needs 92 seconds. The methodology using sample points as conditional data showed an improvement of computational time which is 30 times faster than the non-modified method and 10 times faster than the Cond. TI. This means that the efficiency of the methodology has improved significantly. The structures of the three different methodologies are shown on Figures 4.9 – 4.11.

The analyses from the results are that the use of sample points as conditional data has improved the computational time to reconstruct the 3D porous media of sandstone. The sample points which were extracted from the training image have the same statistical variations with training image. The variogram model also contains the same statistical variability as a training image. With sample point as conditional data, a value of $f(r)$ which is drawn from conditional cumulative distribution function (*ccdf*)

is easily preserved. The time algorithm processes to reconstruct porous media is reduced since there are three inputs that limit the possibility of reconstruction. Porosity states the exact value of training image porosity. A variogram model and sample points made the visited along random path based on *ccdf* of all nodes to create 3D cube easily to conducted since there are two information (variogram and sample points) which give information about *ccdf* of training image.

Figures 4.9, 4.10, 4.11 show the three samples have similar structure of porous media. Variograms from three different orientation (x, y and z) directions show the same structure variability. This means that sample points as conditional data improve the computational time of this method and make it more efficient to use on a standard personal computer.

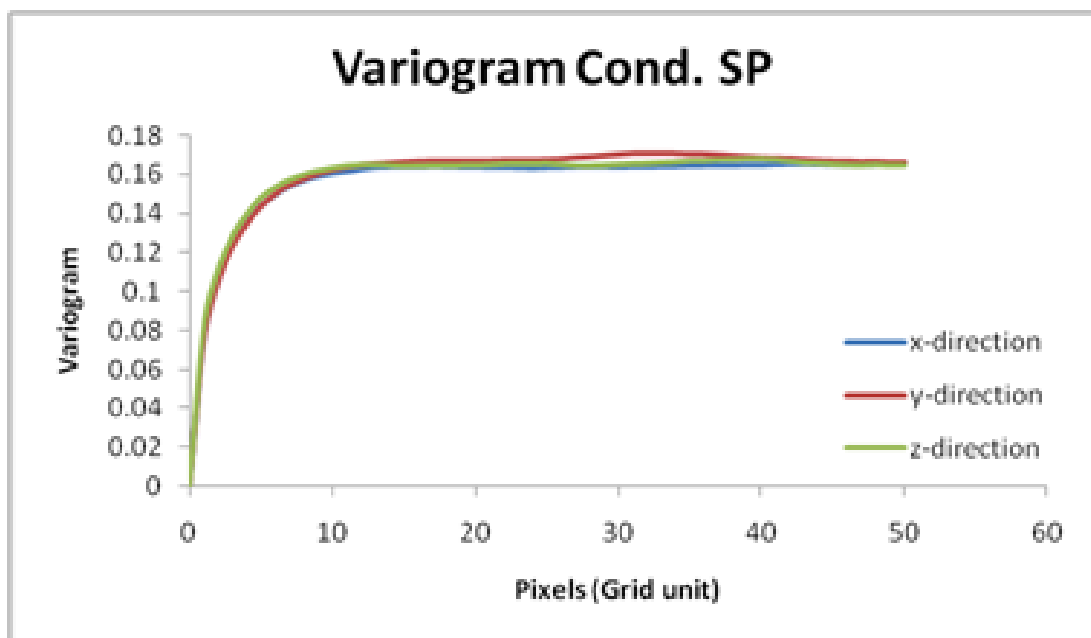
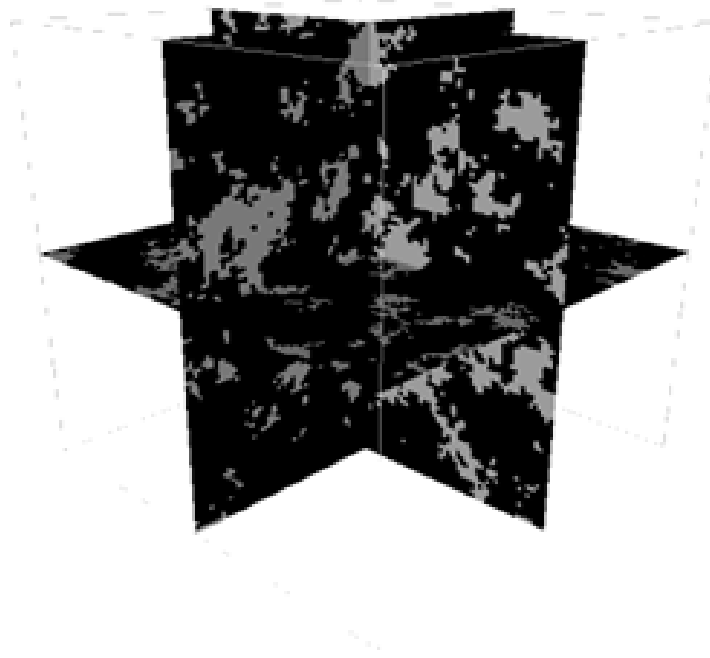


Figure 4.9 Structural and variogram ($x=50$, $y=50$ and $z=50$) using sample points as conditional data. The structure showed that the complexities of porous media are well preserved. The variograms are align showed that the image is isotropic.

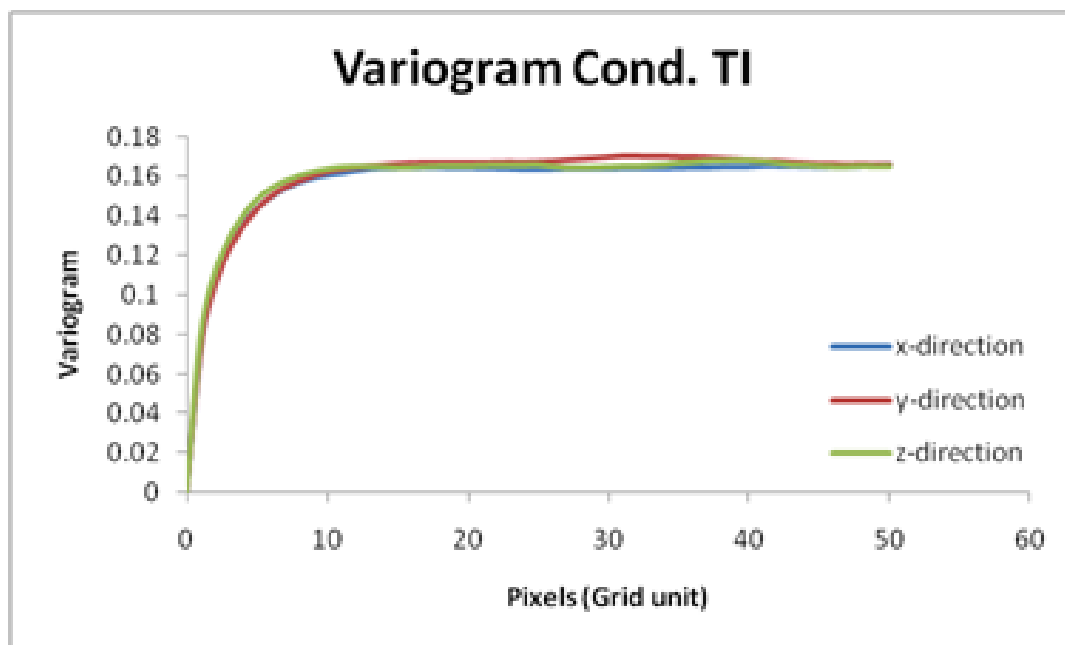
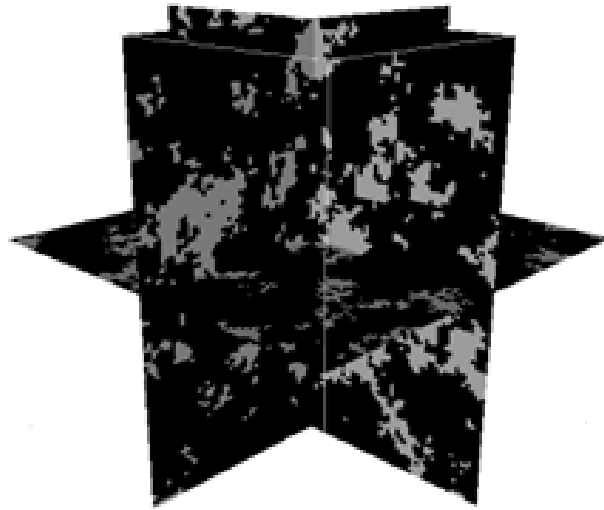


Figure 4.10 Structural and variogram ($x=50$, $y=50$ and $z=50$) using training image as conditional data. The structure showed that the complexities of porous media are well preserved. The variograms are align showed that the image is isotropic.

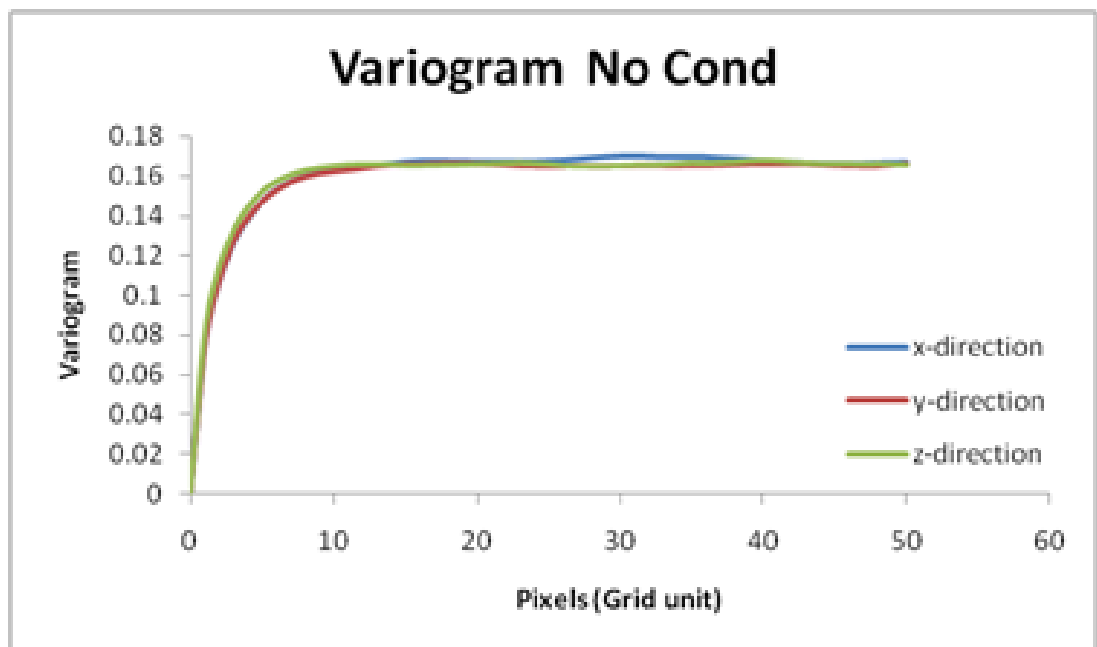
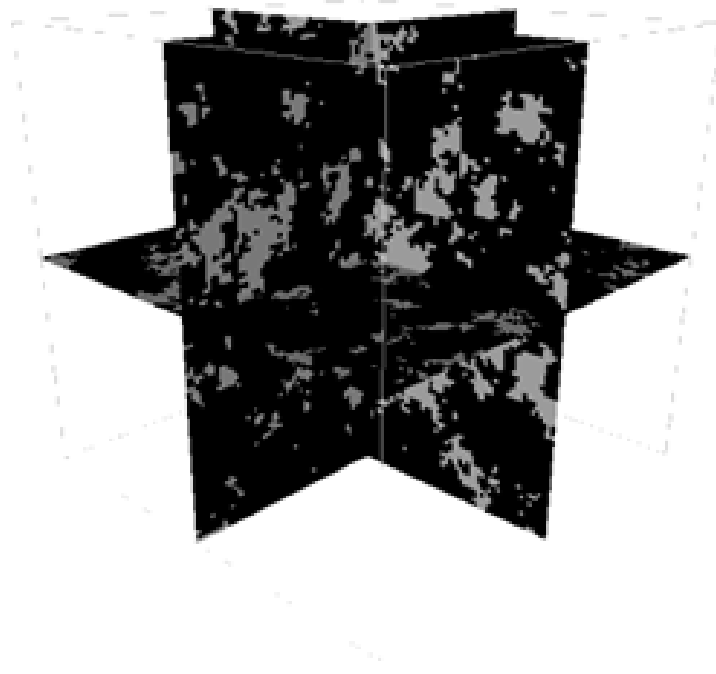


Figure 4.11 Structural and variogram ($x=50$, $y=50$ and $z=50$) without conditional data. The structure showed that the complexities of porous media are well preserved. The variograms are align showed that the image is isotropic.

4.4 Reconstruction from 2D to 3D Porous Media of Sandstone

The porous media reconstruction method needs a 2D image as an input. The validation of this technique requires a 3D image of a porous media. Therefore for this purpose the reconstruction was conducted on 2D cross sections selected from 3D X-ray tomography images. Six samples were used: Berea Sandstone, Sandstone S (8), Fontainebleau Sandstone, Sandstone S (4), Sandstone S (2), Sandstone S (4) and Sandstone S (5). Three first samples will be described in detail in this section and the last three samples will be summarized and discussed briefly in Section 4.5.

4.4.1 Berea Sandstone Reconstruction

The 2D to 3D porous media reconstruction was first tested on Berea sandstone. The 2D image was cut from a 3D x-ray tomography image of Berea sandstone. The purpose is to compare and validate the results of the reconstruction method with experimental CT-Scan data. The sample has a size of 400^3 voxels with a resolution of $5.3 \mu\text{m}$ per pixel. The porosity and permeability calculated and simulated from the 3D image of the reference data was 19.6% and 1360 mD respectively. A training image (2D image) was selected in terms of REV and porosity within a 2D slice along a 3D CT-Scan image of Berea sandstone. REV is required to identify the minimum sizes that represent the whole sample. With minimum sizes the fluid flow simulation can be conducted in real time on a standard personal computer. Reducing the resolution directly to minimum sizes without conducting REV will affect the connectivity and simulated fluid flow as shown in Section 4.2.

Representative elementary volume (REV)

The minimum size of elementary volume can be determined from REV calculation. Porosity can be used to determine the REV. There were 20 subsections from the center of the original 400 voxels, ranging from 20 to 400 voxels at intervals of 20 voxels on each edge which were taken to calculate the REV of the CT-scan image of

Berea sandstone. The porosity was calculated on each subsection and the edge lengths at which porosity converged was used to decide the REV range.

Figure 4.12 shows the calculated porosities from 20 subsections of the Berea sandstone 2D images. The cube figure on the right shows the initial 3D image of the Berea sandstone on which REV was conducted. The blue line shows the trends of porosity values. The REV range for Berea sandstone was decided based on the trends. The fluctuations of porosity values are significantly less from 200 to 400 voxels.

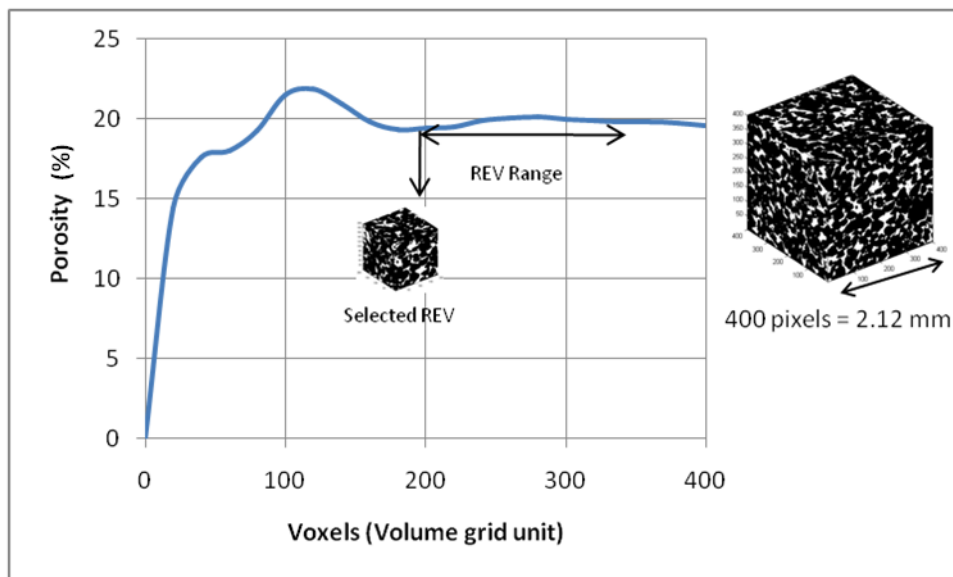


Figure 4.12 The REV graph for porosity on 3D CT-Scan of Berea Sandstone. The cube on the right shows the original size of 3D image and the cube on the left shows the selected REV cube.

The size of 200 voxels was selected as the minimum elementary volume. This size was taken as the input for training image selection. This size was also considered based on the preliminary study on impact of image resolution. The size of 200 square pixels of 2D image is still a considerable size if it was reduced to 100 square pixels since the size of input for the reconstruction method and fluid flow simulation on a personal computer which can be running in real time is at this size.

Selection of training image

The 3D CT-scan image is a set of closely spaced consecutive 2D slices. These slices can be analogous as thin sections. In order to reconstruct a 3D porous media from a 2D image, a representative 2D image should be selected in terms of porosity. Porosity from each consecutive 2D slices was calculated. Each of image gave different porosity and showed fluctuations as shown on Figure 4.9. The selected REV size for the Berea sandstone sample is 200 voxels, which means there are 200 images of 2D slices within the cube. The average porosity was calculated from all 2D slices within 3D porous media of selected REV size. The average porosity was taken as a benchmark and the training image was selected based on this value.

Figure 4.13 shows porosity fluctuations within the 200 voxels cube of Berea sandstone sample. The arrow shows the interval at which the training image was selected. This image was selected at interval 0.23 mm which had a porosity close to the average porosity from 200 images and original size of the reference data.

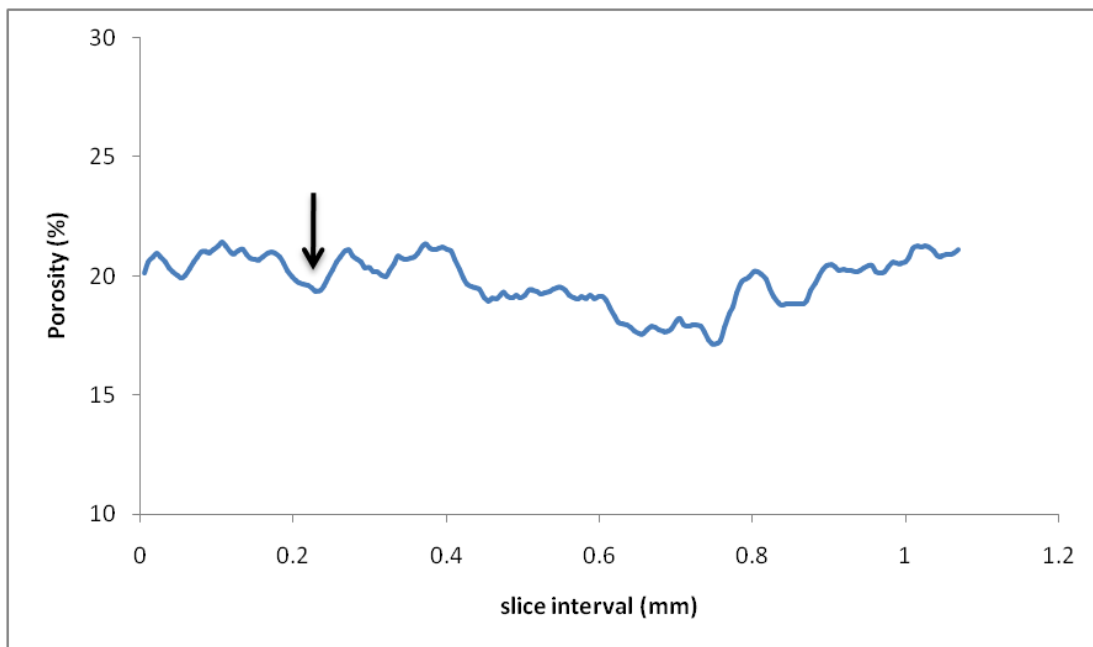


Figure 4.13 Porosity fluctuations within the 3D CT-Scan of Berea Sandstone sample. Arrow indicates the slice which was taken as training image.

Two point correlation function (TPCF)

The assumption to reconstruct 3D porous media from a 2D image is the input which should represent a homogenous and isotropic sample [9] [17] [68]. TPCF was used to determine the geometrical micro structural spatial arrangement of the Berea sandstone training image which was selected in the training image selection part.

Figure 4.14 shows two orthogonal (vertical and horizontal) TPCF graph from the training image of Berea sandstone. Since TPCF shows the spatial probability of certain simple geometrical arrangements of the image, TPCF can be used to identify the structural type of sample. The differences between vertical and horizontal TPCF graphs are negligible and indicate that the training image is nearly isotropic. With the assumption of mm scale, a training image also can be assumed as homogenous. With this condition, the training image is ready to be used for porous media reconstruction. The porosity of the training image is 19.8 %. The porosity is calculated based on Equation 3.4.

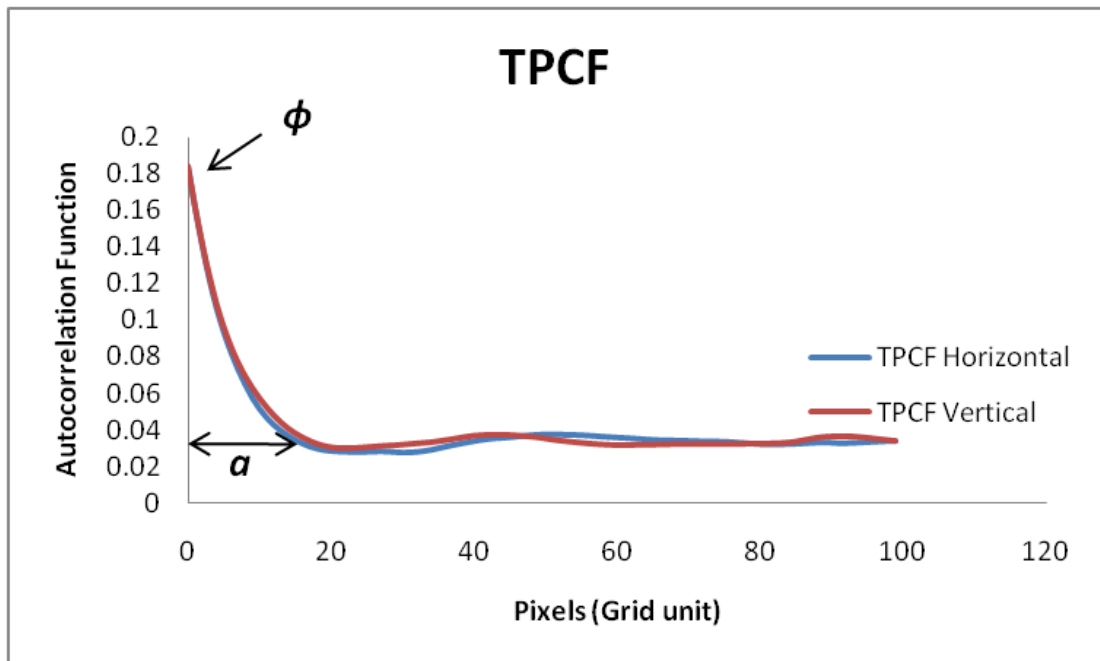


Figure 4.14 Horizontal and vertical TPCF graph from Berea sandstone training image. The graphs of TPCF are align showed that the training image is isotropic.

The autocorrelation length (a) observed from the graph is about 20 grid units (Figure 4.14). Based on previous work [17] [68], for accurate simulation of absolute permeability, the size of the samples should be $10 a$, which means that 200×200 pixels is an appropriate size for training image

2D to 3D porous media reconstruction of Berea Sandstone

There are three input parameters to reconstruct porous media; porosity, variogram and sample points. All parameters were calculated and extracted from the training image (2D image). The porosity and variogram were calculated using Equations 3.4 and 3.6.

Figure 4.15 shows the selected training image from a sample of the Berea sandstone on SGEMS user interface. The training image was initially on image format (JPEG or BMP). The training image was reformatted to SGEMS format before it was used for simulation. The effective size for 2D to 3D porous media reconstruction method and fluid flow simulation is 100 voxels. Since the input was 200 square pixels, the image needed to be reduced to 100 square pixels. Due to the change of size, the resolution of the image changed from $5.3 \mu\text{m}$ (200 square pixels) to 10.6 (100 square pixels) μm . This resolution is still in good agreement based on the preliminary study in Section 4.2.

Figure 4.16 shows the variogram calculated from the x and y directions of Berea sandstone training image. The variogram model for input simulation was decided based on these variograms. Equation 3.8 was used to calculate variogram model and used as an input for simulation.

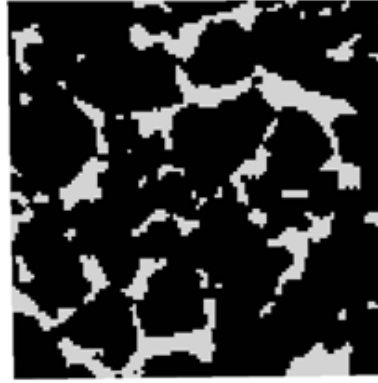


Figure 4.15 Berea sandstone Training image on SGEMS user interface. The image was reformatted from JPEG format to SGEMS format.

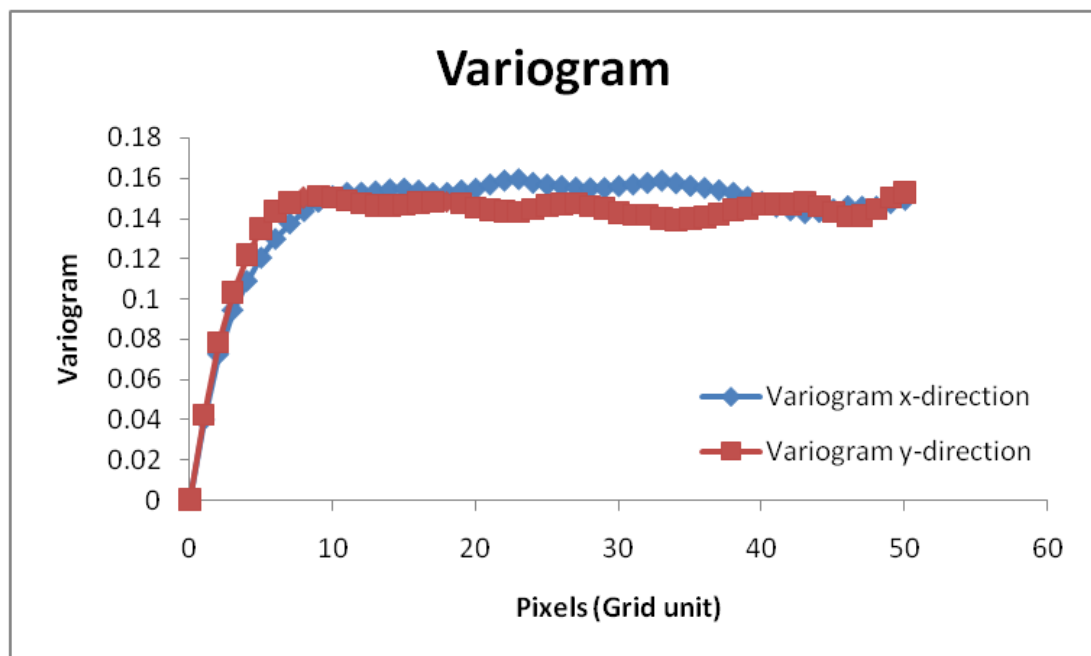


Figure 4.16 Variogram calculated from training image from x and y direction. The variograms are aligned showing that the image is isotropic.

Figure 4.17 shows the sample points extracted from the training image of Berea sandstone. The sample points are the new input parameter for proposed 3D porous media reconstruction method. The sample points were created using MATLAB and a 3 x 3 extracting template was applied and as a result 0.5 % pixels were extracted from training image. This sample points was used as a conditional data for simulation. This new parameter reduces the computational time to reconstruct 3D porous media from 2D image. The analysis of the computational time improvement is shown in Section 4.5.

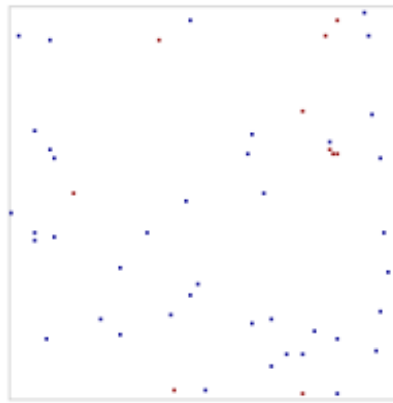


Figure 4.17 Sample points extracted from Berea sandstone training image.

Geostatistical algorithm was used to reconstruct the 3D porous media. The porosity, variogram and sample points as conditional data were used as inputs for this reconstruction. The algorithm was the sequential indicator simulation (SISIM) from SGEMS. Figure 4.18 shows the cross sectional area of a simulated 3D porous media. The statistical parameters were calculated from XY, YZ and ZX planes to verify that the simulated 3D porous media have the same statistical properties as the training image. The variograms of three planes are very close to the variogram model calculated from the training image (Figure 4.19). This verifies that the simulated 3D porous media of Berea sandstone has the same variability with the training image.

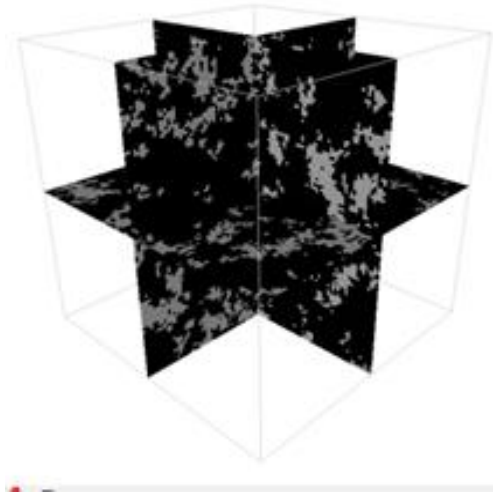


Figure 4.18 Cross sectional areas ($x = 50$, $y = 50$ and $z = 50$) of a reconstructed 3D porous media from 2D image of Berea sandstone. The structure showed that the complexities of Berea sandstone porous media are well preserved.

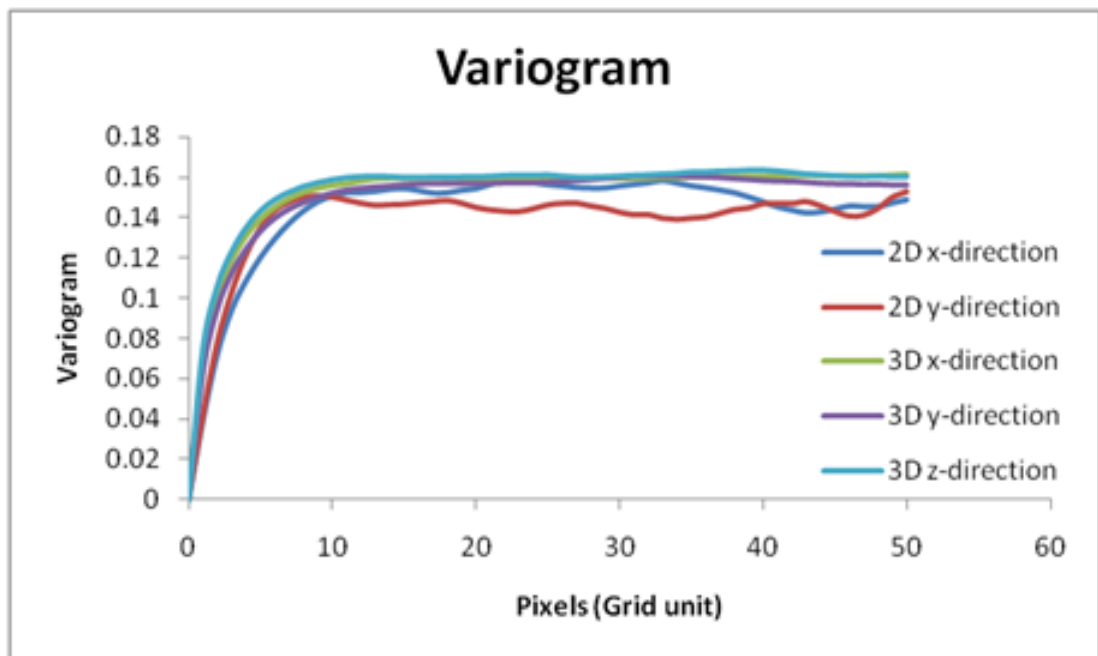


Figure 4.19 Variogram comparison between training image (2D image) and reconstructed 3D porous media. The variograms are aligned for 2D and 3D showing that the images are isotropic.

Figure 4.20 shows the exterior of the simulated 3D porous media of Berea sandstone by geostatistics. The color of pore is shown in white color and grain in black color. MATLAB was used to visualize the exterior and the pore space of the simulated 3D porous media. The absolute permeability was computed in a manner analogous to a laboratory measurement according to the Darcy's equation which directly applied to a simulated 3D porous media. The permeability on the simulated 3D porous media was 1562 mD and on the 3D CT-Scan image was 1360 mD. The permeability from the simulated 3D porous media was in reasonably good agreement with 3D CT-Scan image. The accuracy of this method is about 87%, which shows implicitly that this method produces correct connectivity.

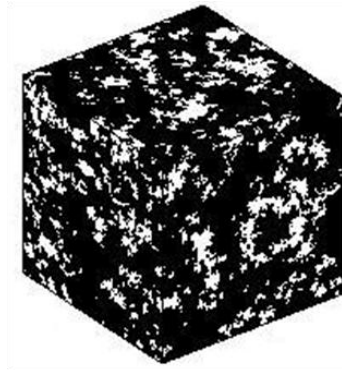


Figure 4.20 Exterior 3D realization of Berea sandstone by geostatistics. The pores are shown in white and grains in black color.

4.4.2 Sandstone S (8) Reconstruction

The 3D porous media reconstructed from 2D image was tested on the second sample, Sandstone S (8). This sample has a size of 300 voxels with a resolution of 4.9 μm per pixel. The calculated porosity of the reference 3D CT-Scan of Sandstone S (8) was 34% and the simulated permeability was 13169 mD. The training image (2D image) was selected in terms of REV and porosity within a 2D slice along with the 3D CT-Scan image of Sandstone S (8).

Representative elementary volume (REV)

There are 30 subsections from the center of the original 300 voxels, ranging from 10 to 300 voxels at an interval of 10 voxels on each edge which were taken to calculate the REV of the CT-scan image of Sandstone S (8). The porosity was calculated on each subsection and the edge length at which porosity converged was used to decide the REV range.

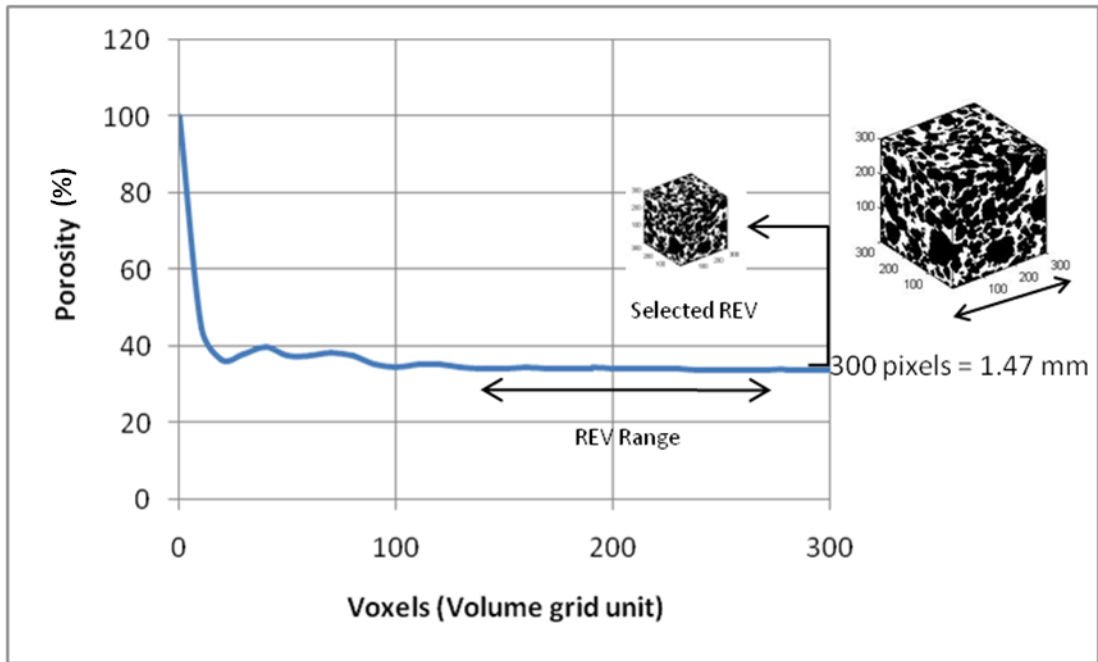


Figure 4.21 The REV graphs for porosity on 3D CT-Scan of Sandstone S (8). The cube on the right shows the original size of 3D image and the cube on the left shows the selected REV cube.

Figure 4.21 shows the calculated porosities of 30 subsections. From the graph the range of REV was decided for 300 voxels cube of Sandstone S (8). The REV range for Sandstone S (8) is from 150 to 300 voxels. To give better representation, 300 voxels was selected as the minimum elementary volume based on REV trends. This size was taken as the input for training image selection. The sample has a good

resolution ($4.9\text{ }\mu\text{m}$ per pixel) and porous (about 34% of porosity), and reducing the size to 100 voxels ($14.7\text{ }\mu\text{m}$ of resolution) is still in good agreement for fluid flow simulation.

Selection of training image

A training image of Sandstone S (8) was selected from 300 voxels of CT-Scan Image. The porosity from each consecutive 2D slices within the cube was calculated. Each of the images gave a different porosity as shown in Figure 4.22. The average porosity was taken as a benchmark and the training image was taken based on this value.

The arrow in Figure 4.23 shows the selected training image to reconstruct the 3D porous media. This image was selected from a 2D slice with an interval of 1.2 mm which had porosity close to the average porosity of 300 images.

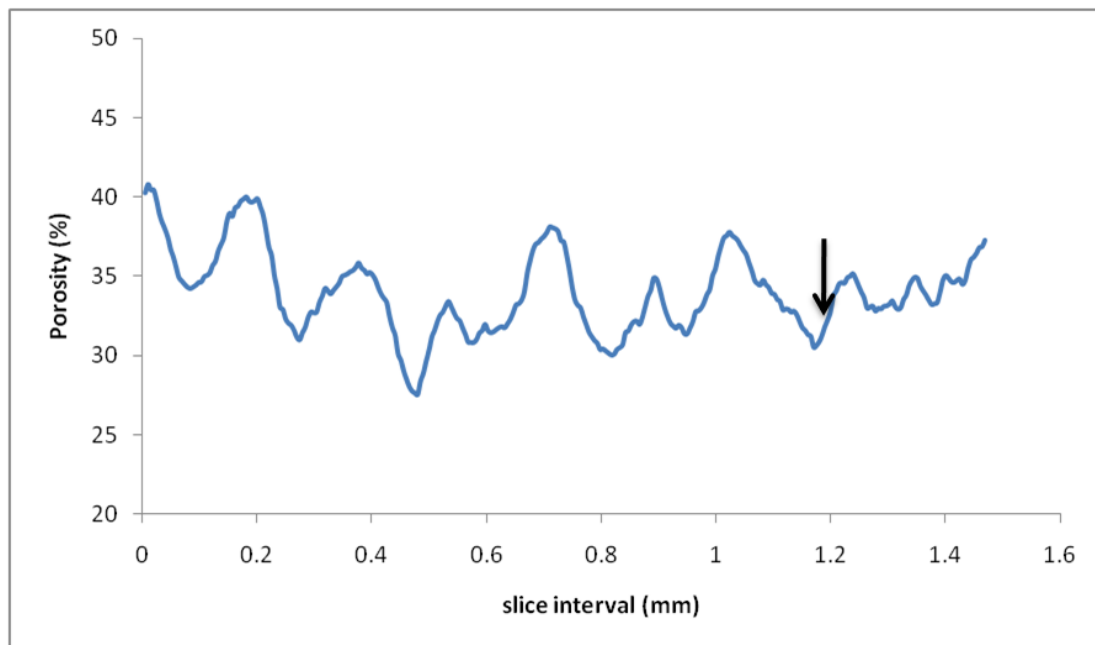


Figure 4.22 Porosity fluctuations within the 3D CT-Scan Sandstone S (8) sample. Arrow indicates the slice which was taken as training image.

Two point correlation function (TPCF)

TPCF was used to characterize the microstructural spatial arrangement of Sandstone S (8) training image. The training image of Sandstone S (8) was selected in training image selection part.

Figure 4.23 shows a two orthogonal (vertical and horizontal) TPCF graph from the training image of Sandstone S (8). The differences of vertical and horizontal TPCF graphs are negligible and indicate that the training image is nearly isotropic. The autocorrelation length (a) is about 20 grid units which can be observed from the TPCF graph (Figure 4.23). The porosity of Sandstone S (8) training image is 35%. The appropriate size for accurate simulation of absolute permeability is $10 a$. The size of 300 x 300 pixels is an appropriate size for training image.

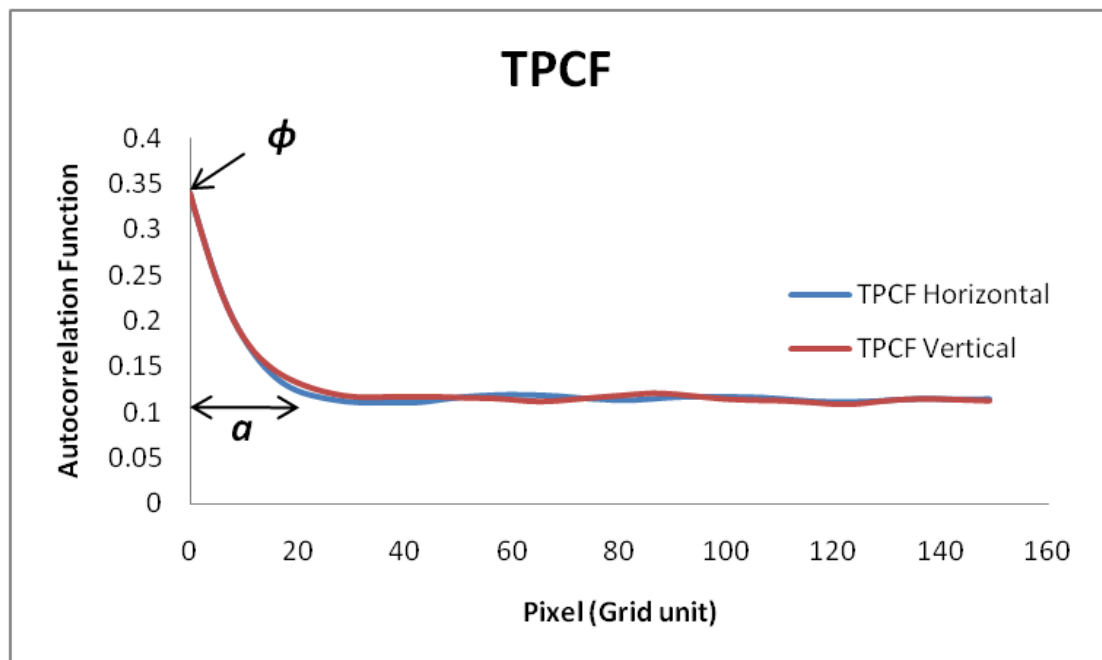


Figure 4.23 Horizontal and vertical TPCF graph from Sandstone S (8) training image. The graphs of TPCF are aligned showing that the training image is isotropic.

2D to 3D porous media reconstruction of Sandstone S (8)

Figure 4.24 shows the selected Sandstone S (8) training image on SGEMS user interface. The training image of Sandstone S (8) was first reformatted to SGEMS format before it was used for simulation. MATLAB was used to reformat the image. The effective size for 2D to 3D porous media reconstruction method and fluid flow simulation is 100 voxels. Since the input was 300 square pixels, the image needs to be reduced to 100 square pixels.

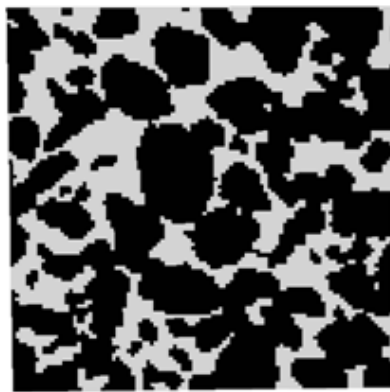


Figure 4.24 Sandstone S (8) training image on SGEMS user interface. The image was reformatted from JPEG format to SGEMS format.

Figure 4.25 shows the variogram calculated from x and y direction of Sandstone S (8) training image. The variogram model for input simulation of Sandstone S (8) was decided based on these variograms.

Figure 4.26 shows the sample points extracted from the training image of Sandstone S(8). The sample points were created using MATLAB and a 3 x 3 extracting template was applied and as a result 0.5 % pixels were extracted from Sandstone S (8) training image. This sample points are used as conditional data for simulation.

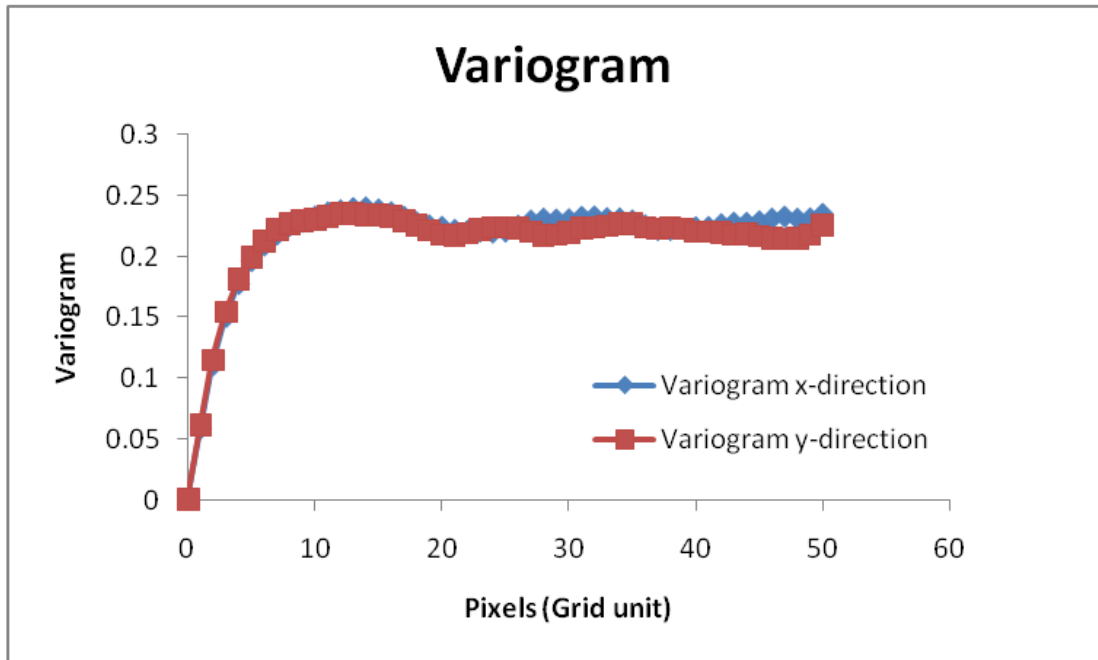


Figure 4.25 Variogram calculated from x and y direction of training image. The variograms are aligned showing that the image is isotropic.

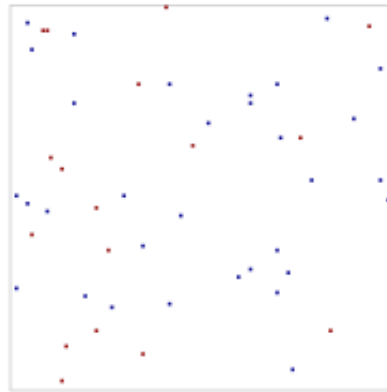


Figure 4.26 Sample points extracted from Sandstone S (8) training image.

The porosity, variogram and sample points as conditional data which were calculated and extracted from Sandstone S (8) training image were used as inputs for this reconstruction. The sequential indicator simulation (SISIM) algorithm from SGEMS was used to reconstruct 3D porous media of Sandstone S (8). Figure 4.27

shows the cross sectional areas of a simulated 3D porous media. The statistical parameters were calculated from XY, YZ and ZX planes to verify that the simulated 3D porous media have the same statistical properties. The variogram of three planes are very close to the variogram model calculated from the training image (Figure 4.28). This verifies that the simulated 3D porous media of Sandstone S (8) has the same variability with Sandstone S (8) training image.

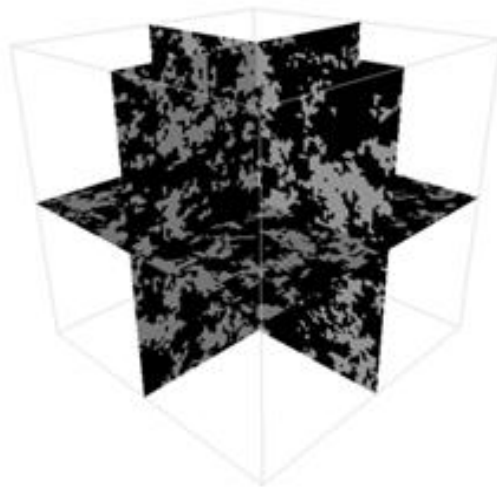


Figure 4.27 Cross sectional areas of a reconstructed 3D porous media from 2D image of Sandstone S (8). The structure showed that the complexities of Sandstone S(8) porous media are well preserved.

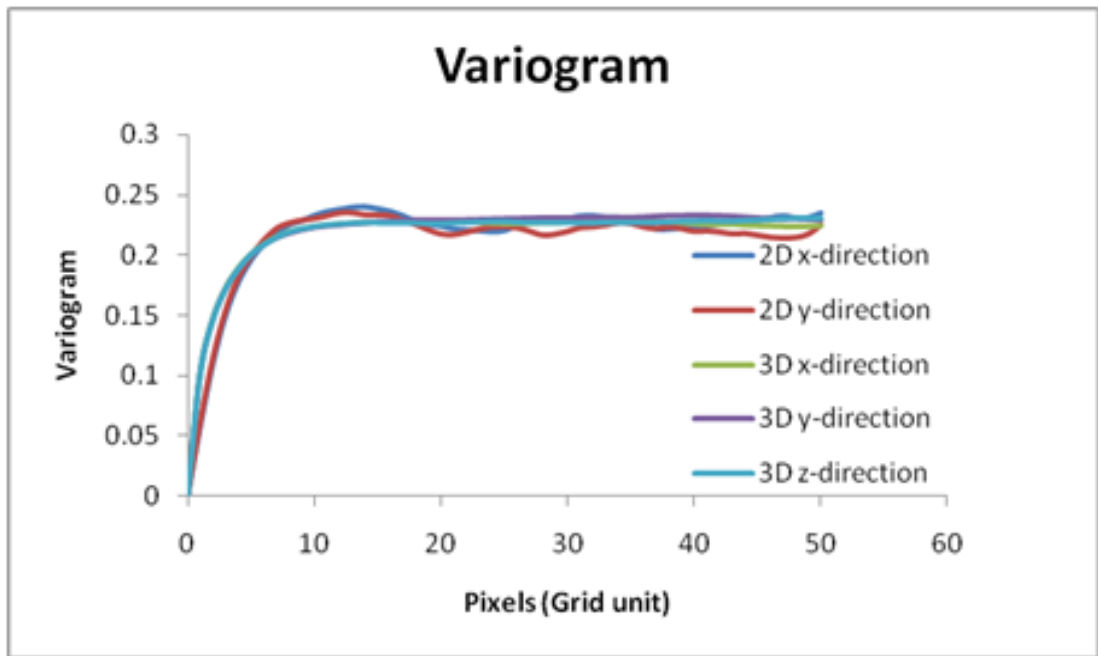


Figure 4.28 Variogram comparison between training image (2D image) and reconstructed 3D porous media. The variograms are aligned for 2D and 3D showing that the images are isotropic.

Figure 4.29 shows the exterior of the simulated 3D porous media of Sandstone S (8) by geostatistics. The pores are shown in white and grains in black color. MATLAB was used to visualize the exterior and the pore space of the simulated Sandstone S (8) porous media. The absolute permeability was computed in a manner analogous to a laboratory measurement according to the Darcy's equation which was directly applied to a simulated 3D porous media. The permeability calculated from the simulated 3D porous media is 13105 mD and 13169 mD on 3D CT-Scan image. Through comparison, the simulated permeability accuracy of this method is about 99%. The permeability from the simulated 3D porous media is in very good agreement with the 3D CT-Scan image, which shows that this method produces correct connectivity of Sandstone S (8).

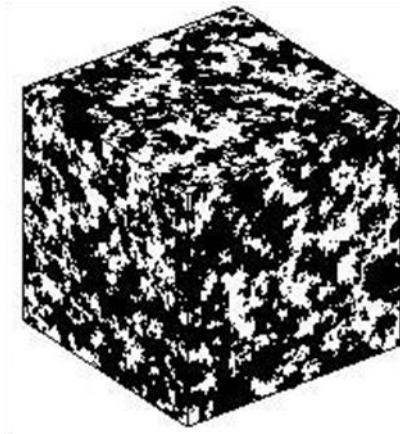


Figure 4.29 Exterior 3D realization of Sandstone S (8) by geostatistics. The pores are shown in white and grains in black color.

4.4.3 Fontainebleau Sandstone Reconstruction

The 3D porous media reconstructed from 2D image was tested on a third sample, the Fontainebleau sandstone. This sample has a size of 144 voxels and a resolution of 15 μm . The porosity of the reference 3D CT-Scan of Fontainebleau is 14.7% and the permeability is 2262 mD. A training image (2D image) was selected in terms of REV and porosity within a 2D slice along a 3D CT-Scan image of Fontainebleau.

Representative elementary volume (REV)

Fourteen subsections from the center of the original 144 voxels, ranging from 10 to 144 voxels at an interval of 10 voxels on each edge were taken to calculate the REV of the CT-scan image of Fontainebleau. The porosity was calculated on each subsection and the edge length at which porosity converged was used to decide the REV range.

Figure 4.30 shows the calculated porosities of the 14 subsections. The cube on the right of the graph in Figure 4.30 is an initial cube of Fontainebleau sandstone. From the graph the range of REV was decided for 144 voxels of Fontainebleau sandstone. The REV range for Sandstone S (8) is from 75 to 144 voxels. The minimum

elementary volume was selected for this sample is 120 voxels. This size was taken as the input for the training image selection prior to the resolution of the image. The resolution of selected REV image is 15 μm per pixel. Reducing the size from 120 to 100 voxels changed the resolution to 18 μm per pixel. This resolution is still in good agreement based on impact of image resolution preliminary study.

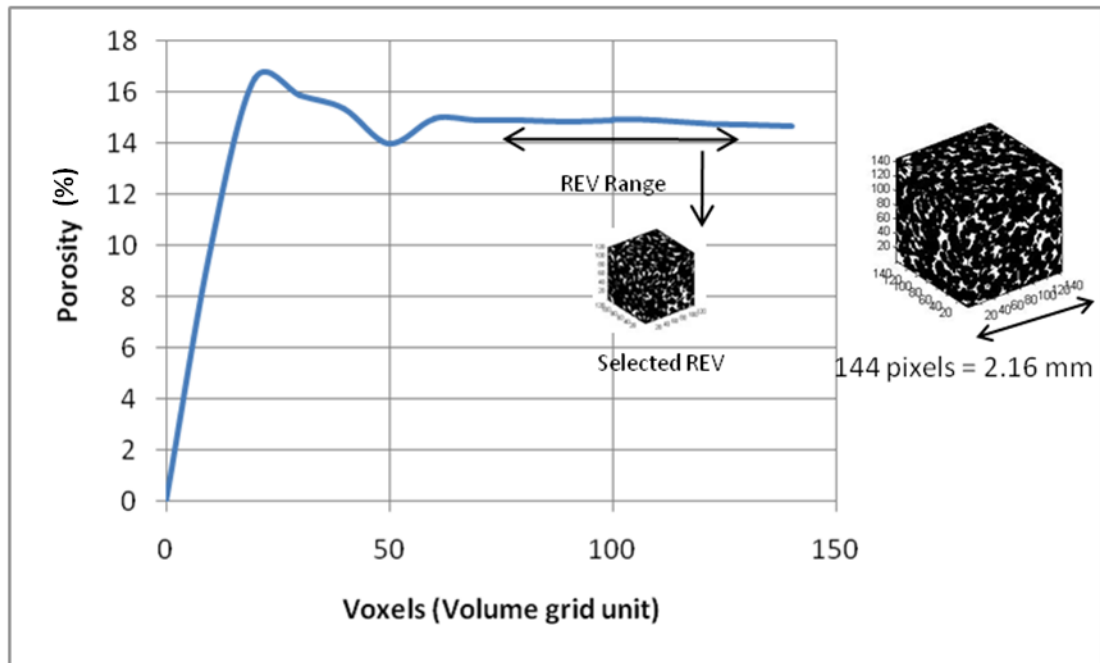


Figure 4.30 The REV graph for porosity on 3D CT-Scan of Fontainebleau sandstone. The cube on the right shows the original size of 3D image and the cube on the left shows the selected REV cube.

Selection of training image

The training image was selected from 120 voxels of Fontainebleau sandstone. The porosity from each consecutive 2D slice within the cube was calculated. Figure 4.15 shows that each of the image gave a different porosity and showed fluctuations. The average porosity was taken as a benchmark and the training image was taken based on this value.

The arrow in Figure 4.31 shows the selected training image to reconstruct the 3D porous media. This image was selected from a 2D slice on interval an interval of 1.1 mm which had porosity close to the average porosity from 120 images.

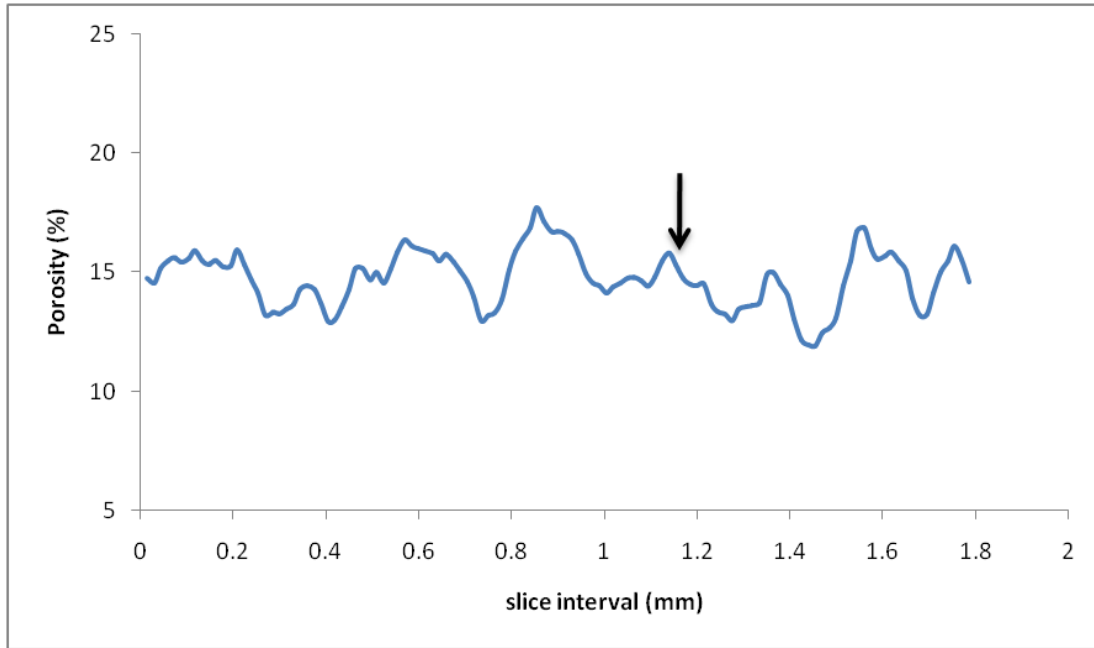


Figure 4.31 Porosity fluctuations within the 3D CT-Scan Fontainebleau sample. Arrow indicates the slice which was taken as training image.

Two point correlation function (TPCF)

TPCF was used to characterize the micro structural spatial arrangement of Fontainebleau sandstone training image. The training image was selected in the training image selection part.

Figure 4.32 shows a two orthogonal (vertical and horizontal) TPCF graph from the training image of Fontainebleau sandstone. The TPCF shows the spatial probability of certain simple geometrical arrangements of the image. The differences of the vertical and horizontal TPCF graphs are negligible and indicate that the training image is nearly isotropic. The autocorrelation length (a) is about 10 grid units which

can be observed from the TPCF graph (Figure 4.32). The porosity of the Fontainebleau sandstone training image is 15.1%. The appropriate size for accurate simulation of absolute permeability is $10a$. A size of 120x120 pixels is appropriate for the training image.

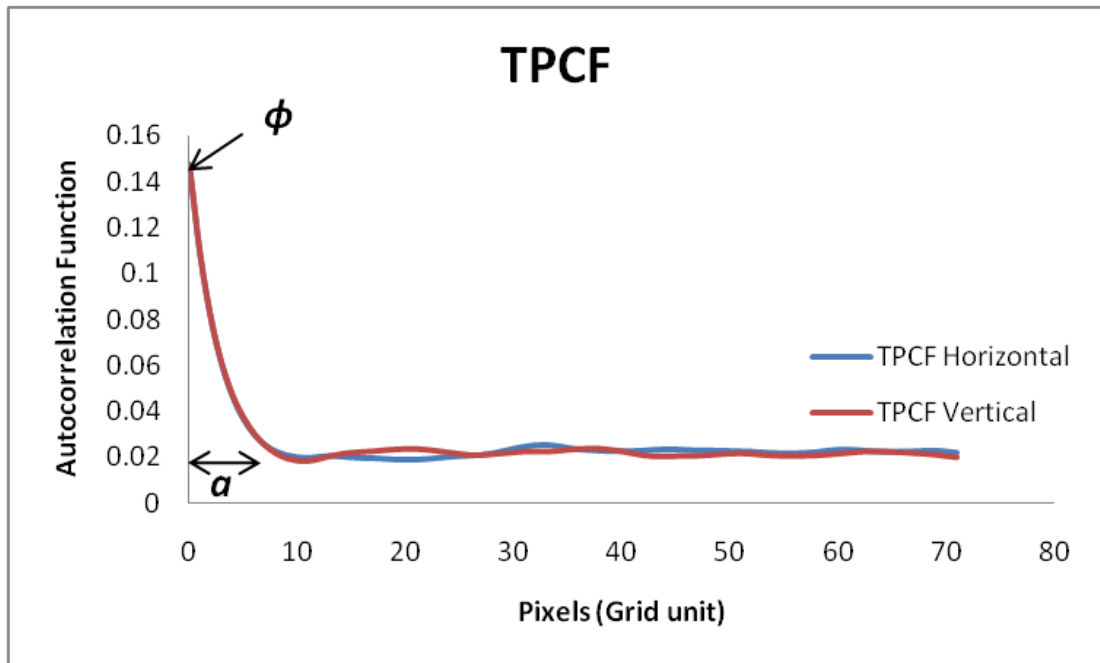


Figure 4.32 Horizontal and vertical TPCF graph from Fontainebleau sandstone training image. The graphs of TPCF are aligned showing that the training image is isotropic.

2D to 3D porous media reconstruction of Fontainebleau sandstone

Figure 4.33 shows the selected training image from Fontainebleau sandstone on SGEMS user interface. The training image was initially on image format (JPEG or BMP). The training image was reformatted to SGEMS format before it was used for simulation. The effective size for 2D to 3D porous media reconstruction and fluid flow simulation is 100 voxels. Since the input was 120 square pixels, the image need to be reduced to 100 square pixels for the input of the 3D reconstruction method.

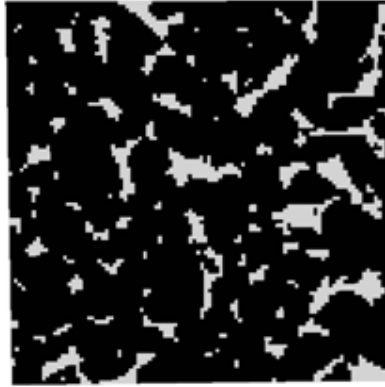


Figure 4.33 Fontainebleau sanstone training image on SGEMS user interface. The image was reformatted from JPEG format to SGEMS format.

Figure 4.34 shows the variogram calculated from the x and y directions of Fontainebleau sandstone training image. The variogram model for input simulation was decided based on these variograms. Figure 4.35 shows the sample points extracted from the training image of Fontainebleau sandstone. These sample points were used as a conditional data for simulation.

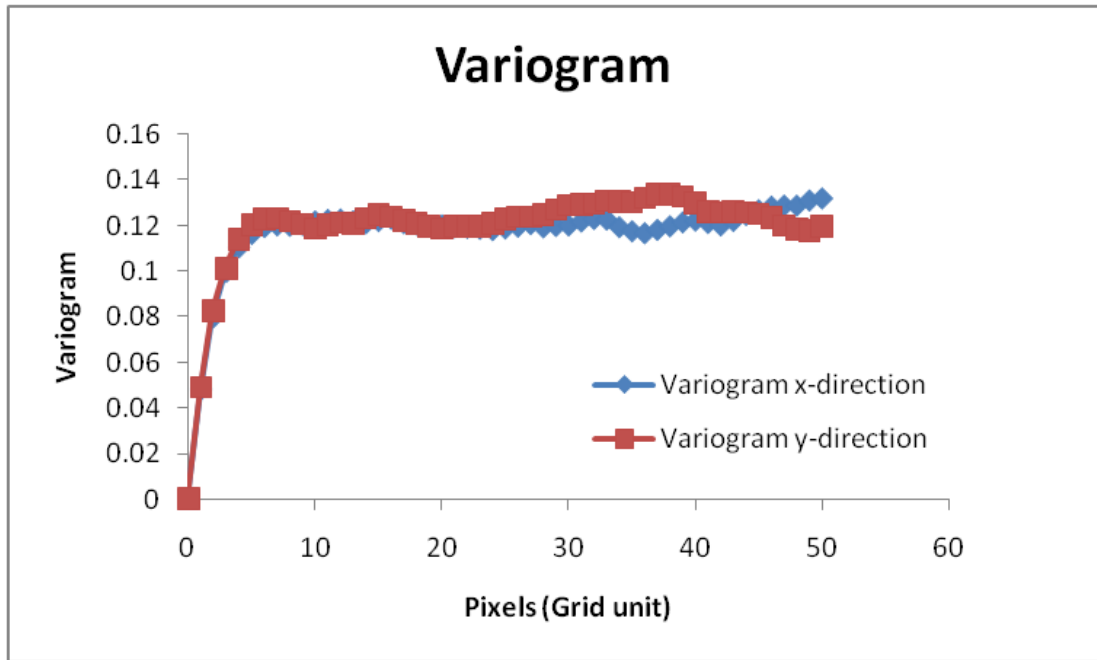


Figure 4.34 Variogram calculated from x and y direction of training image. The variograms are aligned showing that the image is isotropic.

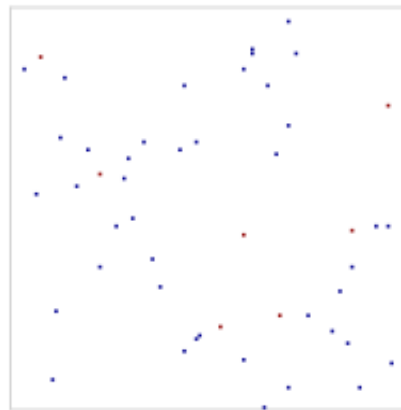


Figure 4.35 Sample points extracted from Fontainebleau sandstone training image.

Geostatistical algorithm was used to reconstruct the Fontainebleau sandstone porous media. The porosity, variogram and sample points as conditional data were used as inputs for this reconstruction. Figure 4.36 shows the cross sectional areas of a simulated 3D porous media of Fontainebleau sandstone. Figure 4.37 shows the

statistical parameters that were calculated from XY, YZ and ZX planes to verify that the simulated 3D porous media have the same statistical properties. The variogram of three planes are very close to the variogram model calculated from the Fontainebleau sandstone training image. This verifies that the simulated 3D porous media has the same variability with training image.

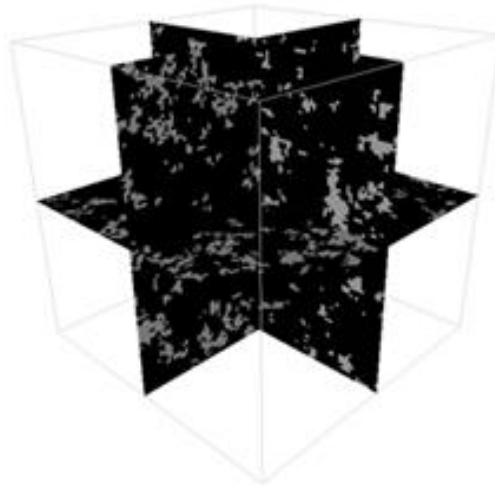


Figure 4.36 Cross sectional areas of a reconstructed 3D porous media from 2D image of Fontainebleau. The structure showed that the complexities of Fontainebleau sandstone porous media are well preserved.

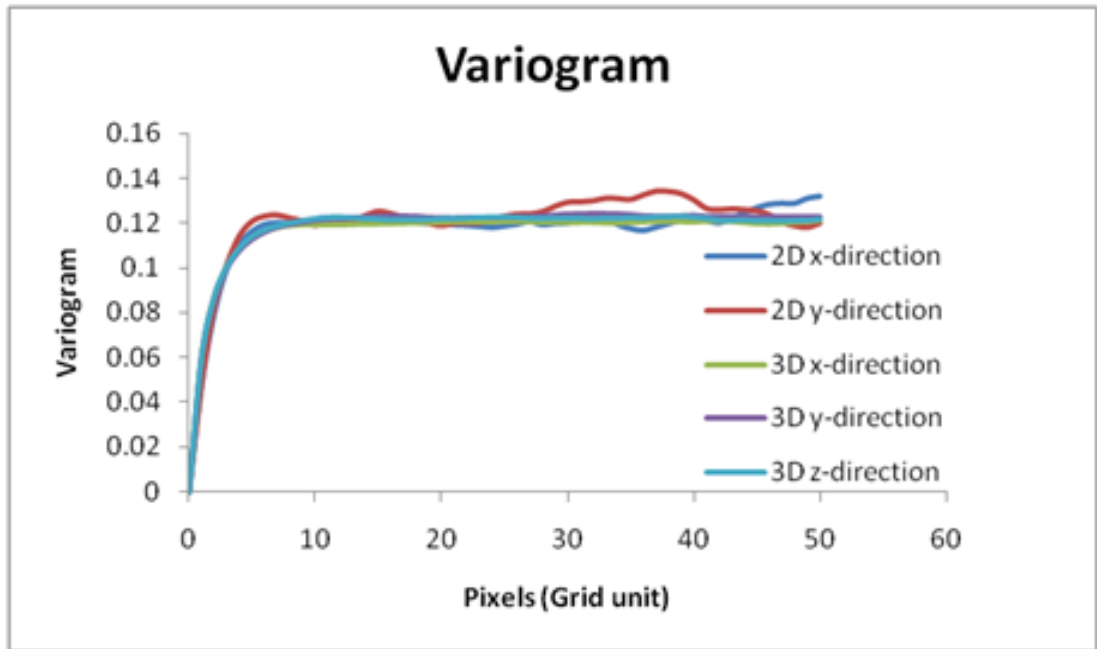


Figure 4.37 Variogram comparison between training image (2D image) and reconstructed 3D porous media. The variograms are aligned for 2D and 3D showing that the images are isotropic.

Figure 4.38 shows the exterior of the simulated 3D porous media of Fontainebleau sandstone by geostatistics. The pores are white and the grains are black in color. MATLAB was used to visualize the exterior of the simulated 3D porous media. The absolute permeability was computed and directly applied to a simulated 3D porous media. Permeability calculated from the simulated 3D porous media is 1550 mD and 2262 mD on the 3D CT-Scan image. The simulated permeability on the 3D porous media is in reasonably good agreement with an accuracy of about 70% when compared with the 3D CT-Scan image. Thus implicitly shows that this method produces good connectivity on Fontainebleau sandstone sample.

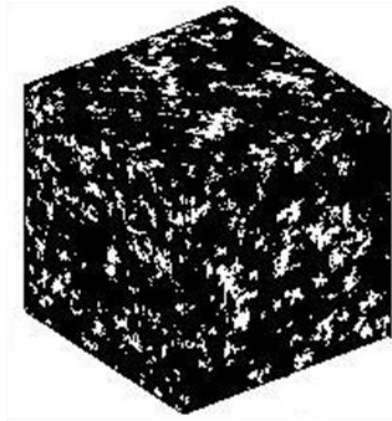
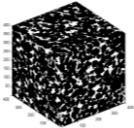
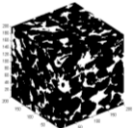

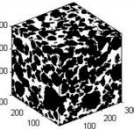
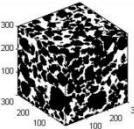

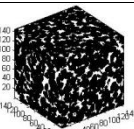
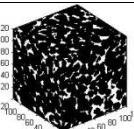

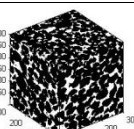
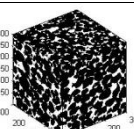

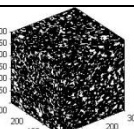
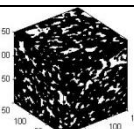
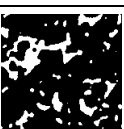
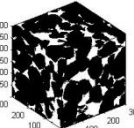
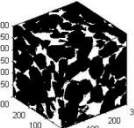



Figure 4.38 Exterior 3D realization of Fontainebleau sandstone by geostatistics.
The pores are shown in white and grains in black color.

4.5 Validation of 2D to 3D Porous Media Reconstruction

The porous media reconstruction method was tested on six samples. The steps and results of three samples have been discussed in detail in the previous section. Table 4.2 below shows briefly the results of six samples after the reconstruction method and simulation of fluid flow.

Table 4.2 Comparison of physical properties obtained from reconstruction and CT-Scan image.

| | Original 3D CT-Scan | Selected REV Size | Training Image | Original 3D CT-Scan | | Reconstructed 3D Porous Media | |
|------|---|---|---|---------------------|----------|-------------------------------|----------|
| | | | | ϕ (%) | k (mD) | ϕ (%) | k (mD) |
| B |  |  |  | 19.6 | 1360 | 19.8 | 1512 |
| | 400 ³ | 200 ³ | 200 ² | | | | |
| S(8) |  |  |  | 34 | 13169 | 35.1 | 13105 |
| | 300 ³ | 300 ³ | 300 ² | | | | |
| F |  |  |  | 14.7 | 2262 | 15.1 | 1550 |
| | 144 ³ | 120 ³ | 120 ² | | | | |
| S(2) |  |  |  | 24.6 | 3898 | 25.8 | 4244 |
| | 300 ³ | 300 ³ | 300 ² | | | | |
| S(4) |  |  |  | 17.1 | 215 | 18.5 | 187 |
| | 300 ³ | 150 ³ | 150 ² | | | | |
| S(5) |  |  |  | 21.1 | 4651 | 21.2 | 3954 |
| | 300 ³ | 300 ³ | 300 ² | | | | |

The REV size was selected based on study on the impact of image resolution and image size in Section 4.2. The autocorrelation length (a) was also used as a parameter to justify the length size of REV. Based on the literature [17], the best length that contain the repetitiveness of the sample should be $L \geq 10 a$. The best resolution grid for fluid flow simulation should be $dx \leq a/10$. The entire selected images for training image fulfill the requirement of $L \geq 10 a$. On the resolution grid not all samples fill the requirement of $dx \leq a/10$. However the selected training image can still be considered a good training image since the samples have good image resolution.

For example, the REV sizes of training image on samples S (8), S (2) and S (5) were taken as 300 x 300 pixels. This is the maximum size of the REV ranges. However, decreasing the resolution to 100 x 100 pixels as an input for simulation on SGEMS is still in good agreement since the samples have good resolution of the image (4.9 μm , 5 μm and 4 μm). For Fontainebleau sandstone and S (4), their respective resolution of 15 μm and 9 μm per pixel is not as good as the other three samples. The best minimum representative volumes were selected on 120 and 150 voxels. The high accuracy on the reconstructed method as compared with CT-Scan data is due to the comparison on the same scale size, which is in millimetre scale.

4.6 Effectiveness of Grain Size Vertical Profile

The grain size vertical profile method is to determine grain size from the digital image of a sediment. The digital image can be acquired from thin sections using microscope or SEM. This method was introduced by Rubin [79]. The basic principle of this method is to calculate the spatial autocorrelation based on the intensities of corresponding pixels of the image. The autocorrelation curve is computed for each row of pixels in the image and grain size is related to the mean autocorrelation for the average of pixels offsets. From this method, the coarsening and fining trends can be determined but not the actual grain size of the sediment [80]. Figure 4.39 shows the effectiveness of this method in the determination of coarsening and fining trends in a digital image of sandstone.

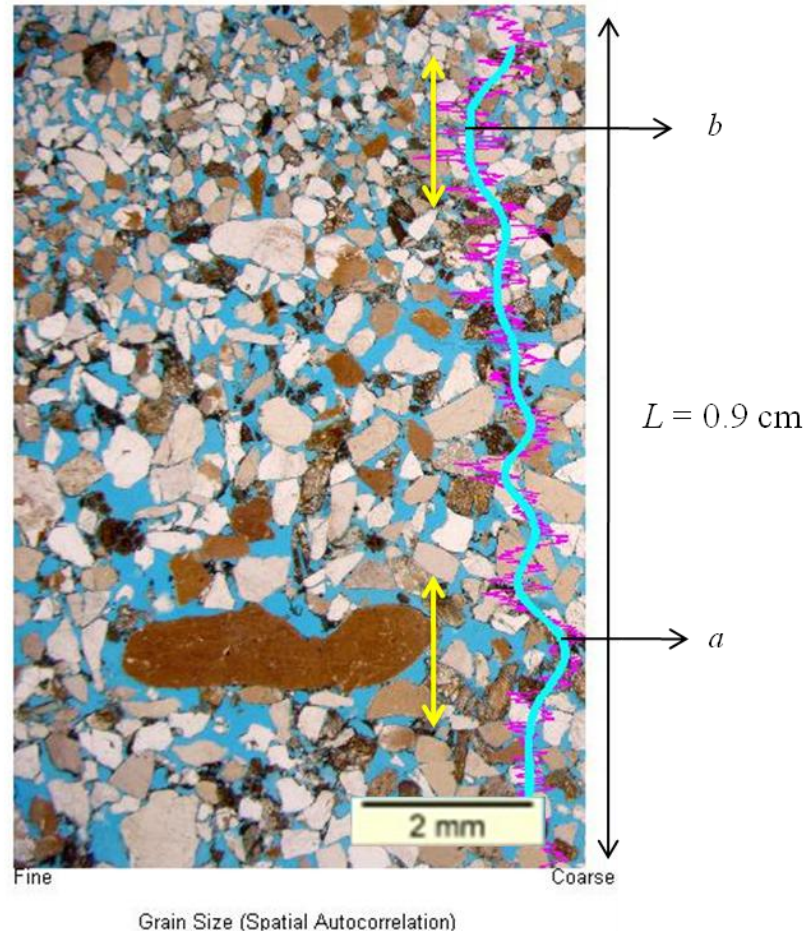


Figure 4.39 Grain size vertical profile in a thin section. The arrow a with the yellow line is the coarse area (porous) and the arrow b with the yellow line is the fine area (tight).

Figure 4.39 shows the trends of coarsening and fining of sandstone. The area marked by the yellow arrow b demarcates the fining part of the thin section. This area can be clearly observed on the image. The area marked by the yellow arrow a demarcates the coarsening part of the thin section. The coarse grains can be observed clearly on the area marked by a . We can assume that the bigger the grain size (coarse) the sample is usually more porous. However, the smaller the grain size (fine) the sample is usually tighter. Using this as quality control from a thin section will differentiate between porous and tight areas in a thin section. From this the heterogeneities of a thin section at cm scale can be resolved.

4.7 Upscaling Permeability: Pore to Core Plug Scale

A combination of 2D to 3D porous media reconstruction and fluid flow simulation can be a robust tool to estimate permeability from a thin section image. Sections 4.4 to 4.5 show the accuracy of permeability determination using these methods. Sample points as conditional data were used to modify the non-modified method. The non-modified method was introduced by Keehm [17]. Results showed that this modification had an effect on the computational time and made reconstruction time more effective (Section 4.3).

Although it is easy to implement, the computational task to generate 3D porous media and fluid flow simulation which can be handled by a standard personal computer and in real time can only be implemented in mm scale. Permeability determination can be accurate if the thin section is homogenous at core plug scale. A comparison through this method can only be precise if it is compared on the same scale (mm to mm scale). At this size, it may not cover sample heterogeneity at laboratory scale (cm scale). A full image of a thin section, in principle, has a similar scale with the laboratory scale.

To overcome these problems upscaling method was applied. Building blocks for upscaling purposes were created based on grain size vertical profile. A grain size vertical profile which shows the trends of coarser and finer parts of a full thin section image was calculated based on Equation 3.11.

There are two inputs to use the upscaling permeability formula, and they are, fraction and permeability from each block. The fraction estimation of the coarse and fine parts can be separated based on information from the grain size vertical profile trends. Each image which represents the coarse and fine part of thin section will be used as an input for the 2D to 3D porous media reconstruction method. The porosity and permeability were calculated from the 3D porous media (mm scale) and used as an input for upscaling (mm to cm scale). These workflows were applied on thin section of the Berea sandstone and sandstone from the Malay Basin.

4.7.1 Application of Upscaling Permeability Workflow to Berea Sandstone Thin Section

A section from the Berea sandstone core plug was cut vertically and made into a thin section. The core plug has a laboratory-measured porosity of 17.5% and a Klinkenberg-corrected air permeability of 196.3 mD. Upscaling permeability workflow was applied on the Berea sandstone thin section. This workflow was compared with laboratory data to demonstrate the accuracy of the workflow.

Figure 4.40 shows scale comparison between the core plug and a full length of a thin section of the Berea sandstone. The core plug used in this study is shown on the left. The core plug has a length of 2 inch (5.08 cm) and a diameter of 1 inch (2.54 cm). A section was cut vertically from the core plug and made into a thin section (right figure). The reason is to create an image from a thin section similar in scale as the core plug scale. There is no information about bedding plane of the core plug. The permeability flow measurement was conducted following the direction of the blue arrow which is shown on Figure 4.40.

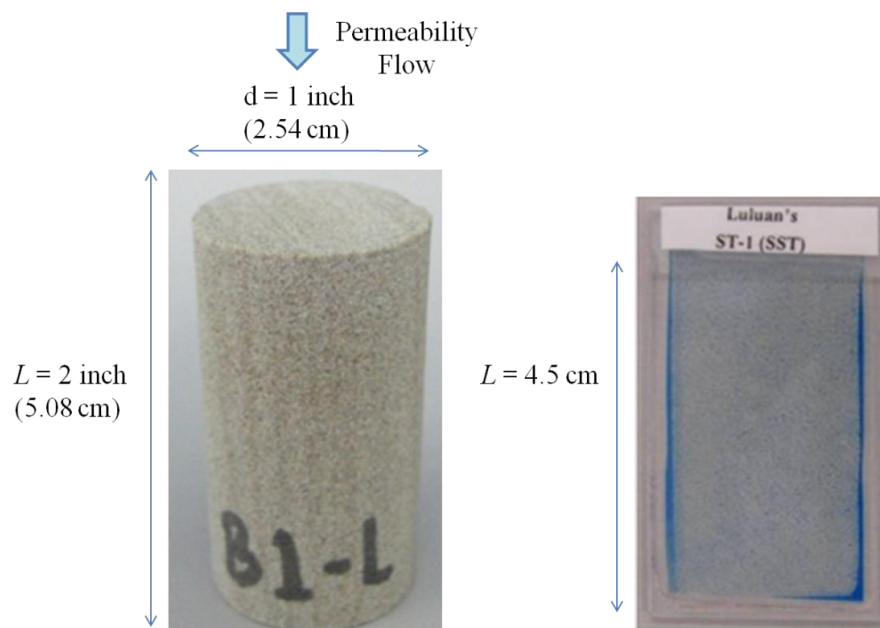


Figure 4.40 Scale comparison between a core plug and the full length of a thin section of the Berea sandstone. The length of a full thin section image is 4.5 cm.

4.7.1.1 Full thin section image of the Berea sandstone

The first step of the workflow is to acquire a full thin section image. The assumption in this study is that a full thin section image has a similar scale (cm scale) with the core plug. Permeability measurement on the core plug is traditionally used as permeability spatial distribution input for reservoir modelling. In this step, a full thin section image was captured using a microscope. A magnification of 12.5 times was selected. This magnification is appropriate to cover all areas of thin section with good resolution and minimal number of images. Through this magnification, a full thin section image at cm scale can be covered with nine images. These images were collected and stitched together into one image. Figure 4.41 shows the workflow and process of image collection and stitching to create a full thin section image.

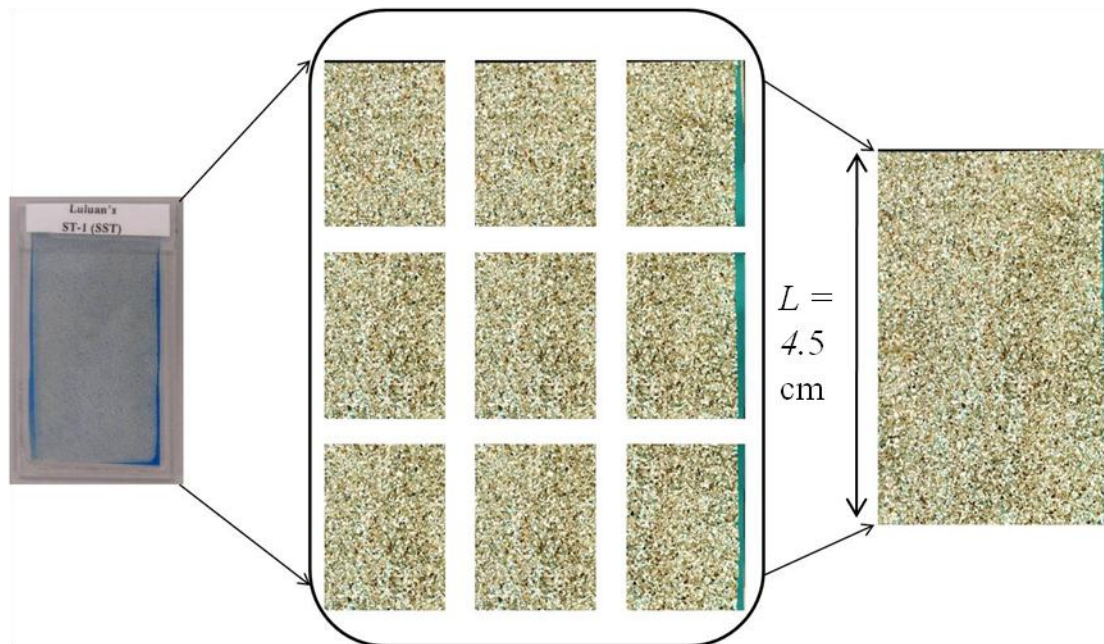


Figure 4.41 Image acquisition and stitching processes on full thin section image of Berea sandstone. Nine images were acquired (middle) by using the 12.5 times magnification. The length of the image (right) after the stitching process is 4.5 cm.

The nine images in the middle of Figure 4.41 are images of the Berea sandstone thin section taken with a 12.5 times microscope magnification. These images were taken under cross-polarization. The cross-polarization light gave a color contrast on each type of mineral. The overlay on each image is around 20%. The purpose of the overlay is to identify the common areas of each image for the stitching process. With these conditions stitching of the images is easier to conduct. The figure on the right of Figure 4.41 shows the result of nine images stitched together to form an image of 4.5 cm length.

4.7.1.2 Grain size vertical profile and building blocks of full thin section image of the Berea sandstone

Once a full thin section image has been acquired, the next step is to calculate the grain size vertical profile trends normal to the length of the thin section. The first reason for calculating in this direction is because the permeability flow (K_n) was measured in this direction. Second, we assume that low variation occurred on the lateral side of the thin section in relation to the permeability flow. The grain size vertical profile was applied on the full thin section image and calculated using MATLAB. The grain size vertical profile was calculated using Equations 3.11.

The spatial autocorrelation was calculated based on the intensities of the corresponding pixels of the image. From this the coarsening and fining trends could be determined. Figure 4.42 shows the grain size vertical profile calculated from a full thin section image of the Berea sandstone.

The grain size vertical profile trends were calculated on a full thin section image of the Berea sandstone. The length of coverage of the grain size vertical profile trend is 4.5 cm. With this length, we assume that these trends profile has a similar scale with the core plug. The autocorrelation curve was computed for each row of pixels on a full thin section image of Berea sandstone. The grain size vertical profile trends are related to the mean autocorrelation for a range of pixel offsets.

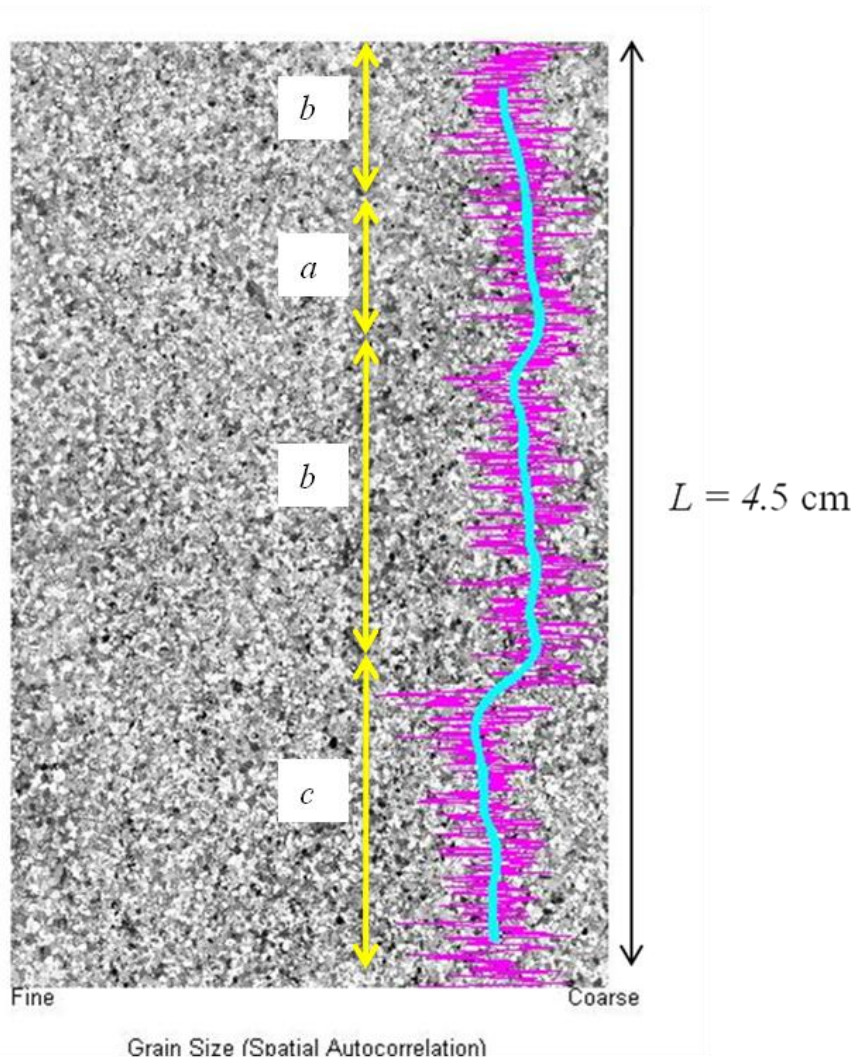


Figure 4.42 Grain size vertical profile trends on full thin section image of Berea sandstone. The pink trends show the profile before smoothing and the blue trends show the profile after smoothing.

The pink trends show the statistical intensity values of each row which were calculated from each pixel. The results were noisy because the statistics of each row were calculated for small samples. The noise on the pink trends was reduced by smoothing and averaging successive rows. The result of smoothing is shown on the blue trends as a smooth line. Calculations for this vertical grain size profile took less than 1 second on an 8 GHz personal computer.

The smoothing (blue) trends on a full thin section image of the Berea sandstone showed the coarsening and fining part of the image. Based on the trends, there were three sections where the blue line had bends. A right bending was observed on area *a* and this right bending indicated that the area had coarse grain. Based on literature [79], the coarse grain area is more porous and fine grain area is less porous.

Since three types of bending were observed, it could be assumed that the far left bending represented an area with fine grains (tight). This type of bending is shown on area *c*. Area *b* is classified as the representative of the patchy area as classified by Kameda [9]. Kameda classified into three types, namely coarse (porous), fine (tight) and mixed (patchy).

From observation on the trends, we could conclude that area *a* has the coarsest grains, area *b* is coarser than area *c*, and area *c* has the finest grain. Building blocks for upscaling were created based on the classification of these areas and it was assumed that low variation occurred on the lateral side of the thin section. The length of each area is indicated by a yellow arrow marked as *a*, *b* and *c*. The fractions for upscaling permeability were determined based on these lengths.

4.7.1.3 Upscaling permeability workflow on the Berea sandstone thin section

The weighted arithmetic and harmonic mean was used to determine the permeability on sandstone/shale reservoir sequences. The weighted arithmetic mean was used to average permeability values parallel to bedding (horizontal) direction, while weighted harmonic mean is used to average the permeability values perpendicular to bedding (vertical) [81] [82].

The same concept was applied to the upscaling permeability workflow. The building blocks were created based on the grain size vertical profile trends of a full thin section image. Since the whole area of thin section was in cm scale (similar to the scale with the core plug), it was assumed that permeability anisotropy of the core plug was covered.

The permeability determined directly using the 2D to 3D porous media was sometimes higher or lower than those derived from core plug measurement. The reason is because of the heterogeneity of the core plug and the input for this was only in mm scale. Since the input for permeability measurement for reservoirs usually come from core plug measurements, permeability determination from this method needs to be upscaled.

In order to test the accuracy of the upscaling permeability workflow, the workflow was applied on a full thin section image where the permeability was already known from laboratory test. In the example, a full thin section image of the Berea sandstone was used. There are two inputs for the upscaling formula, namely, fraction and permeability from each block. The fraction is based on the grain size vertical profile trends. As shown in Figure 4.42, there are three areas: *a*, *b* and *c*. The permeability (*k*) at pore scale size from each image representative building block is estimated using 2D to 3D porous media reconstruction and fluid flow simulation.

A total of 35 images were collected using a microscope with 40 times magnification and plane-polarized light. This magnification was appropriate for the input of 2D to 3D porous media reconstruction. Plane-polarization was used for easier image processing and pore grain segmentation. From the 35 images, three images which represented the *a* or porous area (coarse grain), *b* or patchy area and *c* or tight area (fine grain) were selected. It was assumed that low variation occurred on the lateral side of the thin section. The selection of each image on each block was then justified.

The 2D to 3D porous media reconstruction and fluid flow simulation was applied to estimate the permeability at pore scale from each image. Figure 4.43 shows the building blocks and the application of the upscaling permeability workflow on a full thin section image of the Berea sandstone.

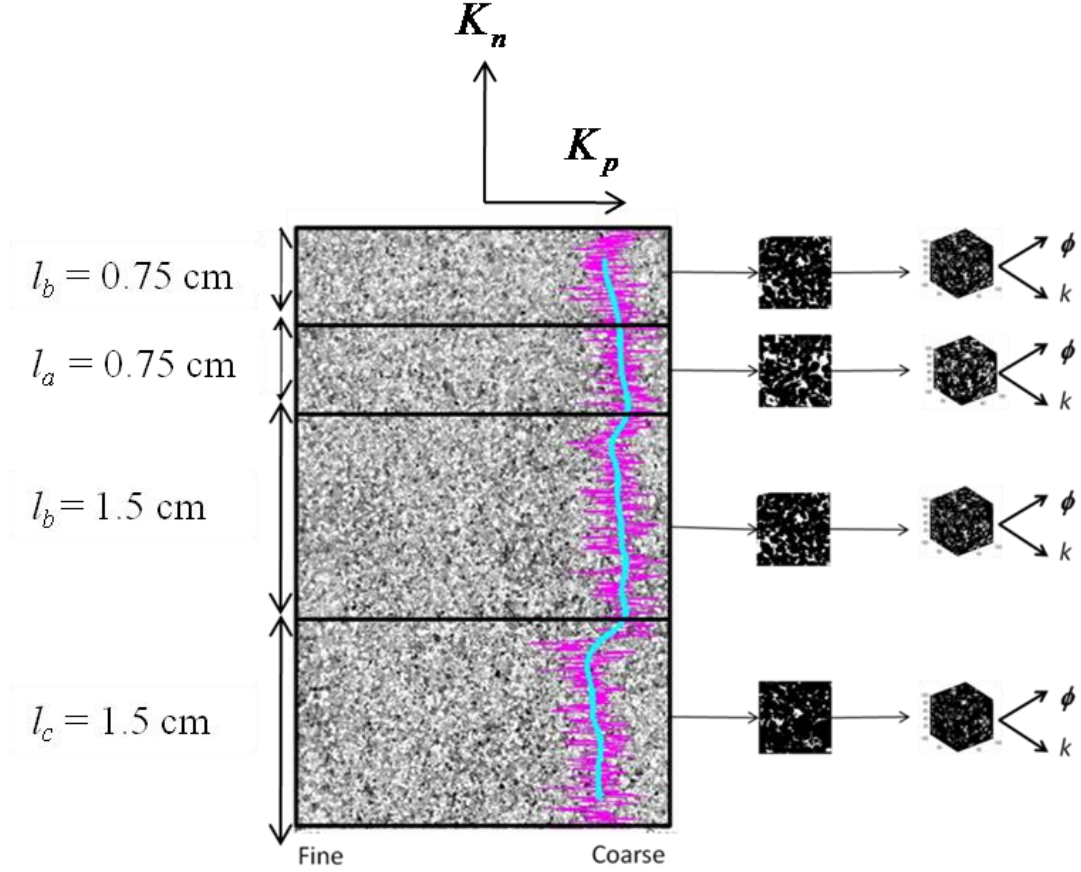


Figure 4.43 Building blocks for upscaling permeability workflow on a full thin section image of the Berea sandstone. The building blocks and fractions of heterogeneity are shown in the middle and the pore scale permeability estimations on each block of the Berea sandstone thin section are shown on the right.

Based on the grain size vertical profile, the length fraction of porous area (l_a) was 0.75 cm, the length fraction of the patchy areas (l_{b1}) was 0.75 cm and (l_{b2}) 1.5 cm and the length fraction of the tight area (l_c) was 1.5 cm.

The three images which represented the porous area, patchy area and tight area were collected. Image processing and segmentation processes were applied on these images to obtain 2D binary images. The resolution of each image after these processes was 10 μm per pixel with a size of 100 square pixels. The size and resolution are of appropriate size as mentioned in Section 4.2. These images were used as inputs to

estimate the permeability from each building block using 2D to 3D porous media reconstruction and fluid flow simulation. The workflow followed the steps in the simulation study. An estimation of the porosity and permeability from each image are summarized in Table 4.3.

Table 4.3 Estimation of porosity and permeability from each representative building block of the Berea sandstone thin section.

| Type | Porosity (%) | Permeability (mD) |
|------------------------------|--------------|-------------------|
| Porous / Coarse (<i>a</i>) | 20.1 | 1002.1 |
| Patchy (<i>b</i>) | 15.2 | 382.5 |
| Tight / Fine (<i>c</i>) | 9 | 73.6 |

Equations 3.12 and 3.13 for upscaling were used to estimate the effective permeability in the vertical and horizontal directions at laboratory (core plug) scale. The resulting estimates of upscaling porosity and permeability are summarized in Table 4.4

Table 4.4 Comparison between the porosity and permeability from upscaling workflow on thin section and core plug measurement on the Berea sandstone.

| Type | Porosity (%) | Permeability (mD) |
|---------------------|--------------|-------------------|
| Core Plug | 17.5 | 196.3 |
| Upscaling (K_n) | 15.1 | 166.5 |
| Upscaling (K_p) | 15.1 | 382.8 |

The porosity was calculated using the arithmetic average from three images. The value was 15.1 % as compared to 17.5 % from laboratory measurement. The permeability which was estimated using upscaling permeability workflow was 166.5 mD when estimation is normal to permeability flow (K_n) and 382.8 mD when parallel to permeability flow (K_p).

Figure 4.44 shows a comparison of the permeability derived from upscaling and direct core plug measurement. The blue dots are the pore scale permeability estimation on each representative image of the building blocks. The red line is permeability measured from core plug and the green line is permeability from a full thin section image by applying upscaling permeability workflow. The red line value is equal to one since it has 100% similarity with the measured value. The green line and blue dots are compared to the measured values and the comparison is shown in the figure below.

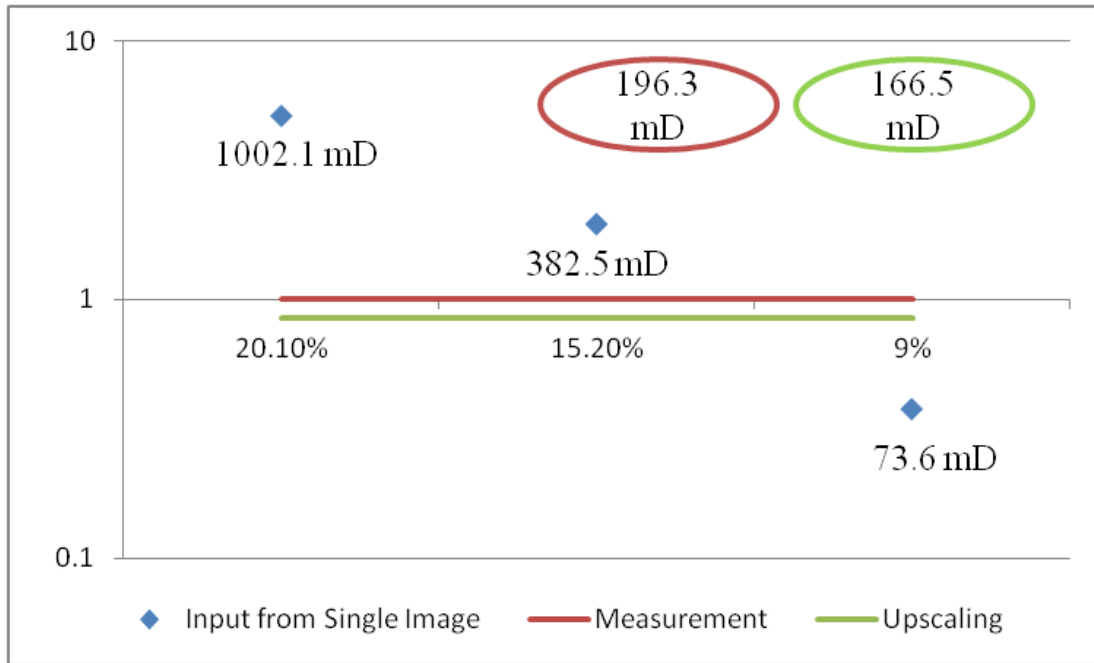


Figure 4.44 Berea sandstone permeability comparison: Estimated permeability of building blocks representative image (blue dots), upscaling permeability workflow (green line and green ellipse) and laboratory data (red line and red ellipse). The y axis is has no unit.

There are two pore scale permeability that are overestimated and one is underestimated. It shows that permeability prediction on mm scale cannot cover the heterogeneity at core plug scale. The accuracy of applying upscaling permeability workflow is about 85 % through comparison on K_n with laboratory measurement. It shows that applying this workflow on a thin section can cover the heterogeneity at core plug scale and improve the prediction of permeability at laboratory scale.

4.8 Case Studies: Application of Upscaling Permeability Workflow to Thin Sections from the Malay Basin

Three thin sections from Wells A, B and C (names of the wells are not real) in the Malay Basin were used to apply upscaling permeability workflow. The information that were available are the porosity and permeability measurements from core plugs. No information was available as to from which parts of the wells were these thin sections obtained. It was assumed that the thin sections were made from the cuttings, sidewall core plug or chips at the same depth as the core plugs were extracted.

4.8.1 Application of Upscaling Permeability Workflow to Thin Section from Well A

The first thin section tested is from the reservoir of Group I, Malay Basin. The data was provided by PETRONAS Research Sdn. Bhd. (PRSB). The sample was from Well A at a depth of 1501.14 m. The sample was a sandstone which was deposited in a fluvial channel. The porosity and permeability of the core plug were 28.7% and 1085 mD respectively. There was no information about the type of bedding. It was assumed that the thin section was made from cuttings or chips from Well A. Permeability was measured on the core plug that was extracted from the same well and depth.

Figure 4.45 shows a thin section from Well A. The length of the full thin section image is 2.8 cm. Since there is no information about the bedding plane of the core plug, the workflow to obtain full thin section image is applied on the normal to the longest length of the thin section. The purpose is to sample the longest length that is near or similar to core plug scale. It was assumed that there is low variation parallel to the longest length of the thin section as the information of bedding plane is unknown.

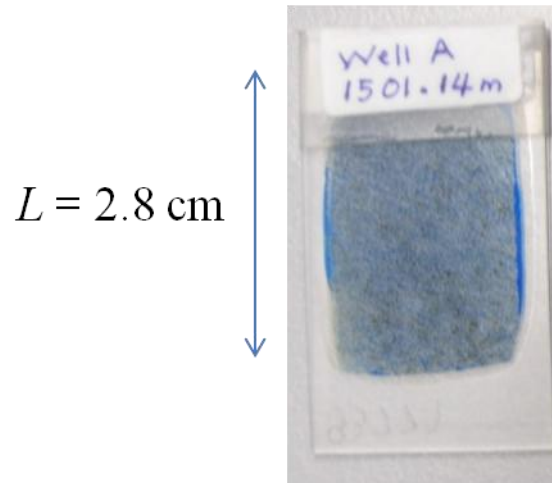


Figure 4.45 Thin section of sandstone from Well A.

4.8.1.1 Full thin section image of sandstone from Well A

To apply upscaling permeability workflow on the thin section from Well A, the first step is to acquire a full thin section image of the thin section. A full thin section image was captured using microscope. Nine images were collected from different parts of the thin section. These images were collected and stitched together into one image. Figure 4.46 shows the process of image collection and stitching into one image.

The nine Images in the middle are the images of the thin section from Well A taken from different parts of the thin section. The figure on the right side shows the result of nine images stitched together to form a single thin section of 2.8 cm length.

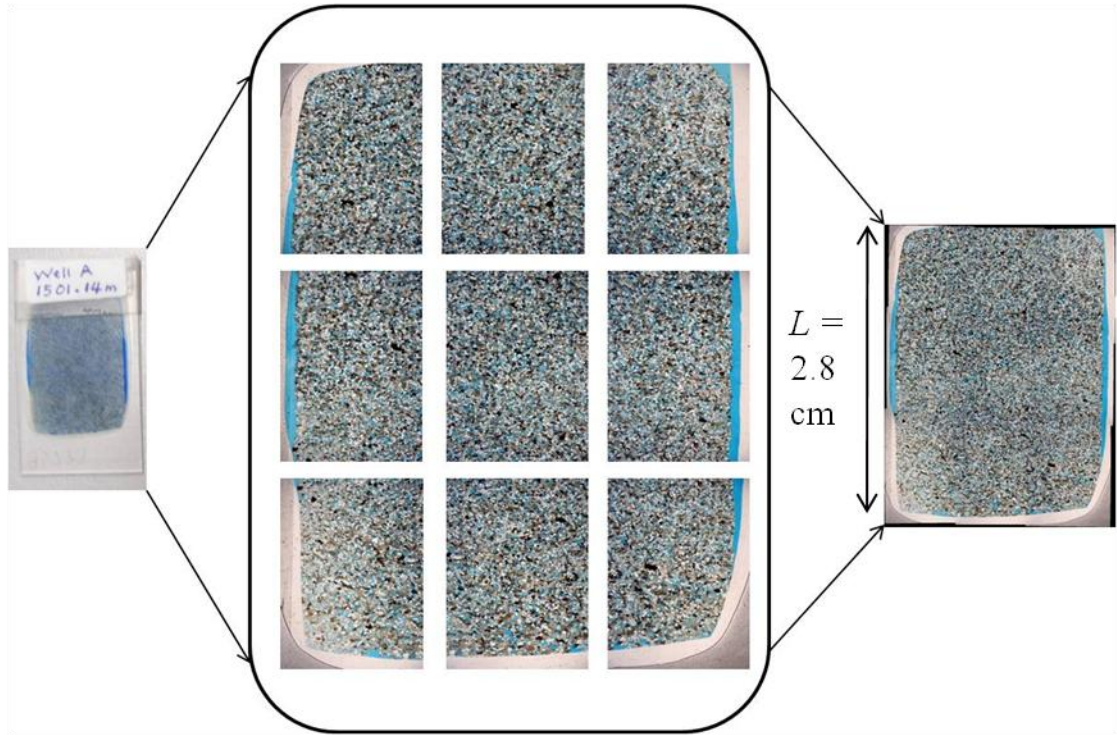


Figure 4.46 Image acquisition and stitching processes on a full image of a thin section of sandstone from Well A. Nine images were acquired (middle) by using the 12.5 times magnification. The length of the image (right) after stitching is 2.8 cm.

4.8.1.2 Grain size vertical profile and building blocks of sandstone from Well A

The next step is to calculate the grain size vertical profile trends from a full thin section image of Well A. The spatial autocorrelation was calculated based on the intensities of corresponding pixels of a full thin section image of Well A. From this the coarsening and fining trends of a full thin section image of Well A could be determined. Figure 4.47 shows the grain size vertical profile calculated from a thin section of Well A from the Malay Basin.

The grain size vertical profile trends were calculated on a full thin section image of Well A. The coverage length of the grain size vertical profile trend was 2.6 cm. The actual length of a total image of the thin section was 2.8 cm. The length was cut and reduced to 2.6 cm to create a full rectangular image of the sandstone.

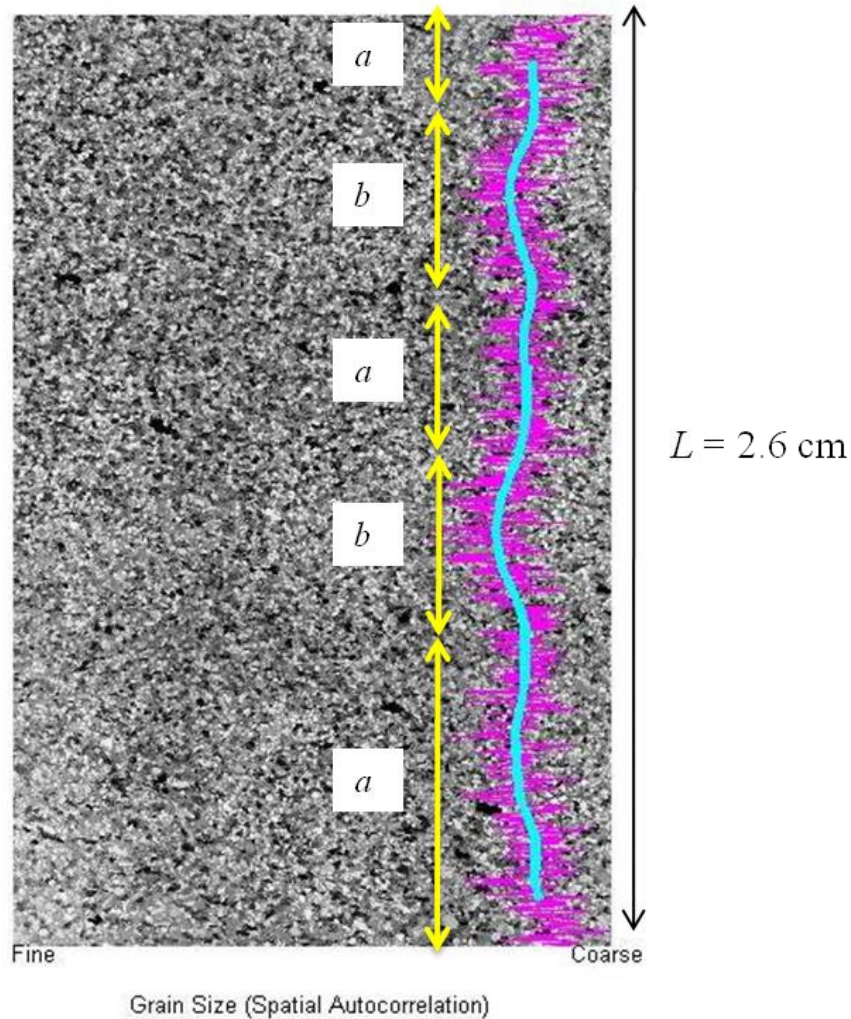


Figure 4.47 Grain size vertical profile trends on a full thin section image of sandstone from Well A. The pink trends show the profile before smoothing and the blue trends show the profile after smoothing.

With this length, it was assumed that this profile had a similar scale with the core plug. The autocorrelation curve was computed for each row of pixels on a full thin section image of the sandstone from Well A. The pink trends show the image statistical intensity values of each row which were calculated from each pixel of the full thin section image. The blue trends showed the reduction and smoothing of noise on the pink trends.

The smoothing (blue) trends on the full thin section image of Well A showed the coarsening and fining part of the image. Based on the trends observed in the full thin section image, there were two areas where the trends had bends. The bend on the left on area *b* was representative of fine/tight grains. Two of the sections had this fine grained material. There were three sections which had coarse grained (area *a*) and were porous. The building blocks for upscaling permeability workflow were created based on the classification of these areas. The length of each area was used as a fraction for the upscaling input.

4.8.1.3 Upscaling permeability workflow on thin section from Well A

The building blocks were created based on the grain size vertical profile trends of the full thin section image of Well A. The length of the full thin section image was 2.6 cm and it was assumed that the anisotropy of core plug was covered and resolved through the grain size vertical profile trends on a full thin section image.

To apply upscaling permeability workflow on the thin section, there were two inputs, namely, the fraction length from grain size vertical profile trends and permeability estimation from each block. The fraction length for the full thin section image is shown in Figure 4.47. As shown in Figure 4.47, there are two areas: *a* and *b* which the trends are bending. The permeability at core plug scale size from each image representative building block was estimated.

A total of 30 images were collected. From the 30 images, two images which represented the *a* area (porous and coarse grained) and *b* area (tight and fine grained) were selected. The assumption is that low variation occurred on the lateral side of the thin section. The 2D to 3D porous media reconstruction and fluid flow simulation was applied to estimate the permeability at pore scale from each image. Figure 4.48 shows the upscaling permeability workflow on a full thin section image of the sandstone from Well A.

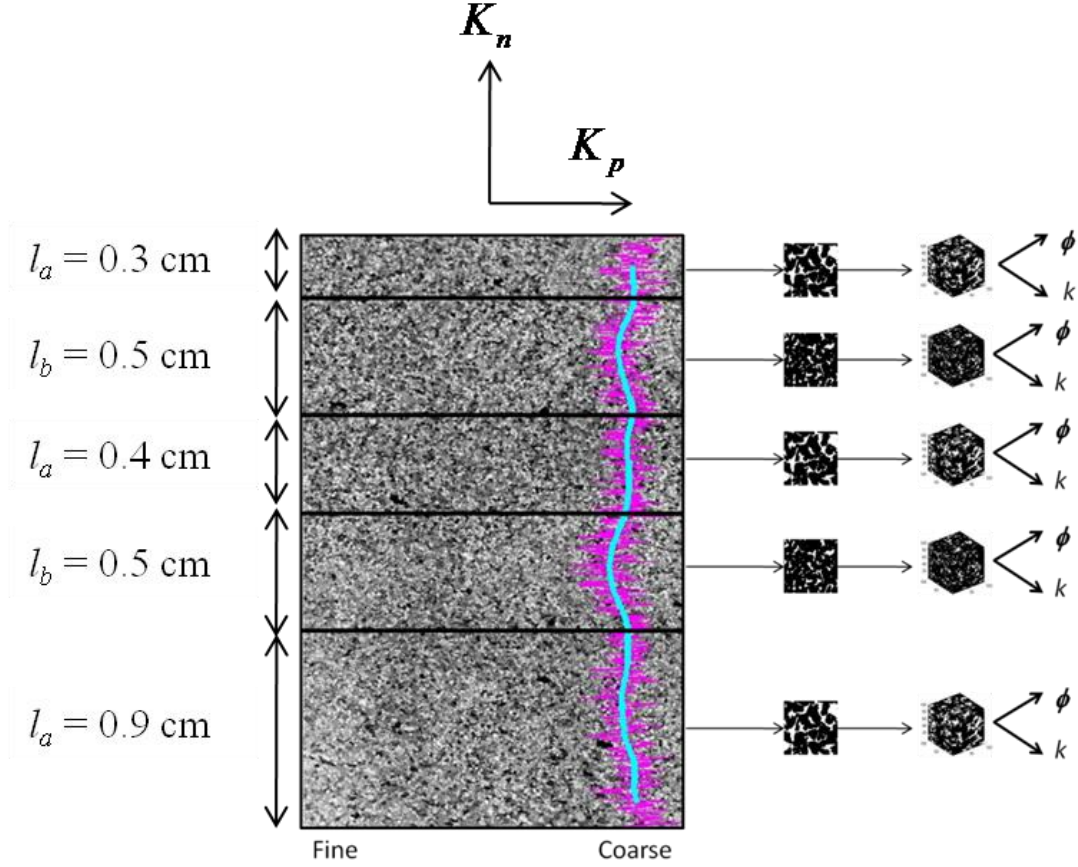


Figure 4.48 Building blocks for upscaling permeability workflow on a full thin section image of sandstone from Well A. The building blocks and fractions of heterogeneity are shown on the middle and the pore scale permeability estimations on each block of sandstone from Well A thin section are shown on the right.

Based on the grain size vertical profile on the full thin section, the length of the fraction of porous area (l_a) is 0.3 cm, 0.4 cm and 0.9 cm. The length of the fraction of tight area, l_b is 0.5 cm and 0.5 cm. Building blocks were created based on the trends.

Two images which represented the porous area and tight area were collected and processed. These images were used as inputs to estimate the permeability from each building block using 2D to 3D porous media reconstruction and fluid flow simulation. The estimated porosity and permeability from each image are summarized in Table 4.5.

Table 4.5 Estimated porosity and permeability from each representative building block of thin section from Well A.

| Type | Porosity (%) | Permeability (mD) |
|------------------------------|--------------|-------------------|
| Porous / Coarse (<i>a</i>) | 32.6 | 1766.7 |
| Tight / Fine (<i>b</i>) | 14.6 | 258.4 |

Upscaling permeability workflow was used to estimate the effective permeability at laboratory scale (core plug scale). The resulting estimates of upscaling porosity and permeability are summarized in Table 4.6.

Table 4.6 Comparison between the porosity and permeability from upscaling workflow on thin section and core plug measurement on sandstone from Well A.

| Type | Porosity (%) | Permeability (mD) |
|---------------------|--------------|-------------------|
| Core Plug | 28.7 | 1085 |
| Upscaling (K_n) | 20.2 | 544.4 |
| Upscaling (K_p) | 20.2 | 1186.6 |

The porosity was calculated using the arithmetic average from three images. The value was 20.2 % as compared to 28.7 % from laboratory measurement. The permeability which was estimated using upscaling permeability workflow was 544.4

mD when estimated normal to the thin section length (K_n) and 1186.6 mD when parallel to the thin section length (K_p).

This estimation was compared with the laboratory results which were measured normal to the thin section length. The value of permeability obtained from PRSB Laboratory was 1085 mD. There was no information about the bedding of the core plug. The accuracy of applying this workflow is about 90 % through comparison on K_p with the laboratory results. Figure 4.49 shows results of the estimated upscaling porosity and permeability.

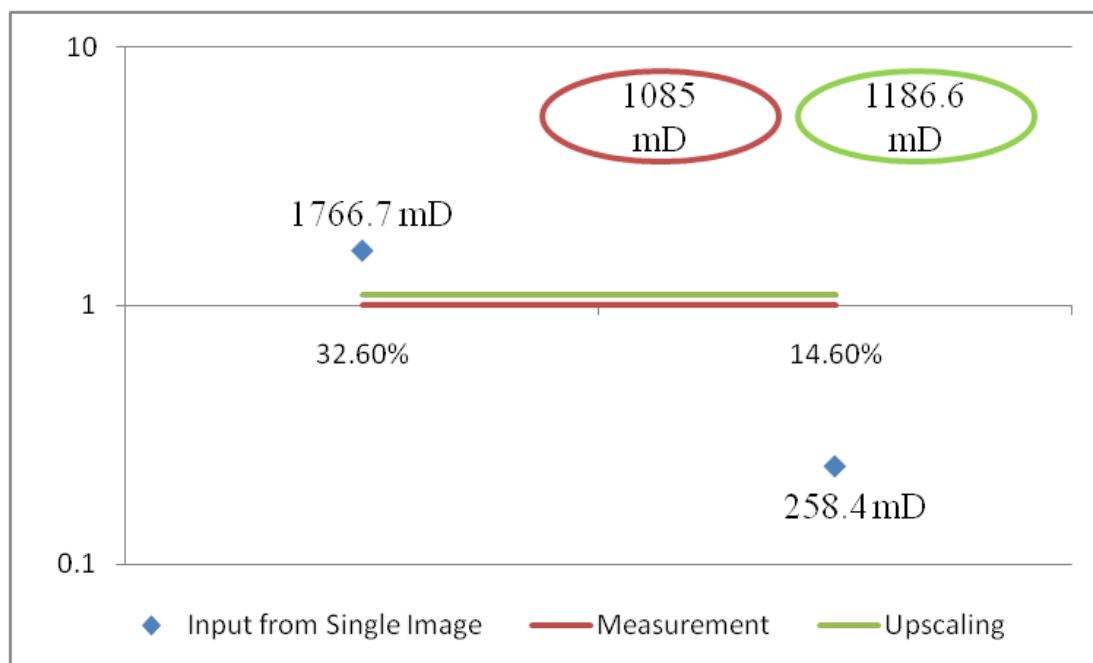


Figure 4.49 Sandstone from Well A permeability comparison: Estimated permeability of building blocks representative image (blue dots), upscaling permeability workflow (green line and green ellipse) and laboratory data (red line and red ellipse). The y axis has no unit.

Figure 4.49 shows a comparison of the permeability derived from upscaling workflow and direct core measurement. The blue dots represent the estimated pore

scale permeability on each representative image of building block of the thin section. The red line is the permeability obtained from PRSB. The green line is the permeability obtained from a full thin section image by applying upscaling workflow. The green line and the blue dots were compared respective to measurement value.

One of the pore scale permeability results was overestimated and the other was underestimated. It shows that permeability prediction on mm scale could not cover the heterogeneity at core plug scale. The accuracy of applying upscaling permeability workflow is about 90 % through comparison on K_p with laboratory measurement. It shows that applying this workflow on a thin section could cover the heterogeneity at core plug scale and improved the prediction of permeability at laboratory scale.

4.8.2 Application of Upscaling Permeability Workflow to Thin Section from Well B

The second thin section tested was from the reservoir of Group J, in the Malay Basin. The data was also provided by PETRONAS Research Sdn. Bhd. (PRSB) from Well B at a depth of 1397.5 m. The rock was deposited in the lower part of an estuary. The porosity and permeability from core plugs were 30.6 % and 3700 mD respectively.

Figure 4.50 shows the thin section from Well B. The length of the full thin section image was 2.8 cm. Since there was no information about the direction of the bedding plane of the core plug, the workflow to obtain a full thin section image was applied normal to the length of thin section. The purpose was to sample the longest length that was near or similar to the core plug scale. Low variation was assumed on the lateral side of the thin section.

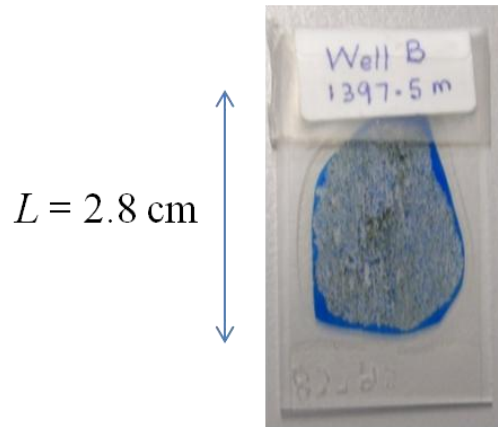


Figure 4.50 Thin section of sandstone from Well B.

4.8.2.1 *Full thin section image of sandstone from Well B*

To apply upscaling permeability workflow on the thin section from Well B, the first step was to acquire a full thin section image of Well B. A full thin section image was captured using a microscope. Nine images were collected from different parts of the thin section. These images were collected and stitched together into one image. Figure 4.51 shows the process of image collection and stitching into one image of a thin section.

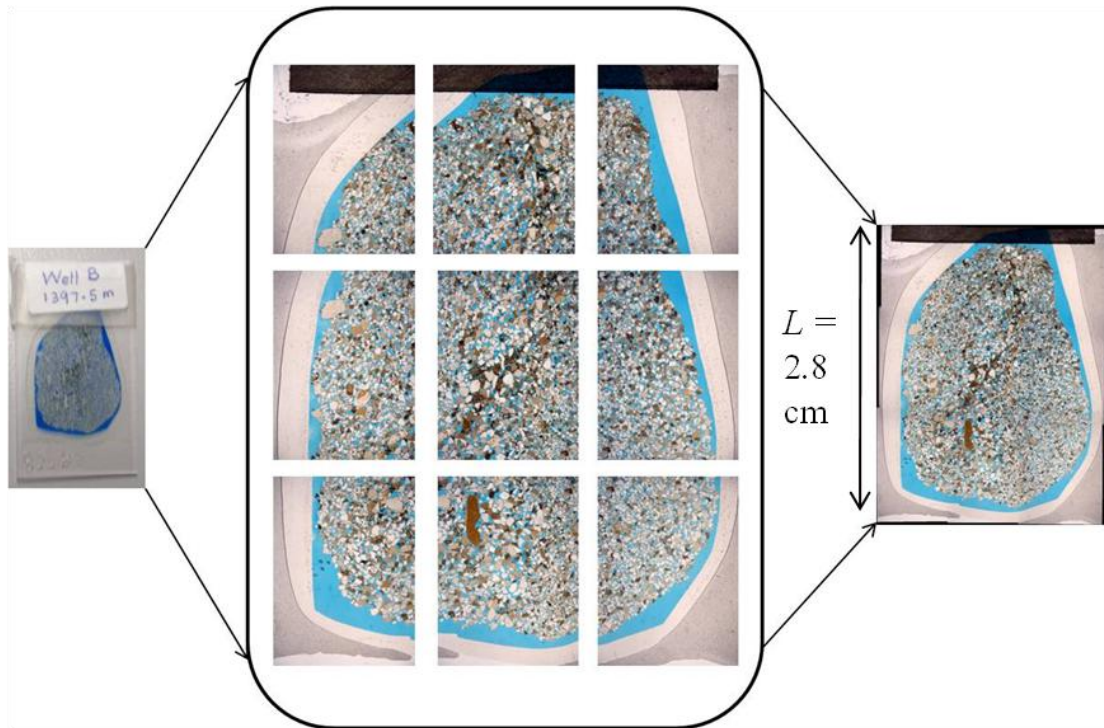


Figure 4.51 Image acquisition and stitching processes on a full image of thin section of sandstone from Well B. Nine images were acquired (middle) by using the 12.5 times magnification. The length of the image (right) after stitching is 2.8 cm.

The nine images in the middle are the images taken from different parts of the thin section. The figure on the right side results from the stitching of the 9 images into a full thin section image with a length of 2.8 cm.

4.8.2.2 Grain size vertical profile and building blocks of Well B sandstone

The next step was to calculate the grain size vertical profile from a full thin section image of Well B. The spatial autocorrelation was calculated based on the intensities of the corresponding pixels of a full thin section image. From this, the coarsening and fining trends of the full thin section image could be determined. Figure 4.52 shows a grain size vertical profile calculated from a thin section of Well B in the Malay Basin.

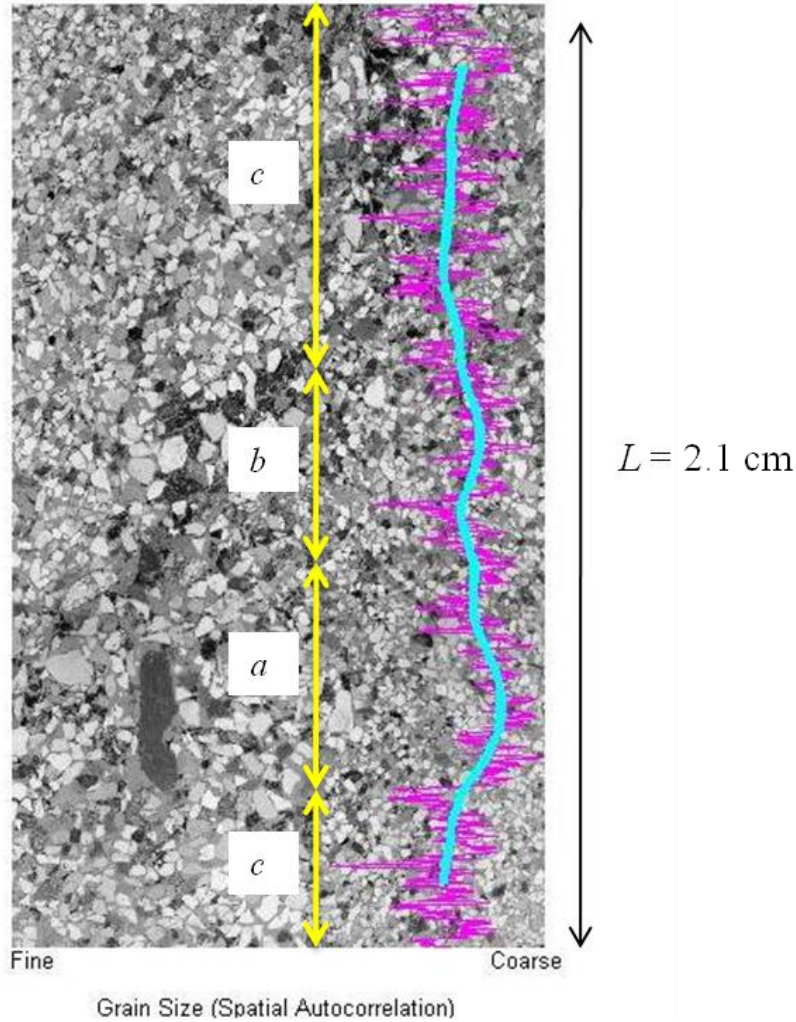


Figure 4.52 Grain size vertical profile trends on a full thin section image of sandstone from Well B. The pink trends show the profile before smoothing and the blue trends show the profile after smoothing.

The grain size vertical profile was calculated on a full thin section image of the rock from Well B. The coverage length of the grain size vertical profile was 2.1 cm. The actual length of the total image thin section image was 2.8 cm. The length was cut and reduced to 2.1 cm to create a full rectangular image.

With this length, it was assumed that this profile had a similar scale with the core plug. The autocorrelation curve was computed for each row of pixels on a full thin

section image. The pink trends show the image statistical intensities value which were calculated from each pixel of the full thin section image. The blue trends show the reducing and smoothing of noise on the pink trends.

The smoothing (blue) trends on a full thin section image showed the coarsening and fining part of the image. Based on the trends observed on the full thin section image, there were three areas where the trends bend. The trends which show bends to the right on the area *a* comprised the coarse and porous sand grains. Two areas with fine and tight grains were present (area *c*). Only one area *b* which comprised moderate grains was observed. The building blocks for upscaling permeability were created based on the classification of these areas. The length of each area was used as a fraction for upscaling input.

4.8.2.3 Upscaling permeability workflow on thin section from Well B

The building blocks were created based on the grain size vertical profile of the full thin section image of Well B. The length of a full thin section image was 2.1 cm and it was assumed that the anisotropy of core plug was covered and resolved through the grain size vertical profile on the full thin section image.

To apply upscaling of permeability on the thin section there were three inputs of fraction length from the grain size vertical profile trends and permeability estimation from each block. The fraction length data for the full thin section image is shown in Figure 4.52. As shown in Figure 4.52, there are three areas: *a*, *b* and *c* which the trends were bending. The permeability at core plug scale size from each image representative building blocks was then estimated.

A total of 24 images were collected. From these 24 images, three images which represented the *a* area, *b* area and *c* area were selected. The assumption was that a low variation occurred on the lateral side of the thin section. The 2D to 3D porous media reconstruction and fluid flow simulation were applied to estimate the permeability at pore scale from each image. Figure 4.53 shows the application of upscaling permeability on a full thin section image of the sandstone from Well B.

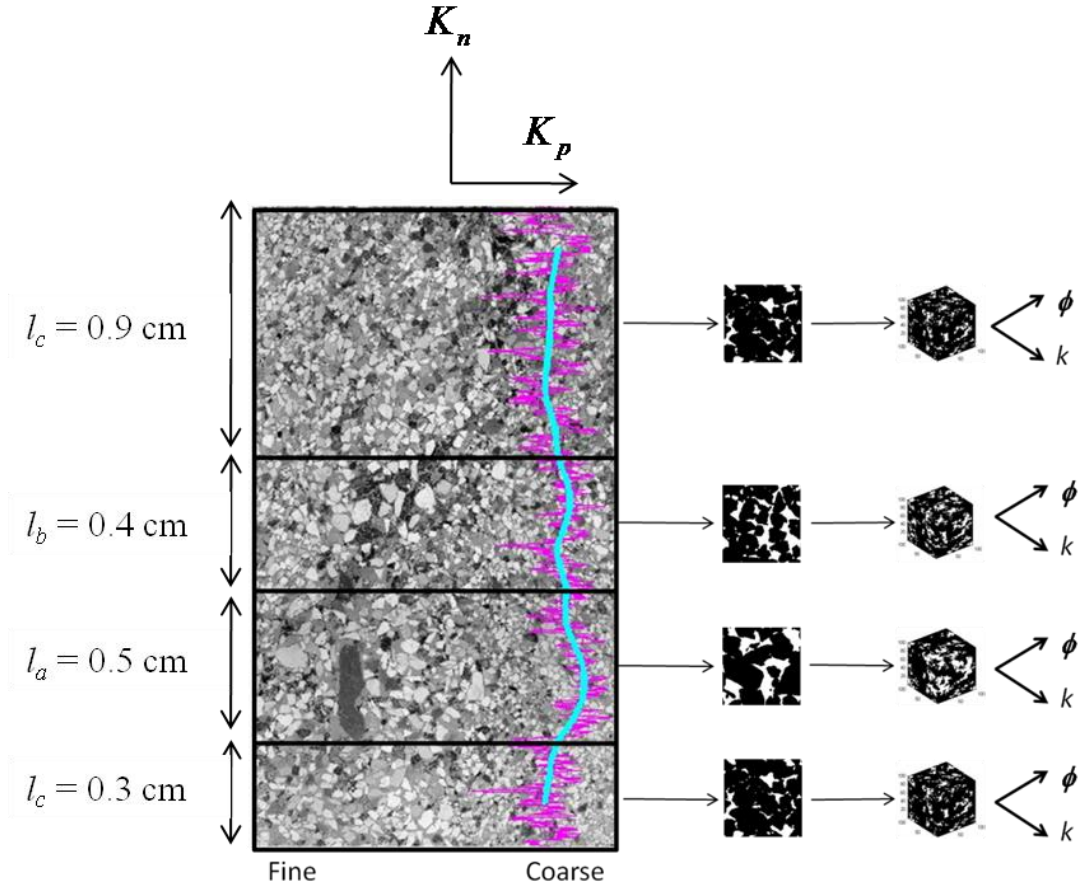


Figure 4.53 Building blocks for upscaling permeability workflow on a full thin section image of sandstone from Well B. The building blocks and fractions of heterogeneity are shown on the middle and the pore scale permeability estimations on each block of sandstone from Well B thin section are shown on the right.

Based on the grain size vertical profile on the full thin section, the length fraction of porous area (l_a) was 0.5 cm. The length fraction of area b , (l_b) was 0.4 cm. The length fraction of area c , (l_c) was 0.9 and 0.3 cm. The building blocks were created based on the trends.

Three images which represented the porous (a), patchy (b) and tight (c) areas were collected and processed. These images were used as inputs to estimate the permeability from each building block using 2D to 3D porous media reconstruction

and fluid flow simulation. The porosity and permeability estimated from each image is summarized in Table 4.7

Table 4.7 Estimated porosity and permeability from each representative building block of thin section from Well B.

| Type | Porosity (%) | Permeability (mD) |
|------------------------------|--------------|-------------------|
| Porous / Coarse (<i>a</i>) | 32.22 | 9921.39 |
| Patchy (<i>b</i>) | 22.06 | 1950.55 |
| Tight / Fine (<i>c</i>) | 15.15 | 843.81 |

Upscaling permeability was used to estimate the effective permeability at laboratory scale (core plug scale). The resulting estimates of the upscaling porosity and permeability are summarized in Table 4.8.

Table 4.8 Comparison of porosity and permeability obtained by upscaling permeability workflow on thin section and core plug measurement from Well B.

| Type | Porosity (%) | Permeability (mD) |
|----------------|--------------|-------------------|
| Core Plug | 30.6 | 3700 |
| Upscaling (Kv) | 22.5 | 715.3 |
| Upscaling (Kh) | 22.5 | 3215.9 |

The porosity which was calculated using the arithmetic average from the three images was 22.5 % as compared to 30.6 % laboratory measurement. The estimated permeability using upscaling workflow was 715.3 mD when conducted normal to the thin section length (K_n) and 3215.9 mD when parallel to the thin section length (K_p).

This estimation was compared with the laboratory results which were measured parallel to the thin section length. The permeability obtained from PRSB laboratory was 3700 mD. There was no information on the bedding of the core plug. The accuracy of applying this workflow is about 86 % through comparison between K_p with the laboratory results. Figure 4.54 shows a plot of the resulting estimates of upscaling porosity and permeability.

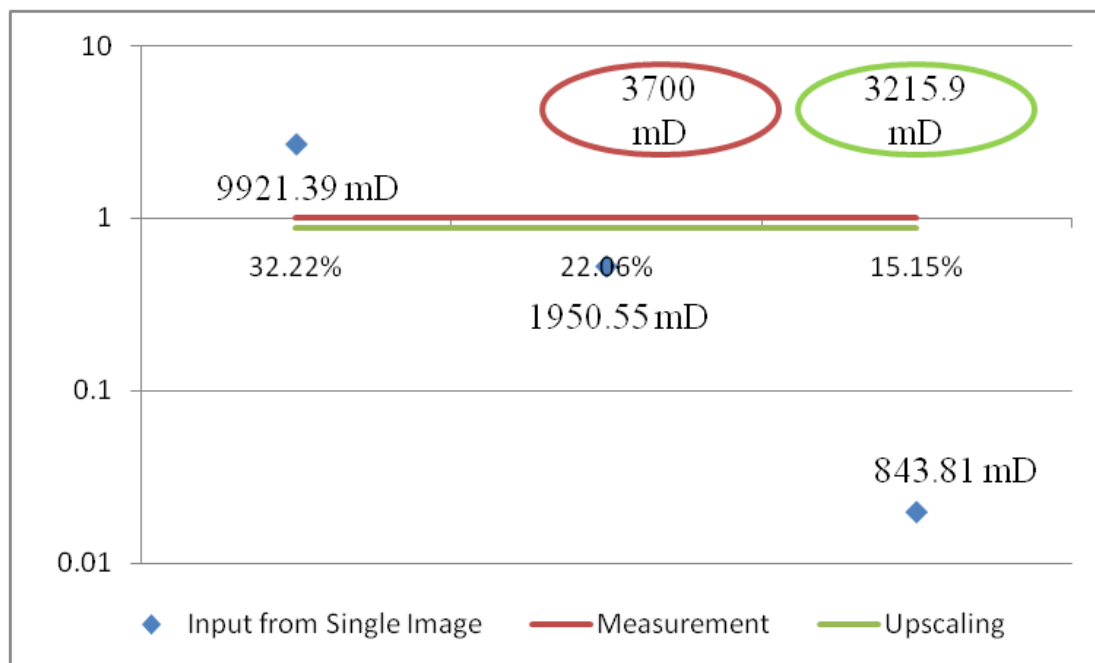


Figure 4.54 Sandstone from Well B permeability comparison: Estimated permeability of building blocks representative image (blue dots), upscaling permeability workflow (green line and green ellipse) and laboratory data (red line and red ellipse). The y axis has no unit.

Figure 4.54 shows a comparison of the permeability derived from upscaling workflow and direct core measurement. The blue dots represent the estimated pore scale permeability on each representative image of building block of the thin section. The red line is the permeability obtained from PRSB. The green line is the permeability obtained from a full thin section image by applying upscaling workflow. The green line and the blue dots were compared respective to measurement value.

One of the pore scale permeability result was overestimated and the others were underestimated. It shows that permeability prediction on mm scale could not cover the heterogeneity at core plug scale. The accuracy of applying upscaling permeability workflow is about 86 % through comparison on K_p with the laboratory measurement. It shows that applying this workflow on a thin section could cover the heterogeneity at core plug scale and improved prediction of permeability at laboratory scale.

4.8.3 Application of Upscaling Permeability Workflow to Well C Thin Section

The third thin section studied was from the reservoir of Group J, in the Malay Basin. The data was also provided by PETRONAS Research Sdn. Bhd. (PRSB) from Well C at a depth of 1812.44 m. The rocks were deposited in a subtidal environment with moderate energy. The porosity and permeability of the core plugs are 24.3 % and 287.6 mD respectively.

Figure 4.55 shows a thin section from Well C. The full length of the thin section image is 2.8 cm. Since no information about bedding plane of the core plug was available, the workflow to obtain the full thin section image was applied normal to the length of the thin section. The purpose was to sample the longest length that was near or similar to the core plug scale. A low variation was assumed on the lateral of the thin section.

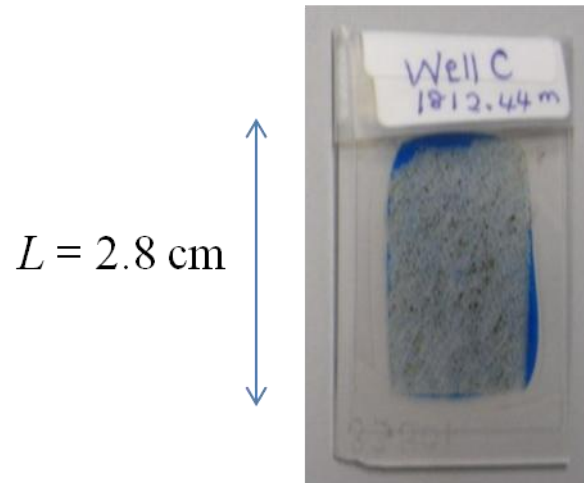


Figure 4.55 Thin section of sandstone from Well C.

4.8.3.1 Full thin section image of sandstone from Well C

To apply upscaling permeability workflow on the thin section, the first step was to acquire a full thin section image of the thin section. A full thin section image was captured using a microscope. Nine images were collected from different parts the thin section. These images were collected and stitched together into one full thin section image. Figure 4.56 shows the process of image collection and stitching into full thin section image.

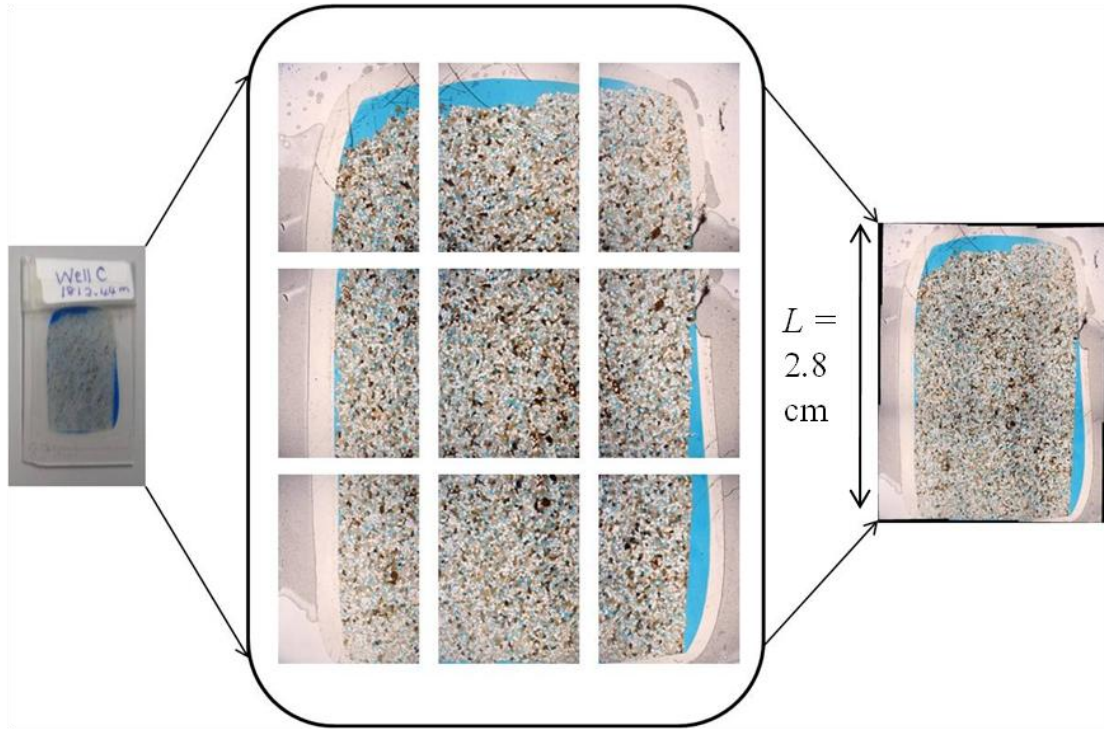


Figure 4.56 Image acquisition and stitching processes on a full image of thin section of sandstone from Well C. Nine images were acquired (middle) by using the 12.5 times magnification. The length of the image (right) after stitching processes is 2.8 cm.

The nine images in the middle are the images taken from different parts of the thin section. The figure on the right side shows the result of stitching the 9 to form a full thin section image of 2.8 cm length.

4.8.3.2 Grain size vertical profile and building blocks of well C sandstone

The next step is to calculate the grain size vertical profile from the full thin section image of Well C. The spatial autocorrelation was calculated based on the intensities of corresponding pixels of the full thin section image. From this the coarsening and fining trends of the full thin section image could be determined. Figure 4.57 shows the grain size vertical profile calculated from the thin section of Well C Malay basin.

The grain size vertical profile trends were calculated on the full thin section image of the Well C. The coverage length of the grain size vertical profile trends was 2.4 cm. The actual length of the total image of the thin section was 2.8 cm, The length was cut and reduced to 2.4 cm to create a full rectangular image of the sandstone.

With this length, it was assumed that this profile has a similar scale with the core plug. The autocorrelation curve was computed for each row of pixels on the full thin section image. The pink trend showed the image statistical intensity value which were calculated from each pixel of the full thin section image. The blue trends show the reducing and smoothing of noise on pink trends.

The smoothing (blue) trends on a full thin section image of Well C sandstone showed the coarsening and fining part of the image. Based on the trends observed, there were two areas where the trends bend. Two areas denoted by the bends on the left on the area *b* had fine grains and were tight. Three sections on area *a* had coarse grains and were porous. The building blocks for the upscaling permeability workflow were created based on the classification of these areas. The length of each area was used as a fraction for upscaling input.

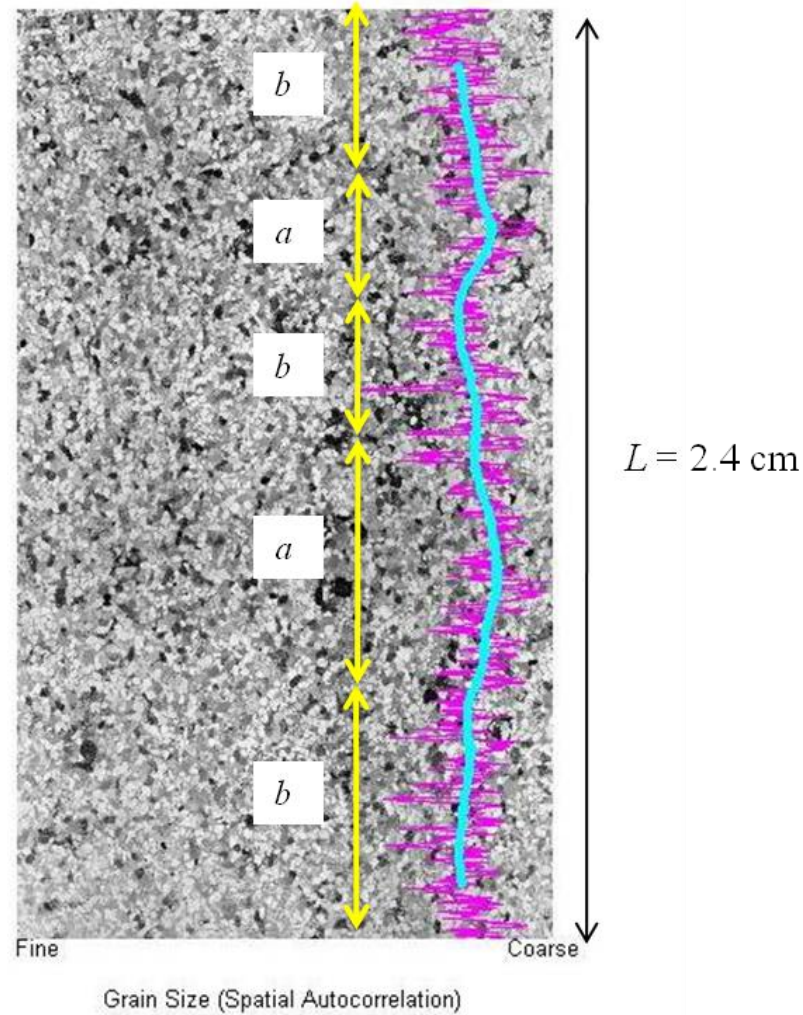


Figure 4.57 Grain size vertical profile trends on a full thin section image of sandstone from Well C. The pink trends show the profile before smoothing and the blue trends show the profile after smoothing.

4.8.3.3 Upscaling permeability and building blocks on sandstone from Well C

The building blocks were created based on the grain size vertical profile of the full thin section image. The length of the full thin section image was 2.4 cm and it was assumed that the anisotropy of the core plug was covered and resolved through the grain size vertical profile trends on the full image of the thin section.

To apply the upscaling of permeability workflow on the thin section there were two inputs, namely, fraction length from grain size vertical profile and the permeability estimated from each block. The fraction length data is shown in Figure 4.57. As shown in Figure 4.57, there are two areas: *a* and *b* where the trends bend. The permeability at core plug scale size was estimated from each representative building block image.

A total of 25 images were collected. From the 25 images, two images which represented the area *a* (porous and coarse grained) and area *b* (fine grained and tight) were selected. The assumption was that low variation occurred on the lateral side of the thin section. The 2D to 3D porous media reconstruction and fluid flow simulation were applied to estimate the permeability at pore scale from each image. Figure 4.58 shows application of upscaling permeability workflow on the full thin section image of sandstone from Well C.

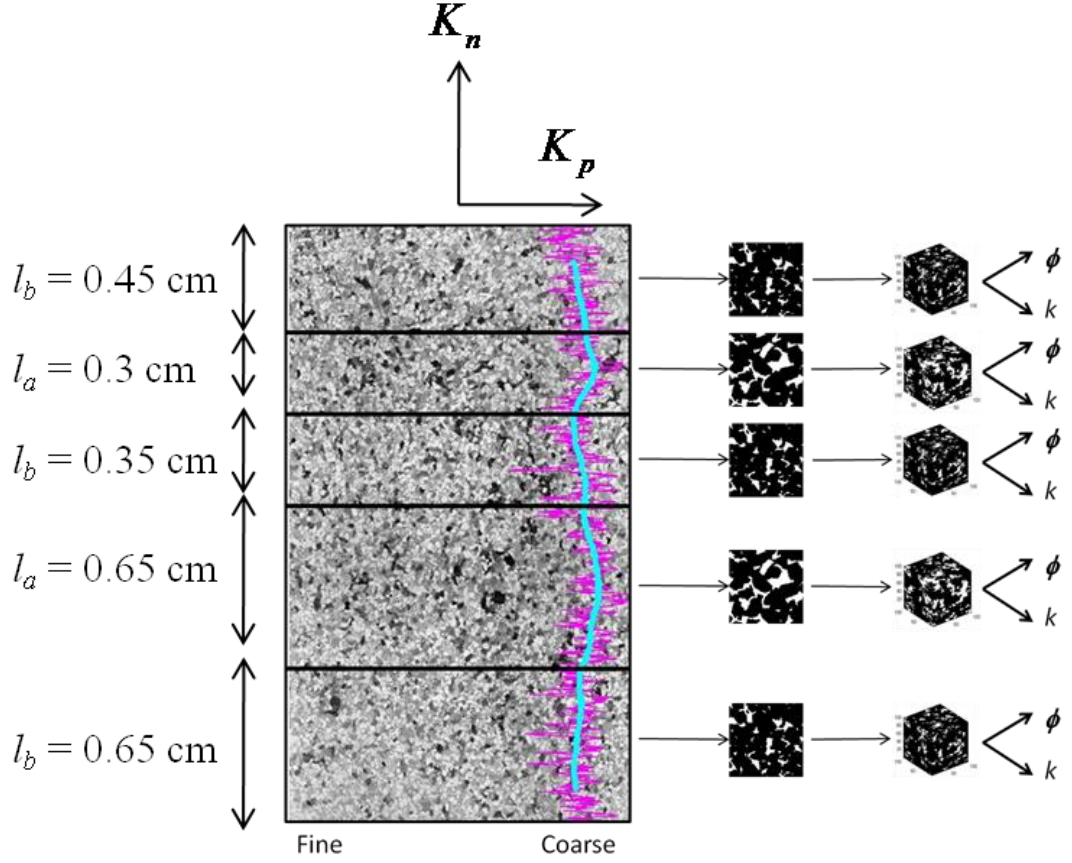


Figure 4.58 Building blocks for upscaling permeability workflow on a full thin section image of sandstone from Well C. The building blocks and fractions of heterogeneity are shown on the middle and the pore scale permeability estimations on each block of sandstone from Well C thin section are shown on the right.

Based on the grain size vertical profile on the full thin section, the length fraction of the porous area (l_a) was 0.3 and 0.65 cm. The length fraction of tight area, l_b was 0.45, 0.35 and 0.65 cm. Building blocks were created based on these trends.

Two images which represented the porous area and tight areas were collected and processed. These images were used as an input to estimate the permeability from each building block using 2D to 3D porous media reconstruction and fluid flow simulation. The porosity and permeability estimated from each image are summarized in Table 4.9.

Table 4.9 Porosity and permeability estimated from each representative building block of the thin section from Well C.

| Type | Porosity (%) | Permeability (mD) |
|------------------------------|--------------|-------------------|
| Porous / Coarse (<i>a</i>) | 27.8 | 1213.7 |
| Tight / Fine (<i>b</i>) | 14.9 | 181.8 |

Upscaling permeability workflow was used to estimate the effective permeability at laboratory scale (core plug scale). The resulting estimates of upscaling porosity and permeability are summarized in Table 4.10.

Table 4.10 Comparison of porosity and permeability obtained by upscaling permeability workflow on thin section and core plug measurement from Well C.

| Type | Porosity (%) | Permeability (mD) |
|---------------------|--------------|-------------------|
| Core Plug | 24.3 | 287.6 |
| Upscaling (K_n) | 20.0 | 274.1 |
| Upscaling (K_p) | 20.0 | 590.3 |

The porosity which was calculated using the arithmetic average from the two images was 20 % as compared to 24.3 % from laboratory measurement. The estimated permeability using upscaling workflow was 274.1 mD when conducted normal to the thin section length (K_n) and 590.3 mD when parallel to the thin section length (K_p).

This estimation was compared with the laboratory results which were measured normal to the thin section length. The permeability obtained from PRSB laboratory was 287.6 mD. There was no information on the bedding of the core plug. The accuracy of applying this workflow is about 95 % through comparison between K_n with laboratory results. Figure 4.59 shows a plot of the resulting estimates of upscaling porosity and permeability.

Figure 4.59 shows a comparison of the permeability derived from upscaling workflow and direct core measurement. The blue dots are the estimated pore scale permeability on each representative image of building block of the thin section. The red line is the permeability obtained from PRSB. The green line is the permeability obtained from a full thin section image by applying upscaling workflow. The green line and the blue dots were compared respective to measurement value to show the efficiency of upscaling workflow.

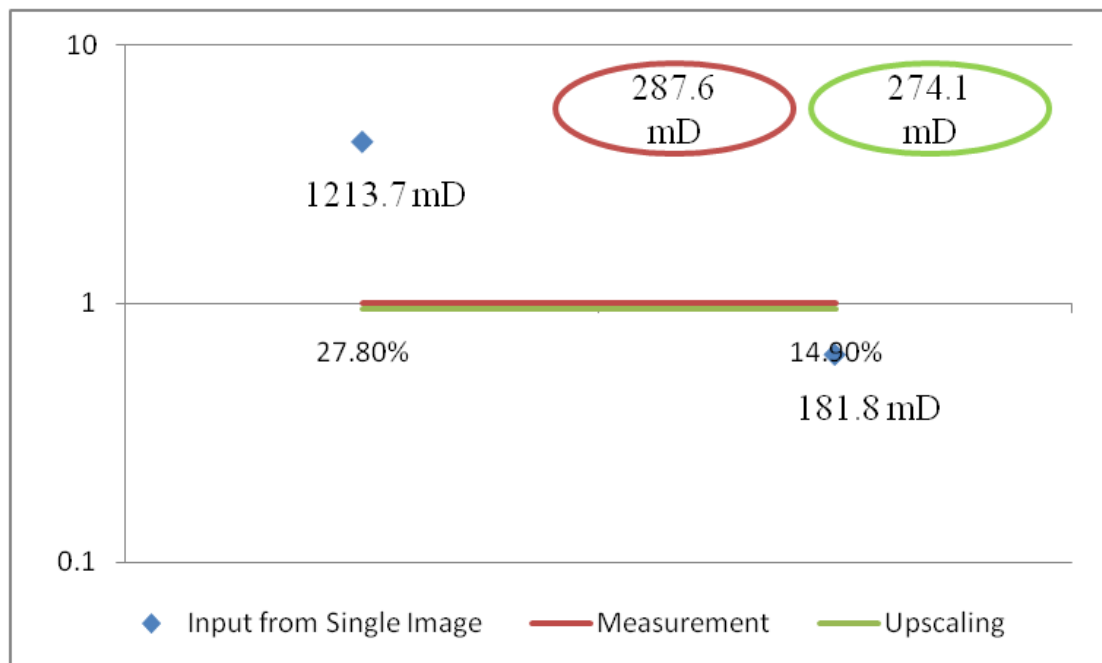


Figure 4.59 Sandstone from Well C permeability comparison: Estimated permeability of building blocks representative image (blue dots), upscaling permeability workflow (green line and green ellipse) and laboratory data (red line and red ellipse). The y axis has no unit.

One of the pore scale permeability results was overestimated and another underestimated. It shows that permeability prediction on mm scale could not cover the heterogeneity at core plug scale. The accuracy of applying upscaling permeability workflow is about 95 % through comparison on K_n with laboratory measurement. It shows that applying this workflow on a thin section could cover the heterogeneity at core plug scale and improved the prediction of permeability at laboratory scale.

4.9 Discussion

Measurement of permeability may be partially replaced by numerical simulation on a 3D porous media of a rock. This porous media can be provided using CT-Scan. The numerical simulation can accurately simulate physical experiments if mimics are provided precisely. Since the physical measurement is conducted at core plug scale, rock digital sample at core plug scale is required as an input to conduct accurate numerical simulation of physical measurement. However, CT-Scan is still prohibitively expensive and the scanning time of large digital sample at core plug scale is too long to be practically useful in massive numerical experimentation. Another problem is that conducting simulation of fluid flow on this large digital scale can only be handled by a supercomputer and still requires hours or days to implement.

CT-Scan is an expensive device, and as such 2D to 3D porous media reconstruction was used as an alternative to obtain 3D porous media of the rock. The methodology from Keehm was adopted and modified to reconstruct the porous media. The sample points as conditional data were added as a new parameter to effectively improve the computational reconstruction time. The results showed that the modification improved the computational reconstruction time by 30 times. The accuracy of this methodology was compared with CT-Scan data. Comparison with a CT-scan image of a sandstone showed that this methodology achieved an accuracy of about 80 – 90 %. This means that this method is accurate in the reconstruction of the porous media connectivity of sandstone.

The task to generate 3D porous media and fluid flow simulation which can be handled by a standard personal computer and in real time can only be implemented at mm scale. This size sometimes cannot cover sample heterogeneity at laboratory scale (cm scale). In this work, the workflow to predict permeability at laboratory scale is presented. The upscaling method combined with 2D to 3D porous media reconstruction was applied. Grain size vertical profile trends were used to isolate variations on coarse and fine parts of the thin section. The building blocks of upscaling purpose were created based on these trends. Each image which represented the coarse and fine parts of the thin section was used as an input for 2D to 3D porous media reconstruction. The porosity and permeability were calculated from 3D porous

media and used as an input for upscaling. These workflows were applied to thin sections of the Berea sandstone and thin sections of sandstones from the Malay Basin. The results on the four thin sections showed good agreement with laboratory data. The accuracy of this workflow is about 85 - 90 % on each thin section compared to physical lab measurement. This workflow can be applied using a standard personal computer with reasonable running time (approximately 180 seconds). Table 4.11 shows the comparison of running time between upscaling permeability workflow with core plug measurement.

Table 4.11 Comparison of running time between upscaling permeability workflow with core plug measurement.

| | Upscaling Permeability Workflow (cm scale) | | | Core Plug Measurement (cm scale) |
|--|--|-----------|-----------|----------------------------------|
| | 2D to 3D | Flow Sim. | GSVP | |
| Running Time | @ ~30 sec | @ ~30 sec | @ < 1 sec | ~30 minutes – 1 hour |
| Sub Total Time (3 image fraction) | ~90 sec | ~90 sec | ~1 sec | --- |
| Total Time | ~ 180 sec | | | ~30 minutes – 1 hour |

*GSVP: Grain Size Vertical Profile

CHAPTER 5

CONCLUSIONS AND RECOMMENDATIONS

5.1 Conclusions

This thesis develops a new workflow to predict laboratory scale permeability using information from a full thin section image which can be applied in real time on a standard personal computer. Several methods are combined as part of the workflow: pore scale 3D porous media reconstruction using 2D to 3D, pore scale fluid flow simulation using LBM, grain size vertical profile calculation at core plug scale and upscaling permeability from pore to core plug scale.

In Chapter 4, a 2D image was sampled and cut from a 3D CT-Scan and porous media reconstruction was applied on a selected 2D image. Based on comparison with the CT-Scan image of a sandstone, 2D to 3D porous media reconstruction using SISIM geostatistical method showed good agreement with the experimental (CT-Scan) image. The accuracy of this method was tested by comparing absolute permeability calculated on generated 3D porous media and 3D CT-Scan Image. By comparison on the same scale (mm to mm) and applying the REV concept, an accuracy of about 80 - 90% was achieved, meaning that this method would still correctly simulate the connectivity of sandstone samples at pore (mm) scale. The 3D porous media reconstruction proposed in this thesis is in real time on a standard personal computer by modifying and adding sample points as new input parameter. This method improved the simulation by running 30 times faster than without conditional data (Keehm's method) and 10 times faster than with conditional data using training image (2D image).

The variograms from the three different methodologies (without conditional data, with conditional data using training image and sample points) showed that the reconstructed images had the same spatial variability, which means the methodology becomes more efficient. The first objective of this study is fulfilled by completing this part of thesis. The writer developed and modified a workflow to reconstruct 3D porous media from thin section images. This method improved the computational time of reconstruction and it could be implemented in real time on a standard personal computer with good accuracy as compared to CT-Scan.

Based on this study, resolution of the image gave a major impact on computed fluid flow. Decreased resolutions led to a decrease on the computed permeability. Decreased resolution gave an impact to the connectivity of porous media. Image resolution has not given a major impact on porosity. Reducing the size of 3D porous media to 50% of the original is a reasonable size for fluid flow simulation (Noted on Berea and S (8)).

However, 3D porous media with a lower resolution (poor quality of image, as noted by Fontainebleau) will give a reasonable size less than 50%. Study on the impact of resolution gave a clear understanding about a minimal size input for fluid flow simulation. The computation time is related to the size of the input. 3D porous media with a big grid or size will affect the computational time. Several studies on fluid flow simulation on different types of size and resolution fulfilled the second objective of this study.

The third objective was fulfilled by applying upscaling permeability workflow on thin sections of Berea Sandstone and from sandstones from the Malay Basin. The first input of this workflow is to obtain a full thin section image and then calculate the grain size vertical profile trends. The grain size vertical profile method on a full thin section image with appropriate resolution could be used to differentiate the heterogeneities parts of a full thin section image. With this information the building blocks input for upscaling can be determined. Based on the results, upscaling permeability workflow using a combination of reconstruction method, fluid flow simulation, grain size vertical profile and upscaling could be applied to accurately estimate the effective permeability at laboratory scale.

The accuracy of this method on thin section samples of sandstone is about 85 – 90% and can be applied on a standard personal computer with reasonable running time (about 180 seconds). Over and underestimation from laboratory measurement could still occur if permeability was only estimated using 2D to 3D porous media reconstruction. Permeability anisotropy at laboratory scale could not be resolved since this method could only be implemented at mm scale. It clearly showed that the prediction of laboratory scale permeability is improved by applying upscaling permeability workflow.

5.2 Recommendation

In light of the findings and conclusions of this study, the author recommends the following:

1. Once the workflow becomes user friendly, the available data from the thin section data base of sandstone can be used as an input and integrated into modeling processes as complimentary data and quality control to logs and seismic for permeability distribution information.
2. For accurate sampling, spacing and to obtain good samples, the built drill bits could be used to take samples from each depth of the well accurately.
3. Deducing a link between laboratory and borehole based NMR measurements for pore space and fluid characterization.
4. Create porosity and permeability trends from thin sections or small cuttings.
5. Adopting fast computational Multiple point statistics algorithm to reconstruct porous media.
6. Numerical experiments with velocity on digital samples and assess permeability from well logging data if the velocity can be calculated on the same digital rocks.

REFERENCES

- [1] Dvorkin, J, Armbruster, M., Baldwin, C., Fang, Q., Derzhi, N., Gomez, C., Nur, B., Nur, A., and Mu, Y., "The future of rock physics: computational methods vs. lab. Testing," EAGE First Break (26), 2008, pp. 63-68.
- [2] Nur, A., "The Emerging Roles of Rock Physics: From 4D Seismic To Pore Scale Imaging," Latin American and Caribbean Petroleum Engineering Conference, 31 May-3 June 2009, Cartagena de Indias, Colombia, 122944-MS, 2009.
- [3] Touati, M., Suicmez, S., Funk, J., Cinar, Y., Knackstedt, M., "Pore network modeling of saudi aramco rocks: a comparative study," Society of Petroleum Engineers, 2009, pp. 1-13.
- [4] Hidajat, I., Rastogi, A., Singh, M. and Mohanty, K. K., "Transport properties of porous media from thin-sections". SPE 69623, SPE LACPEC, March 25-27, 2001.
- [5] Damiani M.C., Fernandes C.P., Bueno A.D., Santos L.O. E., Cunha Neto J.A.B., and Philippi P.C., "Predicting Physical Properties of Reservoir Rocks from the Microstructural Analysis of Petrographic Thin Sections," Submitted to Produccion, 2000
- [6] Tolke, J., Baldwin, C., Mu, Y., Derzhi, N., Fang, Q., Grader, A and Dvorkin, J., "Computer Simulations of Fluid Flow in Sediment: From Images to Permeability" The Leading Edge, Jan, 2010, pp. 68-74.
- [7] Storer, S., "Pore-scale modelling based on microscopic analysis of drill cuttings," first break, vol. 27, July, 2009, pp. 77-83.

- [8] Knackstedt, M. A., Arns, C. H., Limaye, A., Sakellariou, A., Senden, T. J., Sheppard, A. P., Sok, R. M., Pinczewski, W. V. and Bunn, G. F., "Digital Core Laboratory: Properties of Reservoir Core derived from 3D images," SPE 87009, Kuala Lumpur, Malaysia, 2004.
- [9] Kameda, A., "Permeability evolution in sandstone: Digital rock approach," Ph.D. Dissertation, Stanford University, 2005.
- [10] Kayser, A., Kellner, A., Holzapfel, H. W., Van der bilt, Warner, S., and Gras, R., "3D visualization of a rock sample, Rotliegend sandstone, Southern Permian Basin: applications for core analysis and petrophysics," Petroleum Geology Conf. Series, vol. 6, 2005, pp. 1613-1620.
- [11] Marcke, P. V., Verleye, B., Carmeliet, J., Roose, D., and Swennen, R., "An Improved Pore Network Model for the Computation of the Saturated Permeability of Porous Rock," Transport in Porous Media, Vol.85, 2010, pp. 2451-476.
- [12] Grader, A. S., Andrew, B.S., Al-Dayyani, T. and Nur, A., "Computations of Porosity and Permeability of Sparic Carbonate Using Multi-Scale Ct Images," Int. Sym. of the Soc. of Core Analysts, 2009.
- [13] Adler, P. M., Jacquin, C. G. and Quiblier, J. A., "Flow in simulated porous media", Int. J. Multiphase Flow, **16**, 1990, pp. 691-712.
- [14] Yeong, C. L. Y., and Torquato, S., "Reconstructing random media", Phys. Rev. E, **57**, 1998a, pp. 495–506.
- [15] Yeong, C. L. Y., and Torquato, S., 1998b, Reconstructing random media. II. Threedimensional media from two-dimensional cuts, Phys. Rev. E, **58**, 224–233.

- [16] Mese, A., Tutuncu, A., Kameda, A., Nur, A., and Dvorkin, J., “Digital rock physics for sands and shales,” Oil & Gas Network, June, p. 68, 2004.
- [17] Keehm, Y., Mukerji, T., and Nur, A., “Computational rock physics at the pore scale: Transport properties and diagenesis in realistic pore geometries,” The Leading Edge, **20**, 2001, pp. 180–183.
- [18] Bakke, S. and Øren, P. E., “3-D pore-scale modeling of sandstones and flow simulations in the pore networks,” SPEJ, **2**, 136, 1997.
- [19] Mavko, G., and Nur, A., “The effect of a percolation threshold in the Kozeny-Carman relation”, Geophysics, **62**, 1997, pp.1480–1482.
- [20] Walsh, J. B., and Brace, W. F., “The effect of pressure on porosity and transport properties of rock”, J. Geophy. Res., **89**, 1984, pp. 9425–9431.
- [21] Dunsmuir, J. H., Ferguson, S. R., D'Amico, K. L. and Stokes, J. P., “X-ray microtomography. A new tool for the characterization of porous media,” Paper SPE22860 proceedings of SPE Annual Technical Conference and Exhibition held in Dallas, Texas, October 6-9, 1991, pp. 423-430.
- [22] Jasti, J. K., Jesion, G. and Feldkamp, L., “Microscopic imaging of porous media with X-ray computer tomography”, SPE Formation Evaluation, **8**, 1993, pp.189-193.
- [23] Coles, M. E., Hazlett, R. D., Muegge, E. L., Jones, K. W., Andrews, B., Dowd, B., Siddons, P., Peskin, A., Spanne, P. and Soll, W., “Developments in synchrotron X-ray microtomography with applications to flow in porous media,” SPE Reservoir Evaluation & Engineering, **1**, 1998, pp.288-296.

- [24] Okabe, H. and Blunt, M. J., "Pore Space Reconstruction Using Multiple-Point Statistics," *Journal of Petroleum Science and Engineering*, 46, 2005, pp. 121–137.
- [25] Tiab, D. and Donaldson, E., "Petrophysics: Theory and Practice of Measuring Reservoir Rock and Transport Properties," Gulf Publishing Company, Houston, 1996, 706pp.
- [26] Fens, T. W., "Petrophysical properties from small rock samples using image analysis techniques," Ph.D. Dissertation, Delft, 2000.
- [27] Carman, P. C., "L'écoulement des Gaz à Travers les Milieux Poreux," Bibliothèque des Sciences et Techniques Nucléaires, Presses Universitaires de France, Paris, 1961, 194pp.
- [28] Berryman, J. G. and Blair, S. C., "Kozeny-Carman relations and image processing methods for estimating Darcy's constant", *J. Appl. Phys.*, **60**, 1987, pp. 1930-1938.
- [29] Blair, S. C., Berge, P. A., and Berryman, J. G., "Two-point Correlation Functions to Characterize Microgeometry and Estimate Permeabilities of Synthetic and Natural Sandstones," Lawrence Livermore National Laboratory Report, Livermore, 1993.
- [30] Schaap, M. G., and Lebron, I., "Using microscope observations of thin sections to estimate soil permeability with the Kozeny-Carman Equation," *J. Hydrol.*, 251, 2001, pp. 186–201.
- [31] Torabi, A., Fossen, H., and Alaei, B., "Application of spatial correlation functions in permeability estimation of deformation bands in porous rocks," *J. Geophys. Res.*, 113, 2007

- [32] Fauzi, U., “An Estimation of Rock Permeability and Its Anisotropy from Thin Sections Using a Renormalization Group Approach,” *Energy Sources, Part A: Recovery, Utilization, and Environmental Effects*, Vol 33, **6**, 2011.
- [33] Dvorkin, J., “Kozeny-Carman Equation Revisited”, 2009, Notes from www.pangea.stanford.edu/~jack/
- [34] Fatt, I., “The network model of porous media: I. Capillary pressure characteristics,” *Pet. Tran. AIME*, **207**, 1956, pp. 144-159.
- [35] Chatzis, I. and Dullien, F. A. L., “Dynamic immiscible displacement mechanisms in pore doublets: Theory versus experiment”, *J. Colloid Interface Sci.*, **91**, 1983, pp. 199-222.
- [36] Bryant, S. and M. Blunt, “Prediction of relative permeability in simple porous media,” *Physical Review A*, 1992, **46**(4): p. 2004-2011.
- [37] Bryant, S.L., King, P.R. and Mellor, D.W., “Network model evaluation of permeability and spatial correlation in a real random sphere packing,” *Transport in Porous Media*, 1993. **11**: p. 53-70.
- [38] Bryant, S.L., Mellor, D.W., and Cade, C.A., “Physically representative network models of transport in porous media,” *AIChE Journal*, 1993. **39**(3): p. 387-396.
- [39] Lindquist, W. B., Lee, S. M., Coker, D. A., Jones, K. W. and Spanne, P., “Medial axis analysis of void structure in three-dimensional tomographic images of porous media,” *Journal of Geophysical Research-Solid Earth*, **101**, 1996, pp. 8297-8310.

- [40] Lindquist, W. B. and Venkatarangan, A., "Investigating 3D geometry of porous media from high resolution images," *Physics and Chemistry of the Earth, Part A: Solid Earth and Geodesy*, **24**, 1999, pp. 593-599.
- [41] Lindquist, W. B., Venkatarangan, A., Dunsmuir, J. and Wong, T. F., "Pore and throat size distributions measured from synchrotron X-ray tomographic images of Fontainebleau sandstones," *Journal of Geophysical Research: Solid Earth*, **105**, 2000, pp. 21509-21527.
- [42] Silin, D.B., Guodong, J., and Patzek, T.W., "Robust determination of the pore space morphology in sedimentary rocks," in SPE Paper 84296, *Proceedings of the SPE Annual Technical Conference and Exhibition*. 2003. Denver, Colorado.
- [43] Silin, D. and Patzek, T., "Pore Space Morphology Using Maximal Inscribed Spheres," *Physica A*, 2006. **371**: pp. 336 - 360.
- [44] Al-Kharusi, A.S. and Blunt, M.J., "Network Extraction from Sandstone and Carbonate Pore Space Images," *Journal of Petroleum Science and Engineering*, 2007. **56**: pp. 219 - 231.
- [45] Dong, H., Touati, M., and Blunt, M.J., "Pore Network Modeling: Analysis of Pore Size Distribution of Arabian Core Samples," In SPE Paper 105156, *Proceedings of the 15th SPE Middle East Oil & Gas Show and Conference*. 2007. 11-14th March, Bahrain.
- [46] Hardy, J., de Pazzis, O. and Pomeau, Y., "Molecular dynamics of a classical lattice gas: Transport properties and time correlation functions," *Phys. Rev. A*, **13**, 1976, pp.1949-1961.
- [47] Frisch, U., Hasslacher, B. and Pomeau, Y., "Lattice-gas automata for the Navier-Stokes equation," *Phys. Rev. Lett.*, **56**, 1986, pp.1505-1508.

- [48] Gunstensen, A. K., Rothman, D. H., Zaleski, S. and Zanetti, G., “Lattice Boltzmann model of immiscible fluids,” *Phys. Rev. A*, **43**, 1991, pp.4320-4327.
- [49] Rothman, D. H., “Cellular-automaton fluids: a model for flow in porous media,” *Geophysics*, **53**, 1988, pp. 509-518.
- [50] Higuera, F., Succi, S. and Benzi, R., “Lattice gas dynamics with enhanced collisions,” *Europhys. Lett.*, **9**, 1989, pp. 345-349.
- [51] Bosl, W. J., Dvorkin, J., and Nur, A., “A numerical study of pore structure and permeability using a Lattice Boltzmann Simulation,” *Geophy. Res. Lett.*, **25**, 1998, pp. 1475–1478.
- [52] Gunstensen, A. K. and Rothman D. H., “Lattice-Boltzmann studies of immiscible two-phase flow through porous media,” *J. Geophy. Res.*, **98**, 1993, pp. 6431-6441.
- [53] Cancelliere, A., Chang, C., Foti, E., Rothman, D. H. and Succi, S., “The permeability of a random medium: comparison of simulation with theory,” *Phys. Fluids A*, **2**, 1990, pp. 2085-2088.
- [54] Ladd, A. J. C., “Numerical simulations of particulate suspensions via a discretized Boltzmann equation: Part 1”. *Theoretical foundation*, *J. Fluid. Mech.*, **271**, 1994, pp. 285–309.
- [55] Martys, N. S. and Chen, H., “Simulation of multicomponent fluids in complex threedimensional geometries by the lattice Boltzmann method,” *Phys. Rev. E*, **53**, 1996, pp. 743-750.

- [56] Koponen, A., Kandhai, D., Hellén, E., Alava, A., Hoekstra, A. G., Kataja, M., Niskanen, K., Slood, P. and Timonen, K., “Permeability of three-dimensional random fiber webs,” *Phys. Rev. Lett.*, **80**, 1998, pp. 716-719.

- [57] Ladd, A. J. C., “Numerical simulations of particulate suspensions via a discretized Boltzmann equation: Part 2. Numerical results,” *J. Fluid. Mech.*, **271**, 1994, pp. 311–339.

- [58] Spaid, M. A. A., and Phelan, F. R., Jr., “Lattice Boltzmann methods for modelling microscale flow in fibrous porous media,” *Phys. Fluids*, **9**, 1997, pp. 2468–2474.

- [59] Fredrich, J. T., Noble, D. R., O'Connor, R. M., and Lindquist, W. B., “Development, Implementation, and Experimental Validation of the Lattice-Boltzmann Method for Modeling Three-dimensional Complex Flows,” Sandia National Laboratory report SAND99-0369, Sandia National Laboratory, Sandia, 1999.

- [60] Succi, S., “The Lattice Boltzmann Equation for Fluid Dynamics and Beyond,” Oxford University Press, New York, 2001, 304pp.

- [61] Arns, C.H, Knackstedt, M.A., Pinczewski, W.V., and Lindquist, W.B., “Accurate estimation of transport properties from microtomographic images,” *Geophysical Research Letters*, 28, 17, 2001, pp. 3361-3364.

- [62] Arns, C.H., Bauget, F., Limaye, A., Sakellariou, A., Senden, T.J., Sheppard, A.P., Sok, R.M., Pinczewski, V., Bakke, S., Berge, L.I., and Øren, P.E., “Pore-Scale Characterisation of Carbonates Using X-Ray Microtomography,” *SPE Journal*, **10**(4), 2005, pp. 475 - 84.

- [63] Riepe, L., Suhaimi, M. H. B., Kumar, M., Knackstedt, M. A., “Application of High Resolution Micro-CT Imaging and Pore Network Modeling (PNM) for the Petrophysical Characterization of Tight Gas Reservoirs - A Case History from a Deep Clastic Tight Gas Reservoir in Oman,” SPE Middle East Unconventional Gas Conference and Exhibition, 31 January-2 February, Muscat, Oman, 2011.
- [64] Riepe, L., “New Technologies for Petrophysics: Applications of Micro-CT Tomograms and Pore Network Modeling to Evaluate the Storage and Flow Capacity of Tight Gas and Basement Reservoirs,” Technical Talk, Kuala Lumpur, 21 April 2011.
- [65] Hilfer, R., and Manwart, C., “Permeability and conductivity for reconstructed models of porous media,” *Phys. Rev. E*, **64**, 021304, 2001.
- [66] Manwart, C., Torquato, S., and Hilfer, R., “Stochastic reconstruction of sandstones,” *Phys. Rev. E*, **62**, 2000, pp. 893–899.
- [67] Zhang, T., Lu, D. T., and Li, D. L., “A statistical information reconstruction method of images based on multiple-point geostatistics integrating soft data with hard data,” *Proceedings of ISCST 2008*, Shanghai, China, vol.1, Dec. 2008, pp.573-578.
- [68] Keehm, Y., Mukerji, T., and Nur, A., “Permeability prediction from thin sections: 3D reconstruction and Lattice-Boltzmann flow simulation,” *Geophysical Research Letters*, **31**, L04606, 2004.
- [69] Keehm, Y., Sternlof, K. and Mukerji, T., “Computational estimation of compaction band permeability in sandstone,” *Geosci. J.*, 10(4), 2006, pp. 499–505.

- [70] Jin, G., Patzek, T. W. and Silin, D. B., “Physics-based Reconstruction of Sedimentary Rocks,” Proceedings of the SPE Western Regional / AAPG Pacific Section Joint Meeting, SPE 83587, Long Beach, California, 2003.
- [71] Richa, R., “Preservation of Transport Properties Trends: Computational Rock Physics Approach” Ph.D. Dissertation, Stanford University, 2010.
- [72] Dvorkin, J. and Nur, A., “Scale of experiment and rock physics trends,” The Leading Edge, 28(1), pp. 110–115, 2009.
- [73] Bear, J., “Dynamics of fluids in porous media,” American Elsevier. New York, NY, 1972.
- [74] Zhan, X., “Transport and Seismoelectric Properties of Porous Permeable Rock: Numerical Modeling and Laboratory Measurements,” Ph.D. Dissertation, Massachusetts Institute of Technology, 2010.
- [75] Remy, N., Boucher, A., and Wu, J.B., “Applied Geostatistics with SGeMS: A Users’ Guide,” Cambridge: Cambridge University Press, 2009.
- [76] Deutsch, C. V., and Journel, A.G., “GSLIB: Geostatistical Software Library and User’s Guide”, Oxford University Press, New York, 369, 1998.
- [77] Weger, R. J., “Quantitative Pore/Rock Type Parameters in Carbonates and Their Relationship to Velocity Deviations,” Ph.D. Dissertation, University of Miami, 2010.
- [78] Ramil, A., “Petrophysical Characterization and Permeability Upscaling of Fault Zones in Sandstone with A Focus on Slip Surfaces and Slip Bands” M.Sc. Thesis, Stanford University, 2006.

- [79] Rubin, D. M., “A simple autocorrelation algorithm for determining grain size from digital images of sediment,” *Journal of Sedimentary Research* 74, 160–165. 2004.
- [80] Warrick, J.A., Rubin, D.M., Ruggiero, P., Harney, J., Draut, A.E., and Buscombe, D., “Cobble Cam: Grain-size measurements of sand to boulder from digital photographs and autocorrelation analyses,” *Earth Surface Processes and Landforms* (34) pp. 1811-1821, 2009.
- [81] Deutsch, C. V., “Calculating effective absolute permeability in sandstone/shale sequences,” *SPE Formation Evaluation*, **9**, 1989.
- [82] Weber, K. J. and Van Geuns, L.C., “Framework for constructing clastic reservoir simulation models”, *J. Petroleum Technology*, **10**, 1248-1297, 1990.

PUBLICATIONS

- [1] Lubis, L.A. and Harith, Z.Z.T., “Study of Upscaling Permeability from Thin Sections using 3D Pore Space Image and Pore Network Modeling” paper presented at Petroleum Geology Conference and Exhibition (PGCE) 2011, Kuala Lumpur, Malaysia, 06-07 March 2011.
- [2] Lubis, L.A., Harith, Z.Z.T. and Noh, K.A.M., “Workflow to Reconstruct 3D Pore Space from 2D CT-Scan Image of Berea Sandstone” paper presented at National Geosciences Conference (NGC) 2011, Johor Bahru, Malaysia, 11-12 June 2011.

IN PREPARATION PUBLICATIONS

- [1] Lubis, L.A., Harith, Z.Z.T., Khairy, H., Noh, K.A.M. and Salih, A.M., “A New Workflow to Predict Laboratory Scale Permeability of Sandstone using Thin Section Image Information” paper in preparation for Asian Journal of Earth Science, November 2011.

- [2] Lubis, L.A., Harith, Z.Z.T., Fauzi, U, Noh, K.A.M. and Khairy, H., “Pore Scale 3D Porous Media Reconstruction Using Thin Section Images and Its Application to Predict Laboratory Scale Permeability” paper in preparation for Institute of Technology Bandung (ITB) Journal, November 2011.

- [3] Lubis, L.A., Harith, Z.Z.T., Khairy, H., Noh, K.A.M. and Salih, A.M., “Predicting Laboratory Scale Permeability on Berea Sandstone Thin Section using 3D Porous Media Reconstruction and Upscaling Method” paper in preparation for Petroleum Geosciences Conference and Exhibition (PGCE) 2012, Kuala Lumpur, Malaysia, April 2012.

- [4] Lubis, L.A., Harith, Z.Z.T., Noh, K.A.M. and Khairy, H., “Reconstruction of 3D Porous Media from 2D Image of Sandstone on Standard Personal Computer” paper in preparation for National Geosciences Conference (NGC) 2012, Malaysia, June 2012.

- [5] Lubis, L.A., Harith, Z.Z.T., Noh, K.A.M. and Khairy, H., “Application of Upscaling Permeability Workflow: Pore to Core Plug Scale on Malay Basin Thin Sections” paper in preparation for International Conference on Integrated Petroleum Engineering and Geosciences (ICIPEG), Kuala Lumpur, Malaysia, 12-14 June 2012.

APPENDIX A

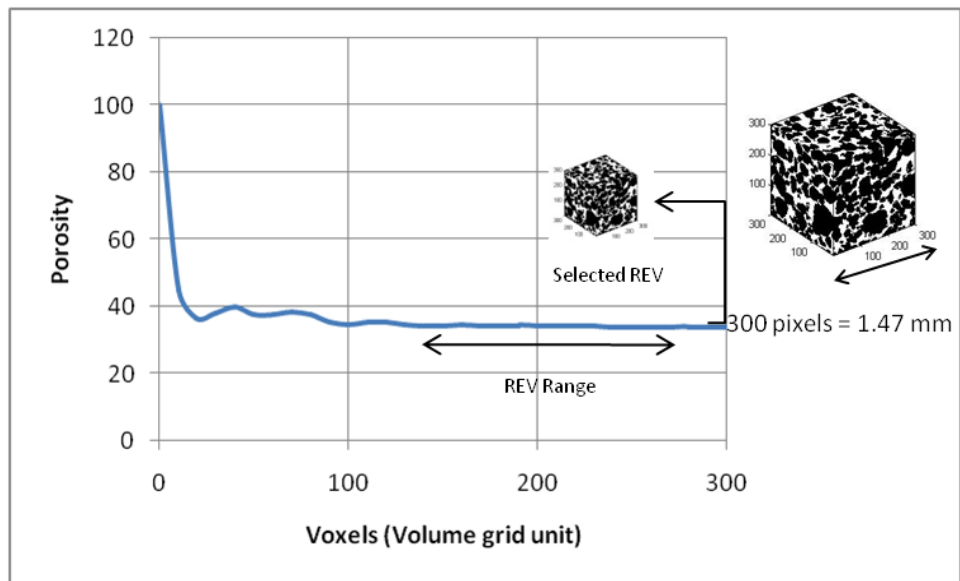


Figure A.1 The REV graph for porosity on 3D CT-Scan of S (2) Sandstone.

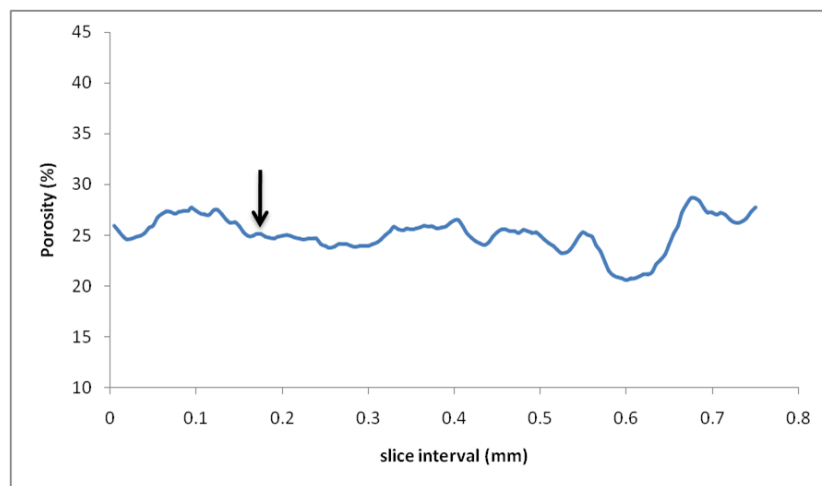


Figure A.2 Porosity fluctuations within the 3D CT-Scan of S (2) Sandstone sample. Arrow indicates the slice which was taken as training image.

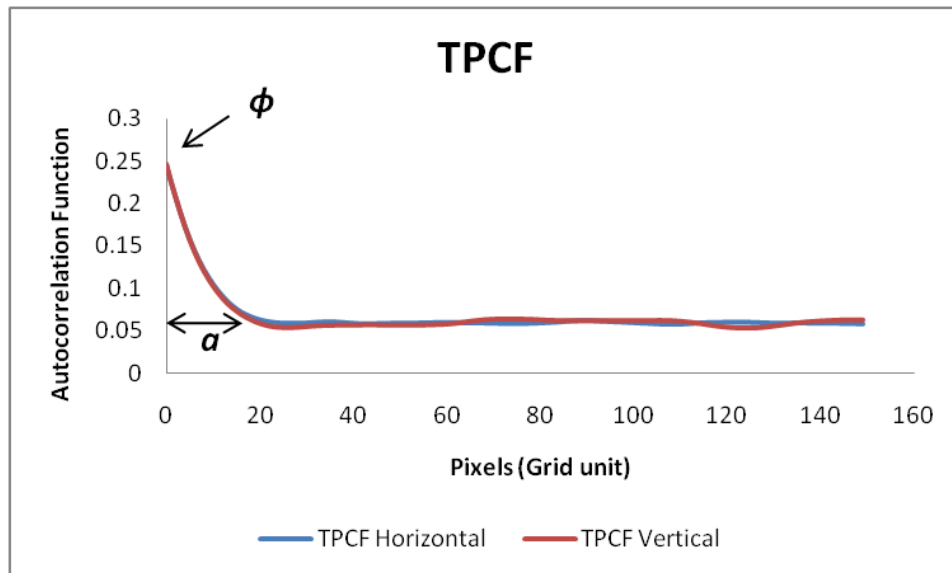


Figure A.3 Horizontal and vertical TPCF graph from S (2) sandstone training image.

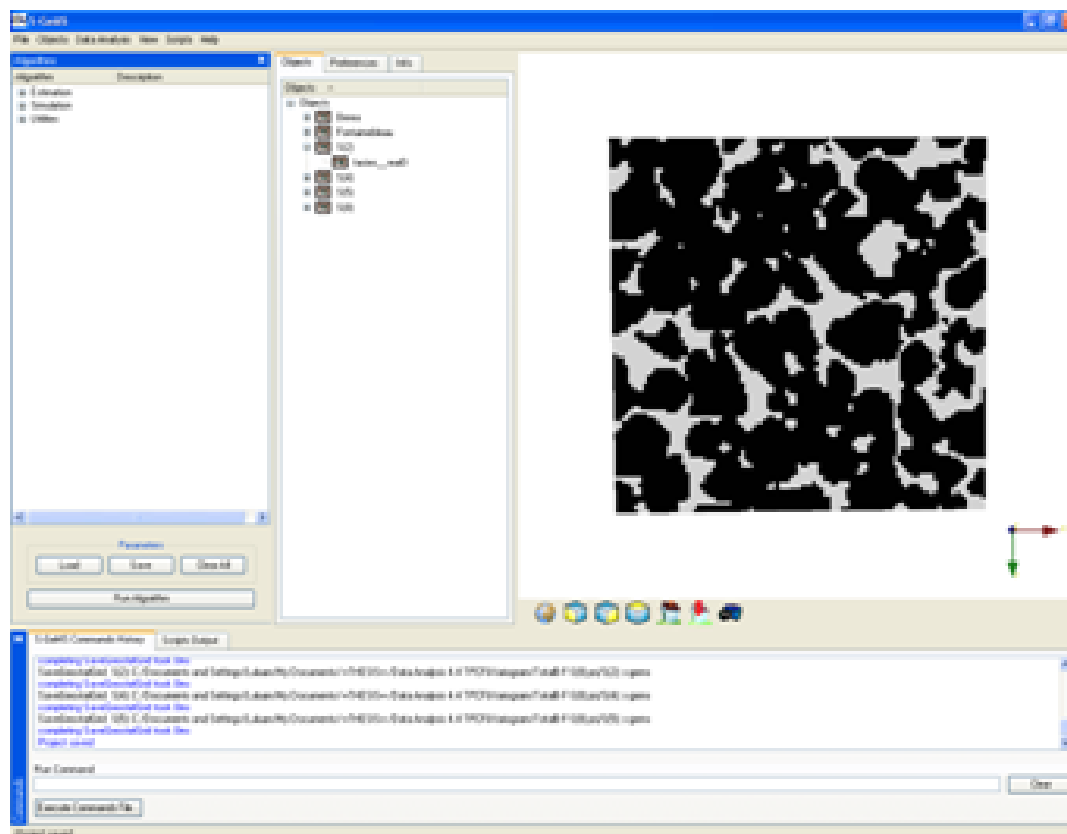


Figure A.4 S (2) sandstone Training image on SGEMS user interface.

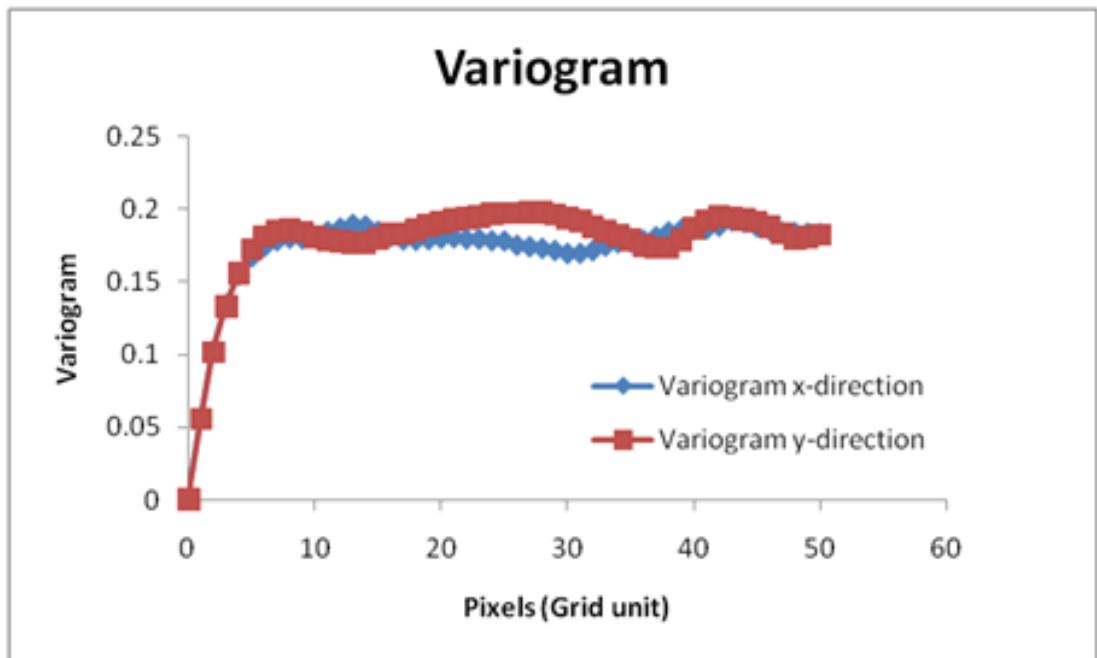


Figure A.5 Variogram calculated from training image from x and y direction.

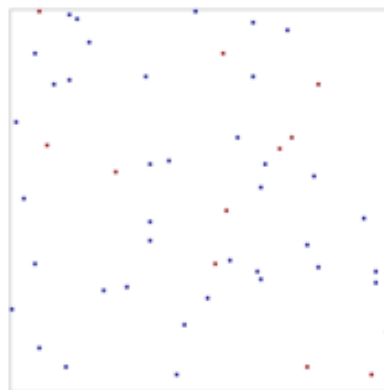


Figure A.6 Sample points extracted from S (2) sandstone training image.

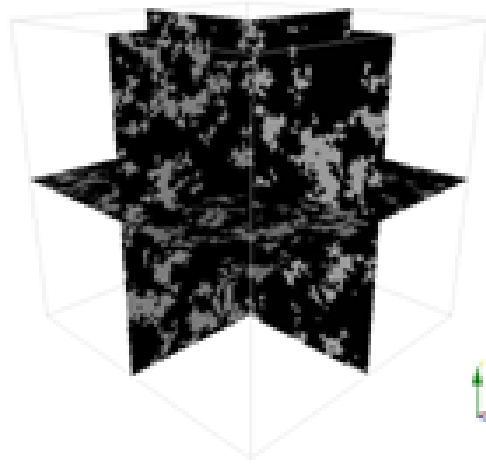


Figure A.7 Cross sectional areas ($x = 50$, $y = 50$ and $z = 50$) of a reconstructed 3D porous media from 2D image of S (2) sandstone.

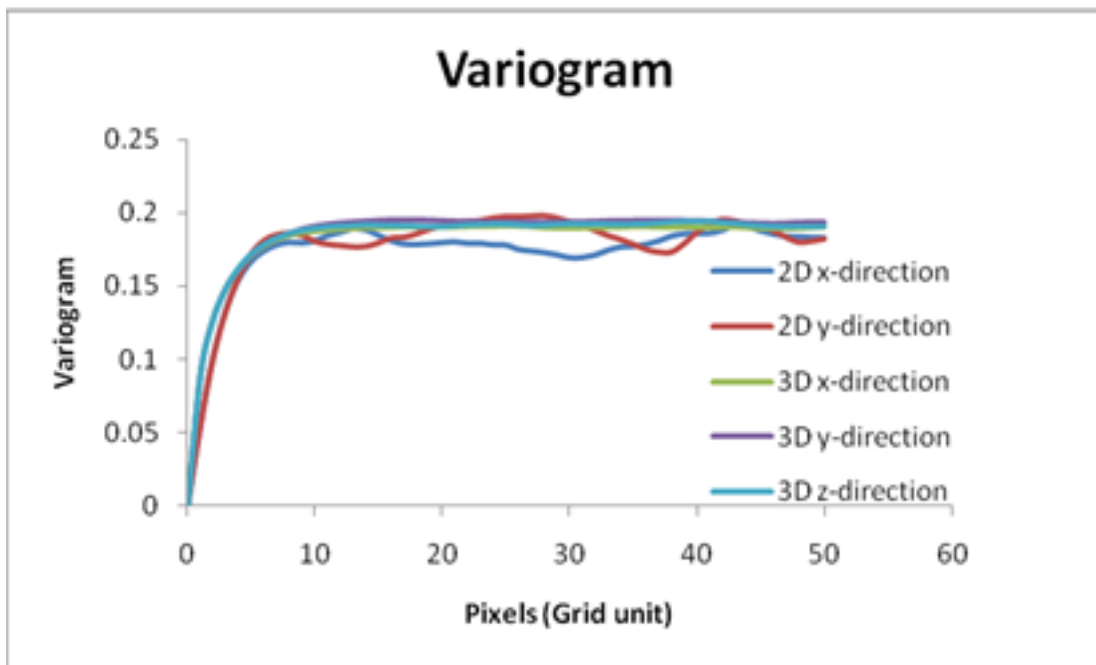


Figure A.8 Variogram comparison between training image (2D image) and reconstructed 3D porous media.

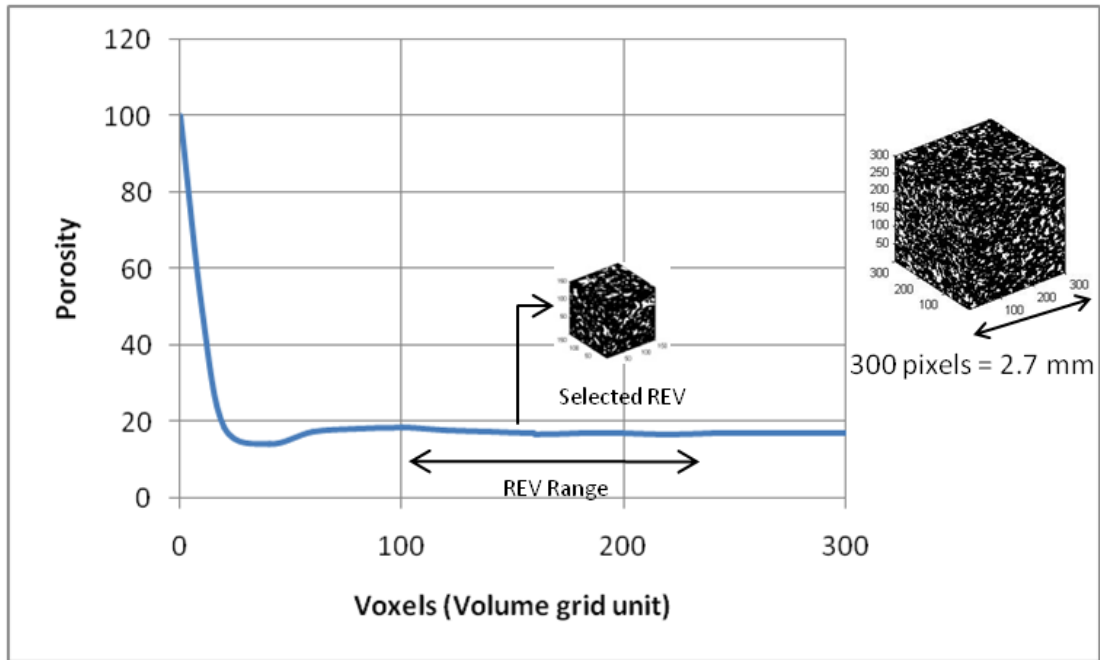


Figure A.9 The REV graph for porosity on 3D CT-Scan of S (4) Sandstone.

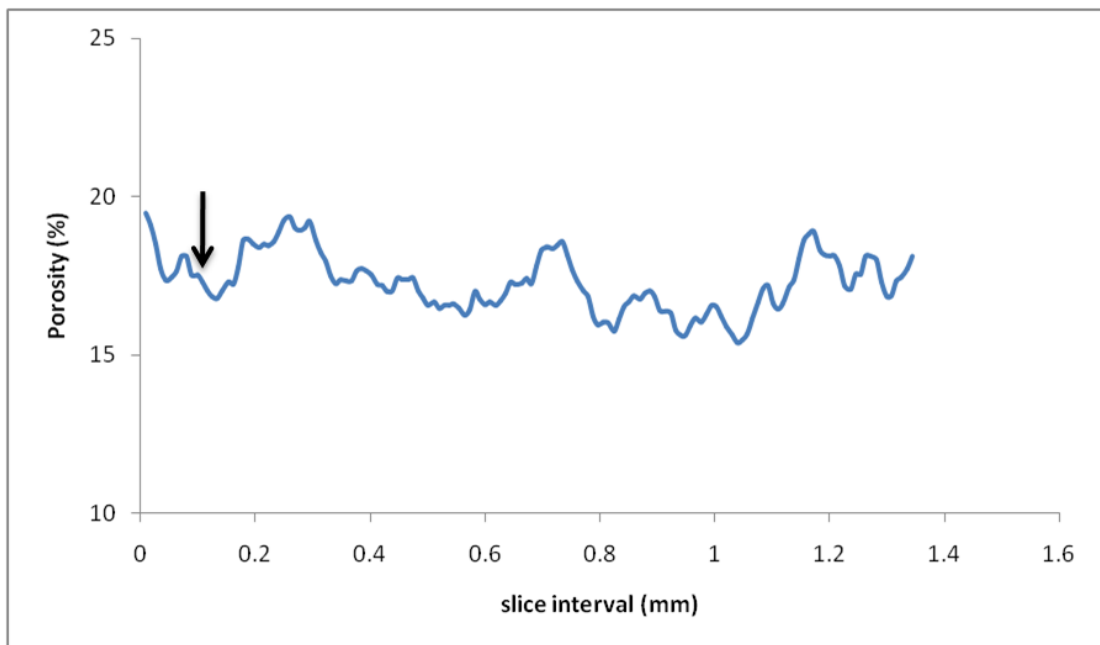


Figure A.10 Porosity fluctuations within the 3D CT-Scan of S (4) Sandstone sample. Arrow indicates the slice which was taken as training image.

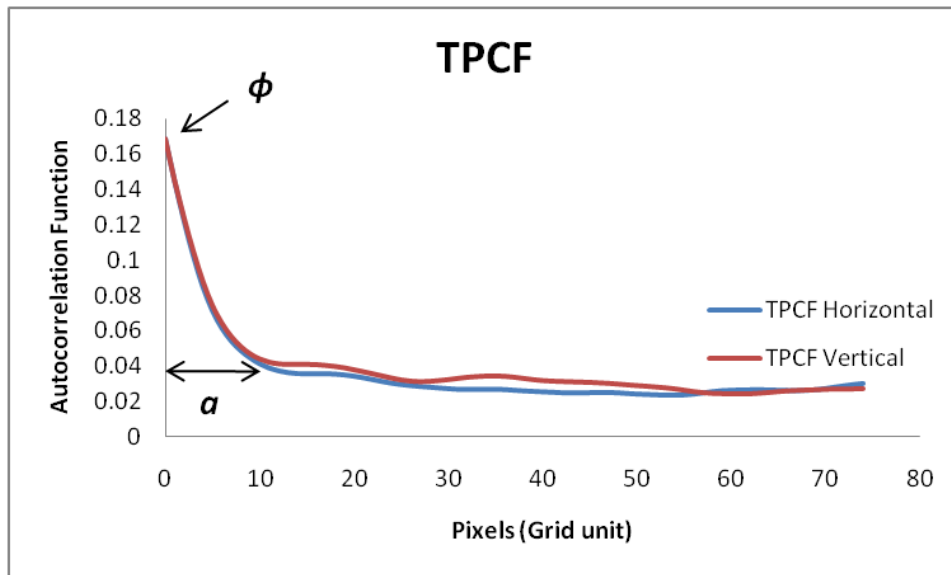


Figure A.11 Horizontal and vertical TPCF graph from S (4) sandstone training image.

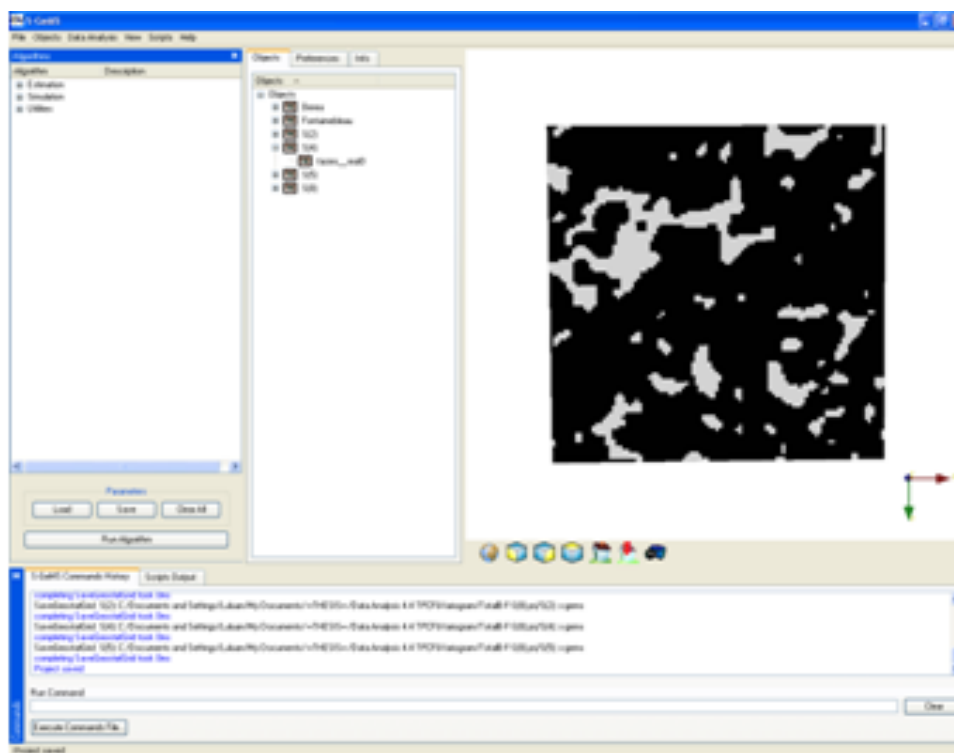


Figure A.12 S (4) sandstone training image on SGEMS user interface.

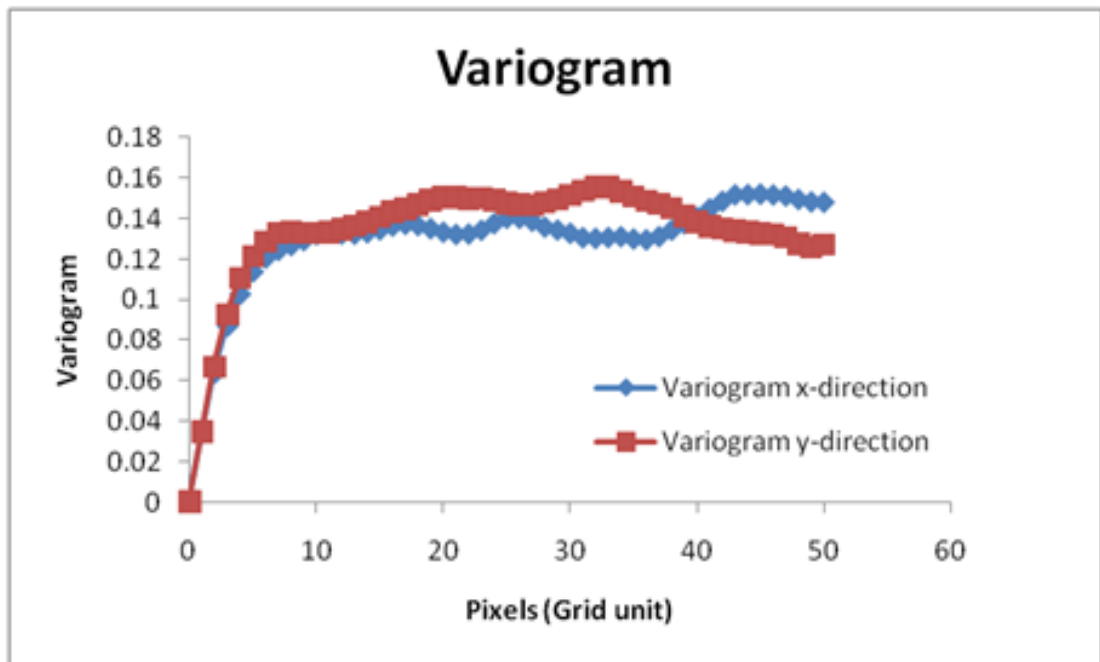


Figure A.13 a) S (4) sandstone training image on SGEMS user interface, b) Variogram calculated from training image from x and y direction.

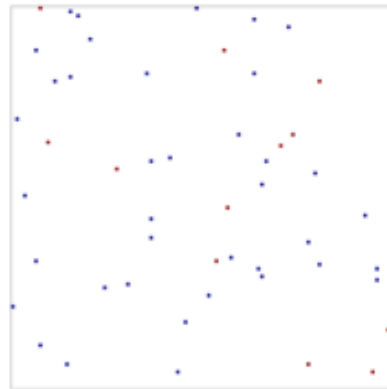


Figure A.14 Sample points extracted from S (4) sandstone training image.

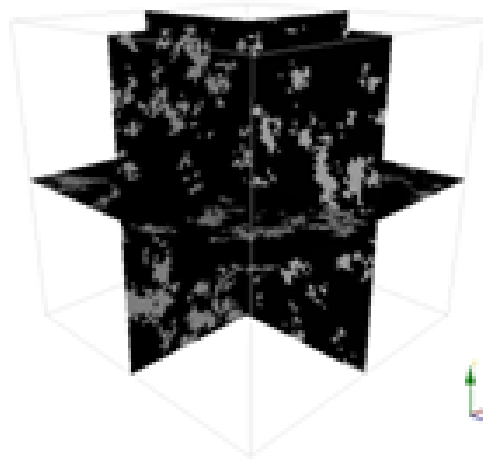


Figure A.15 Cross sectional areas ($x = 50$, $y = 50$ and $z = 50$) of a reconstructed 3D porous media from 2D image of S (4) sandstone.

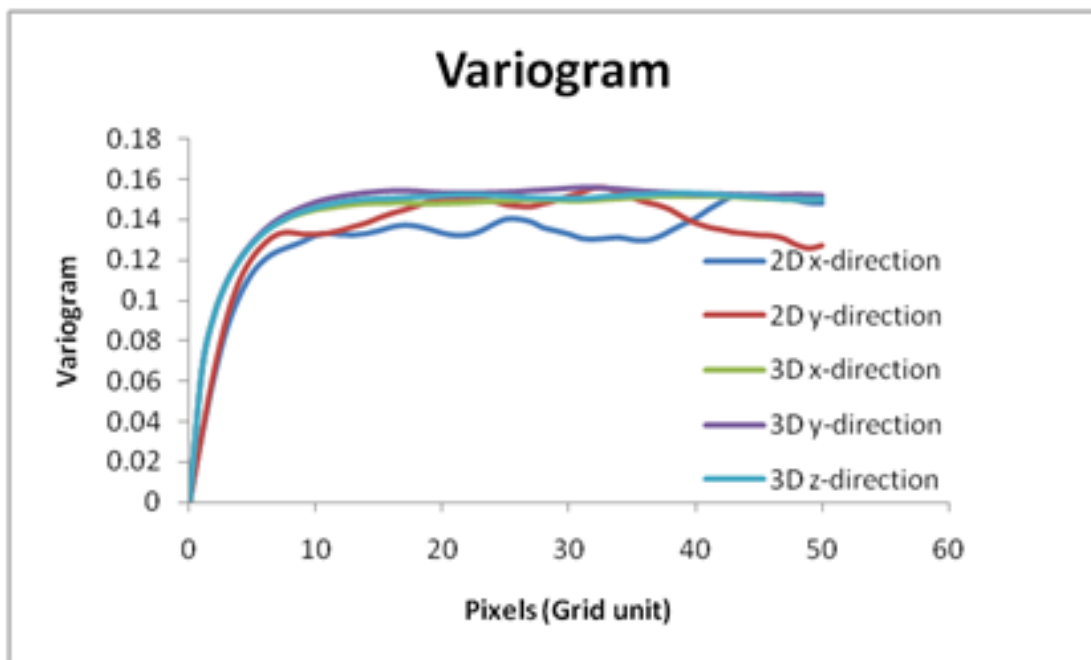


Figure A.16 Variogram comparison between training image (2D image) and reconstructed 3D porous media.

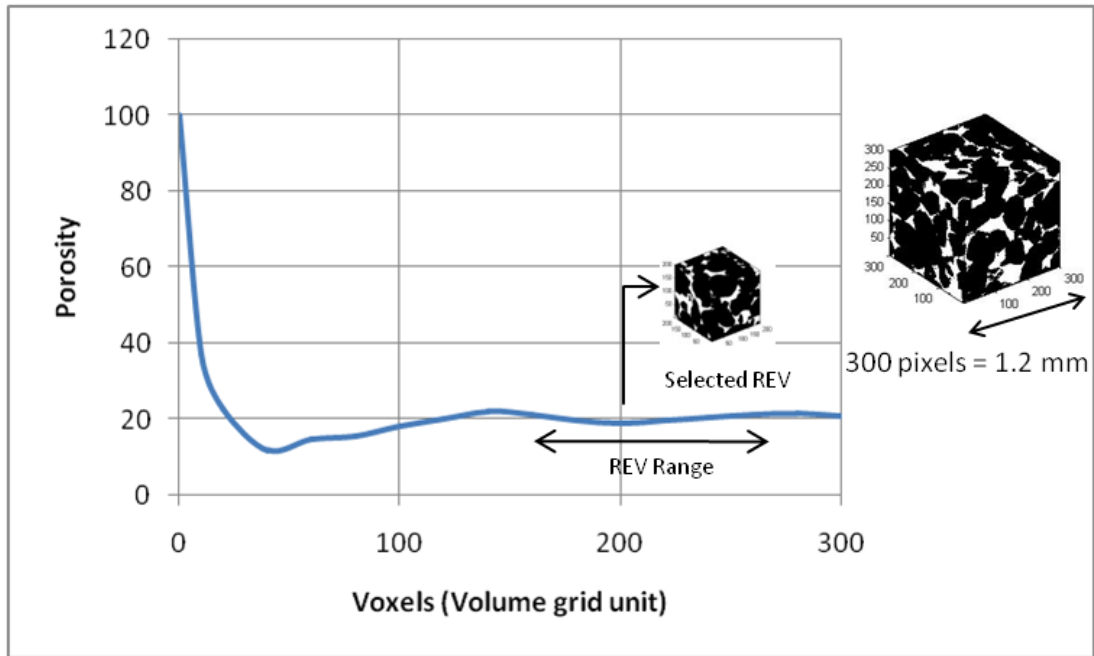


Figure A.17 The REV graph for porosity on 3D CT-Scan of S (5) Sandstone.

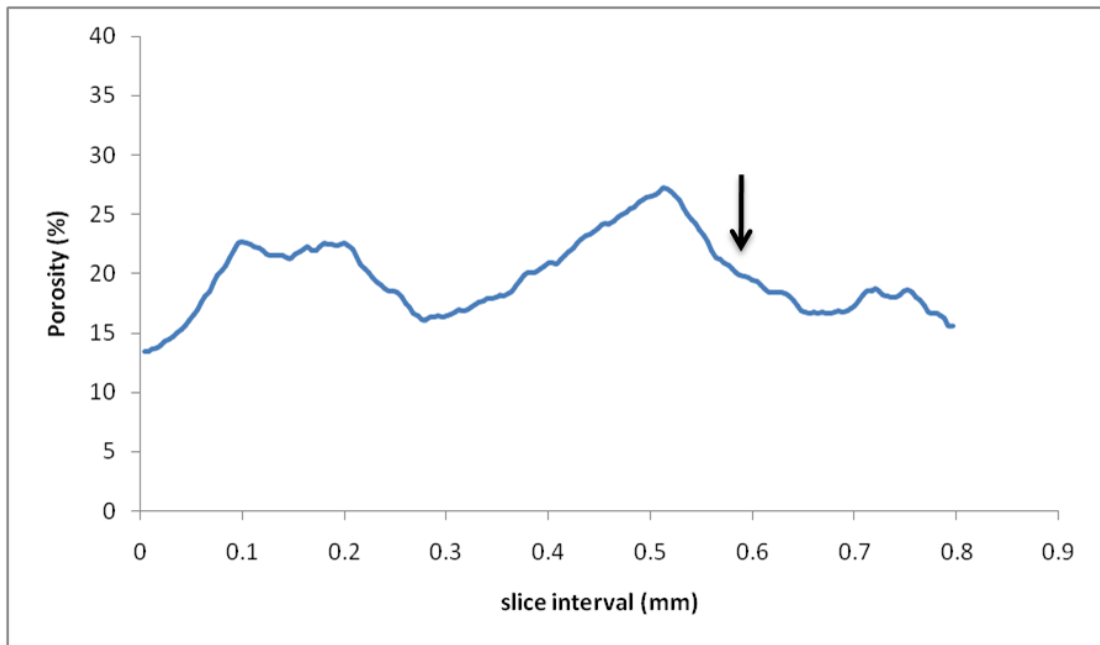
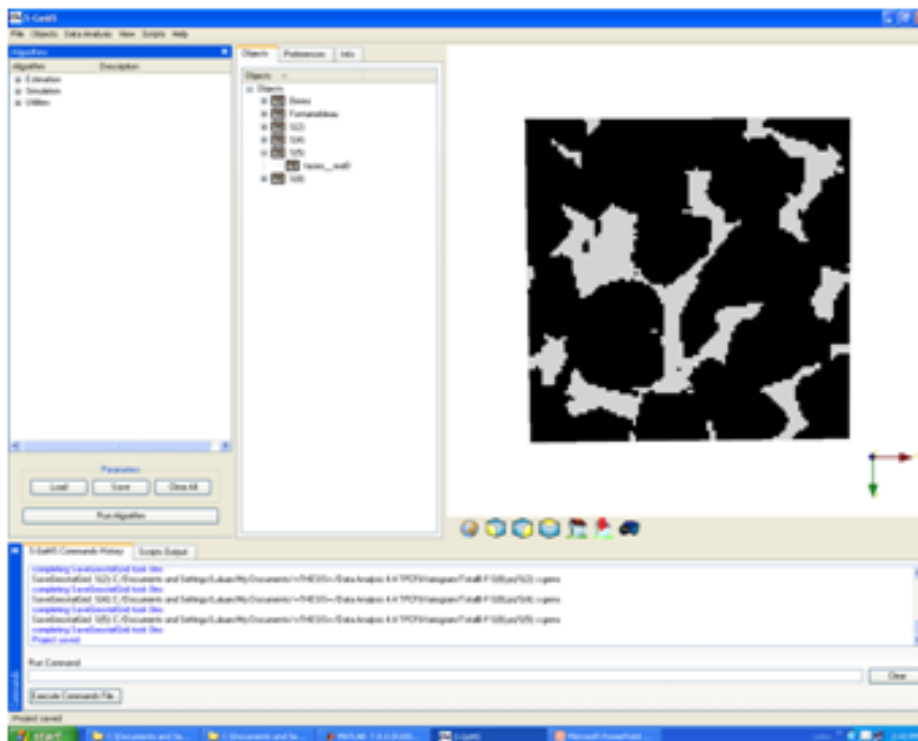
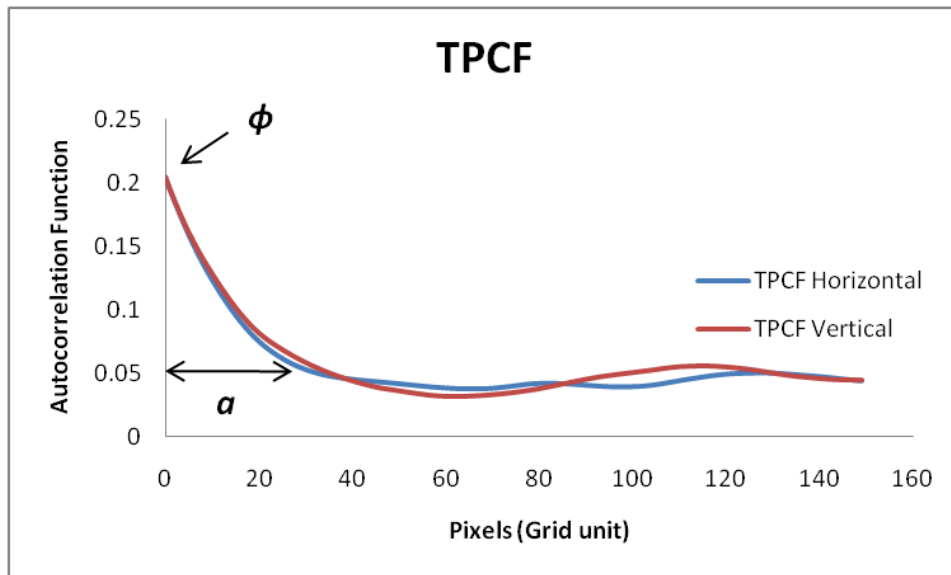


Figure A.18 Porosity fluctuations within the 3D CT-Scan of S (5) Sandstone sample. Arrow indicates the slice which was taken as training image.



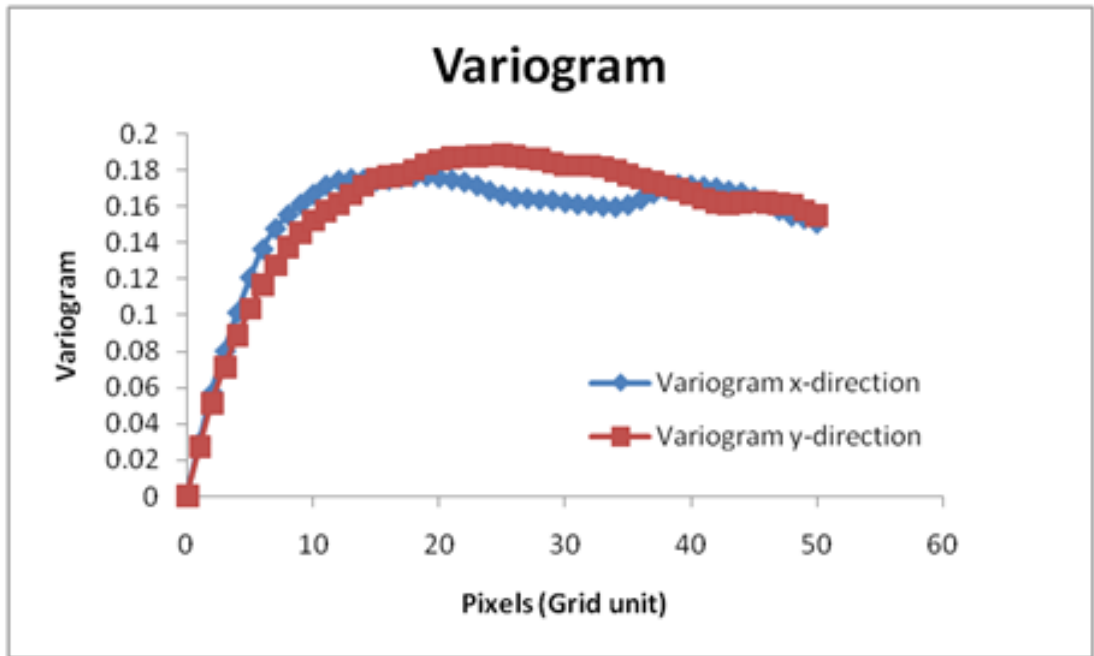


Figure A.21 Variogram calculated from training image from x and y direction.

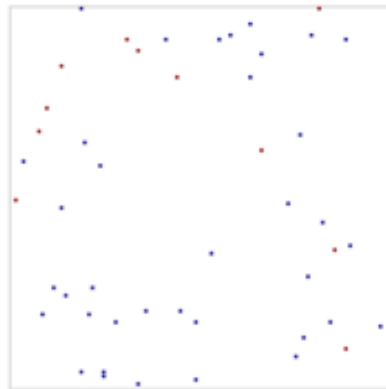


Figure A.22 Sample points extracted from S (5) sandstone training image.

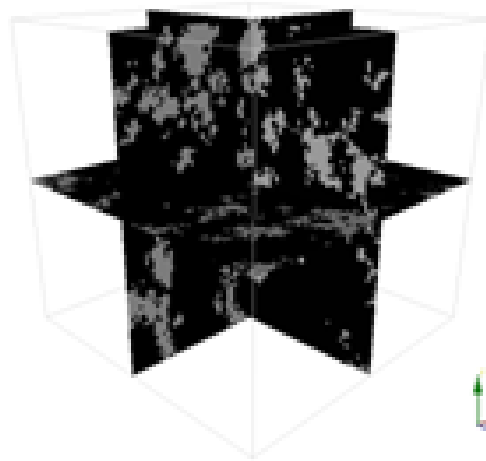


Figure A.23 Cross sectional areas ($x = 50$, $y = 50$ and $z = 50$) of a reconstructed 3D porous media from 2D image of S (5) sandstone.

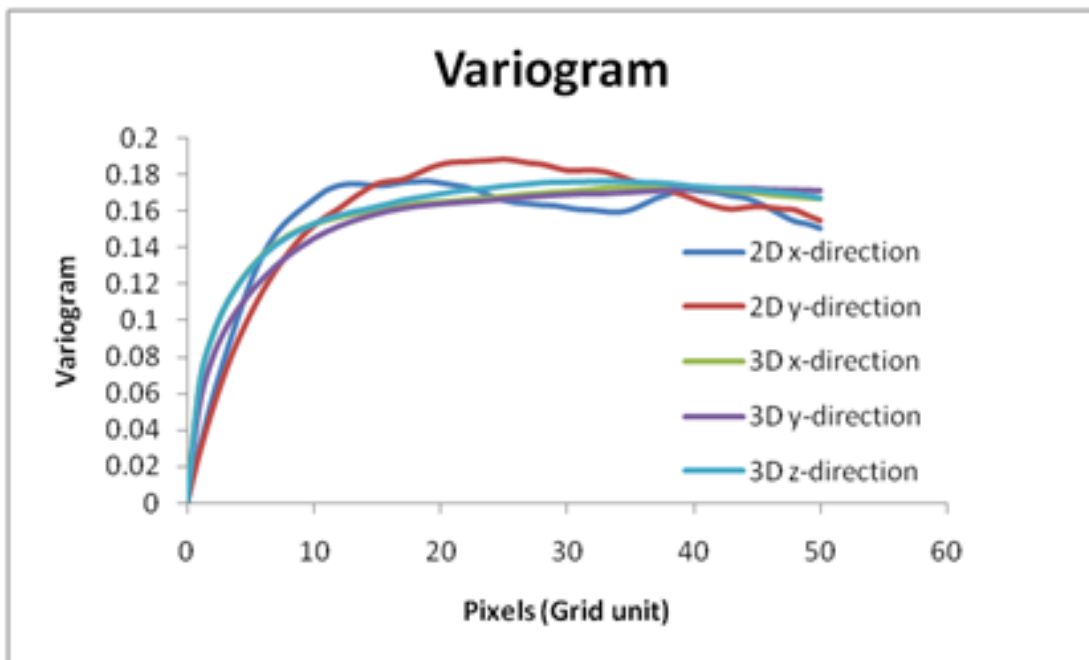


Figure A.24 Variogram comparison between training image (2D image) and reconstructed 3D porous media.

APPENDIX B

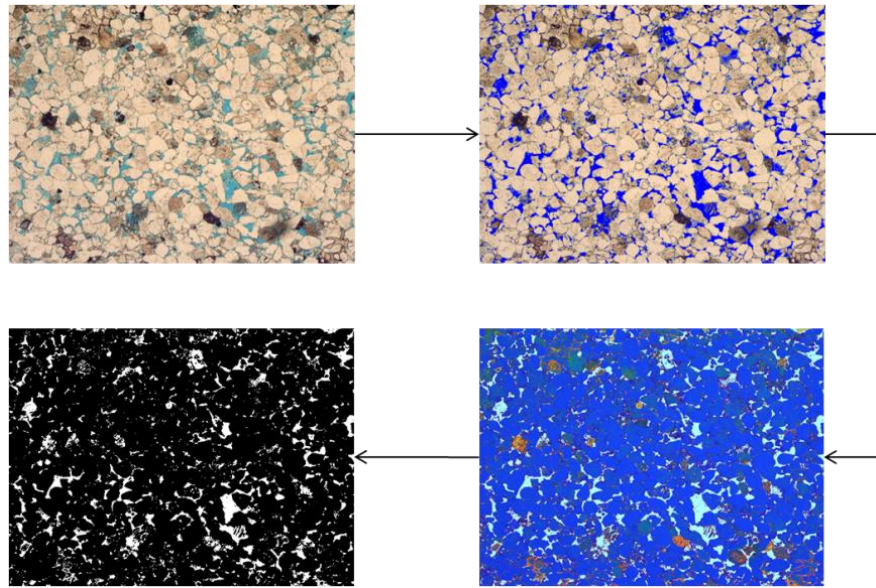


Figure B.1 Steps for image processing and segmentation on selected image (a) from 35 images of Berea sandstone thin section.

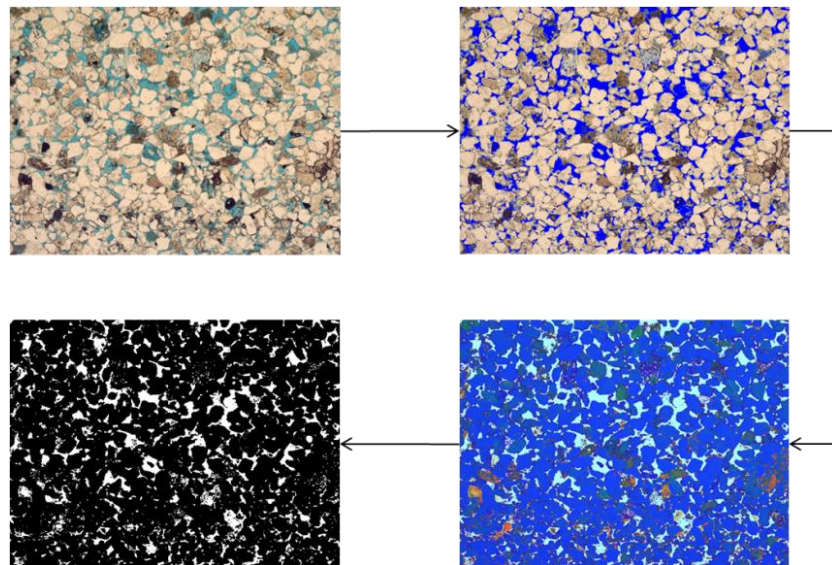


Figure B.2 Steps for image processing and segmentation on selected image (b) from 35 images of Berea sandstone thin section.

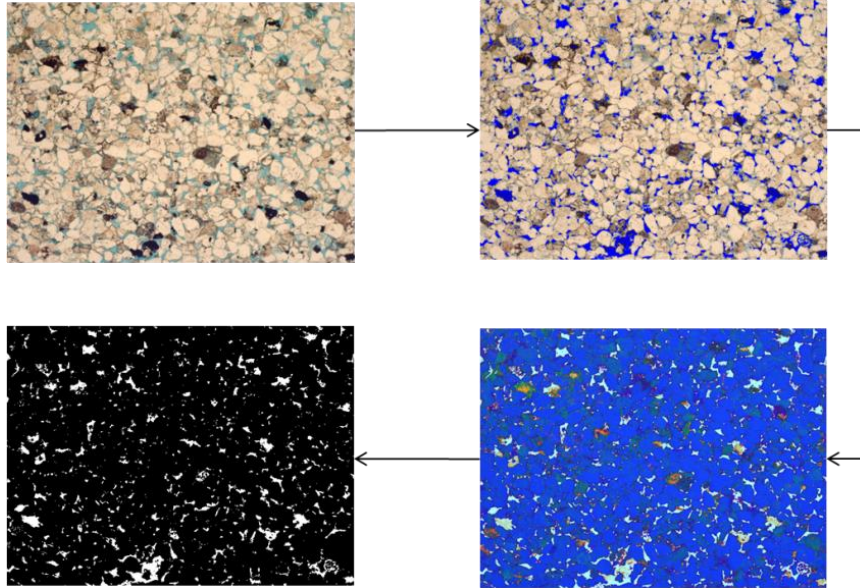


Figure B.3 Steps for image processing and segmentation on selected image (c) from 35 images of Berea sandstone thin section.

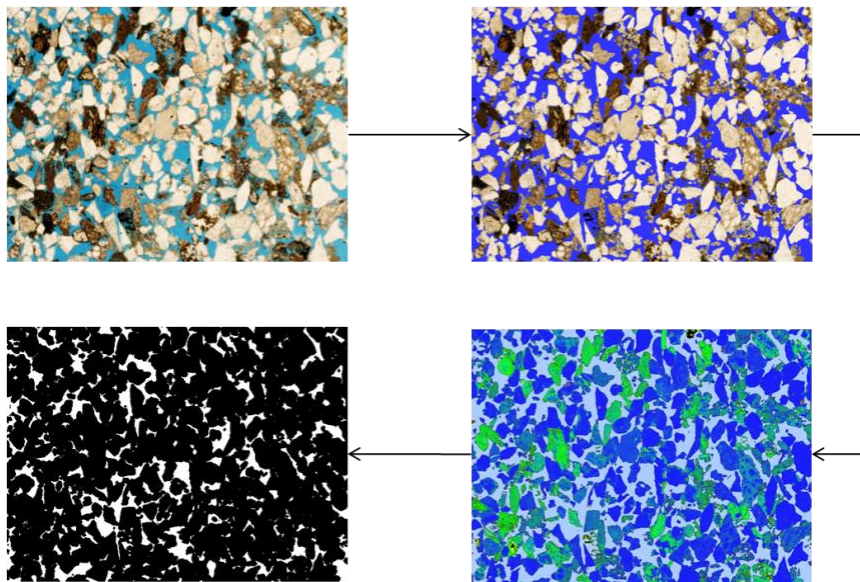


Figure B.4 Steps for image processing and segmentation on selected image (a) from 30 images of Well A sandstone thin section.

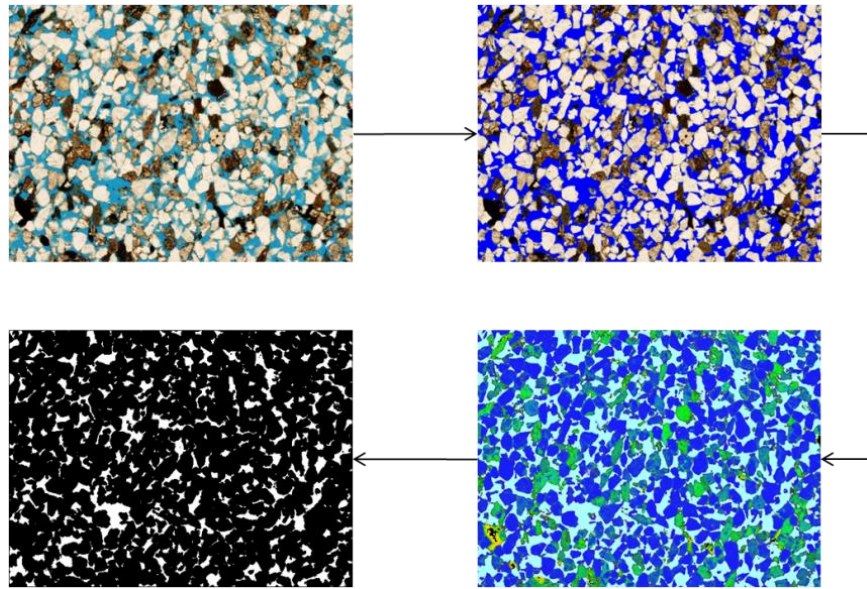


Figure B.5 Steps for image processing and segmentation on selected image (b) from 30 images of Well A sandstone thin section.

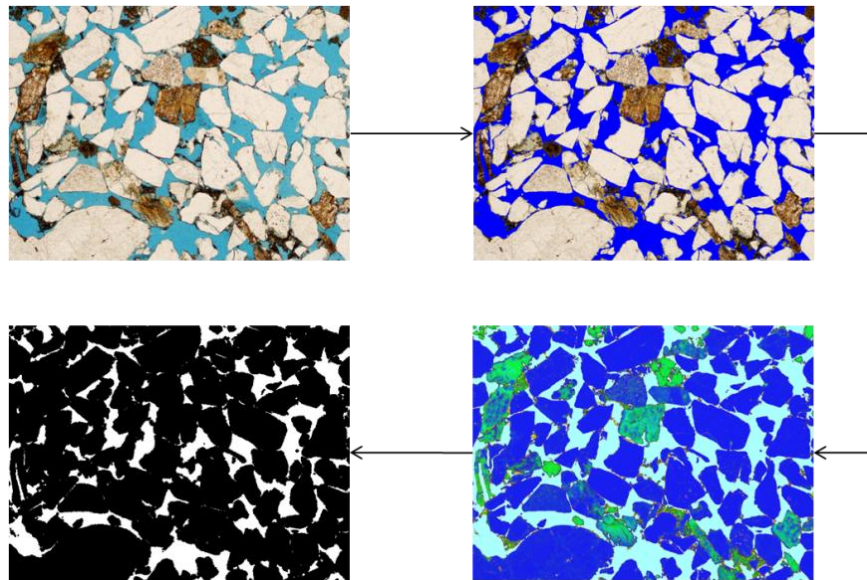


Figure B.6 Steps for image processing and segmentation on selected image (a) from 24 images of Well B sandstone thin section.

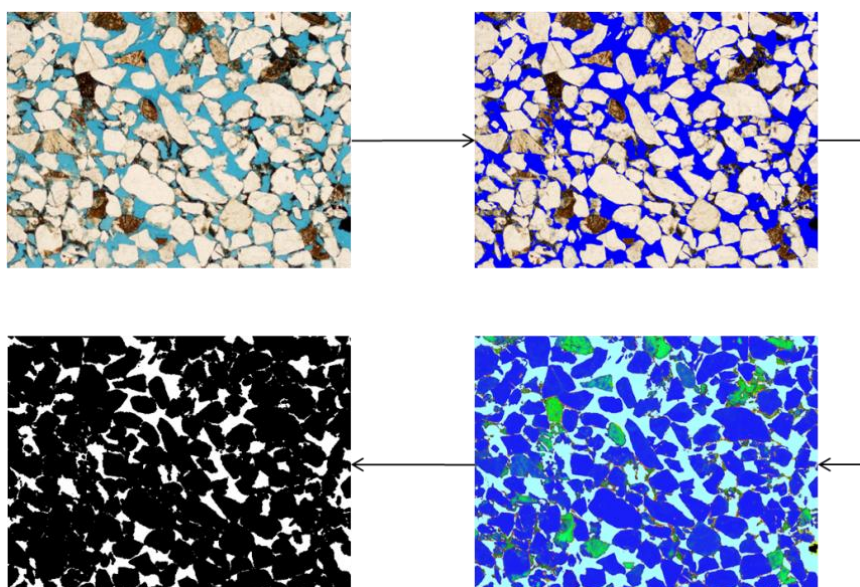


Figure B.7 Steps for image processing and segmentation on selected image (b) from 24 images of Well B sandstone thin section.

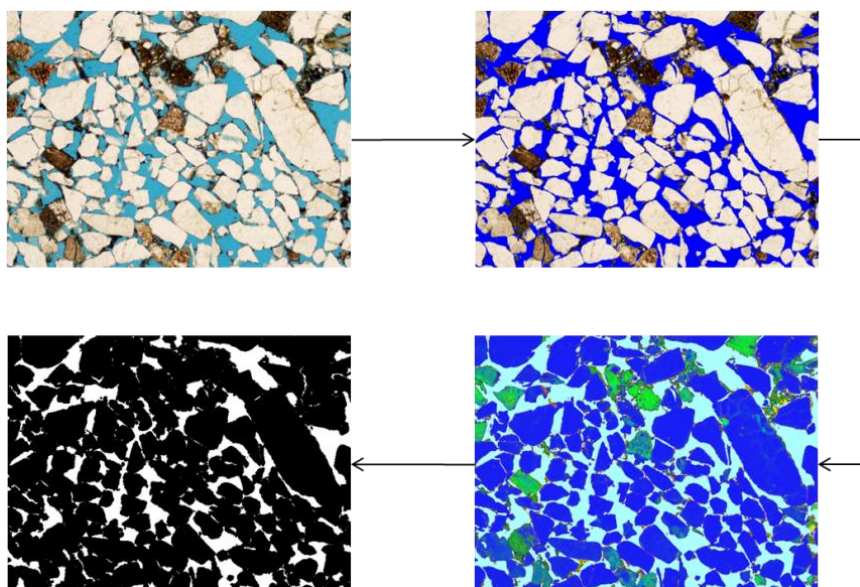


Figure B.8 Steps for image processing and segmentation on selected image (c) from 24 images of Well B sandstone thin section.

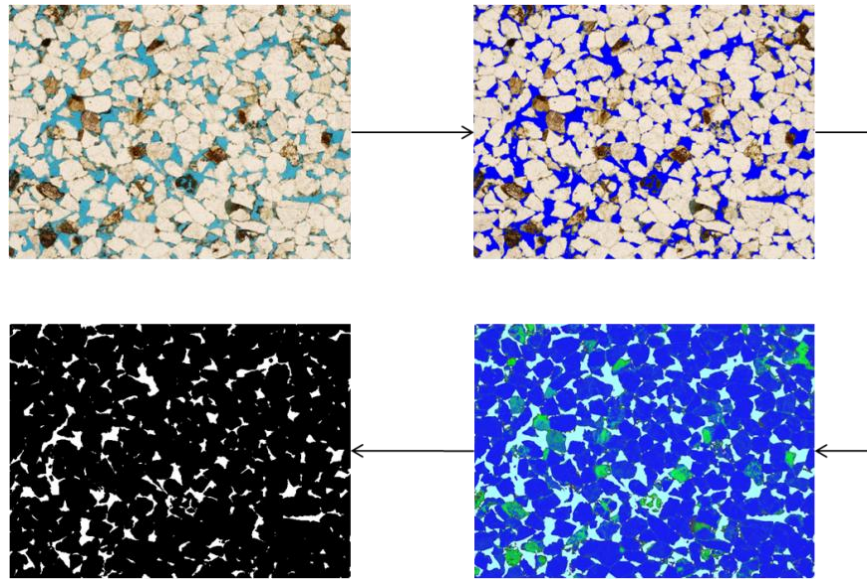


Figure B.9 Steps for image processing and segmentation on selected image (a) from 25 images of Well C sandstone thin section.

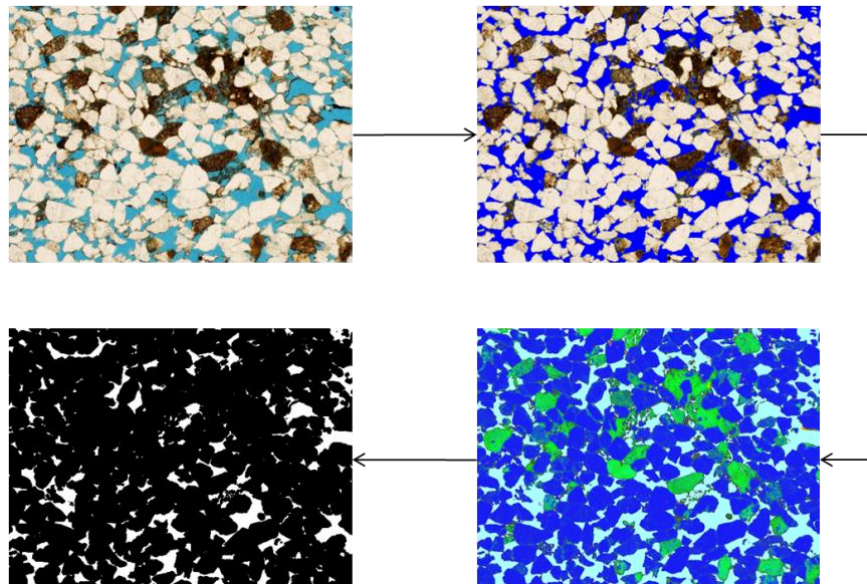


Figure B.10 Steps for image processing and segmentation on selected image (b) from 25 images of Well C sandstone thin section.

